2016-03-01

Lateral Resistance of Pipe Piles Behind a 20-Foot-Tall MSE Wall with Welded-Wire Reinforcements

Ryan Thomas Budd
Brigham Young University

Lateral Resistance of Pipe Piles Behind a 20-Foot-Tall MSE Wall with Welded-Wire Reinforcements

Ryan Thomas Budd

A thesis submitted to the faculty of
Brigham Young University
in partial fulfillment of the requirements for the degree of

Master of Science

Kyle M. Rollins, Chair
Kevin W. Franke
Norman L. Jones

Department of Civil and Environmental Engineering

Brigham Young University

March 2016

ABSTRACT

Lateral Resistance of Pipe Piles Behind a 20-Foot-Tall MSE Wall with Welded-Wire Reinforcements

Ryan Thomas Budd
Department of Civil and Environmental Engineering, BYU
Master of Science

Pile foundations for bridges must often resist lateral loads produced by earthquakes and thermal expansion and contraction of the superstructure. Right-of-way constraints near bridge abutments are leading to an increased use of mechanically stabilized earth (MSE) walls below the abutment. Previous research has shown that lateral pile resistance can be greatly reduced when piles are placed close to MSE walls but design codes do not address this issue. A full-scale MSE wall was constructed and 24 lateral load tests were conducted on pipe, square and H piles spaced at distances of about 2 to 5 pile diameters from the back face of the wall. The MSE wall was constructed using welded-wire grid and ribbed strip inextensible reinforcements. This paper focuses on four lateral load tests conducted on steel pipe piles located behind a 20-ft section of MSE wall reinforced with welded-wire grids. Results showed that measured lateral resistance decreases significantly when pipe piles are located closer than about 4 pile diameters from the wall. LPILE software was used to back-calculate P-multipliers that account for the reduced lateral resistance of the pile as a function of normalized spacing from the wall. P-multipliers for this study were 0.95, 0.68, and 0.3 for piles spaced 4.3, 3.4 and 1.8 pile diameters from the wall, respectively. Based on results from this study and previous data, lateral pile resistance is relatively unaffected (p-multiplier = 1.0) for piles spaced more than approximately 3.9 pile diameters (3.9D) from the MSE wall. For piles spaced closer than 3.9D, the p-multiplier decreased linearly as distance to the wall decreased. P-multipliers were not affected by differences in reinforcement length to height (L/H) ratio or reinforcing type.

Lateral pile loads induce tensile forces in the soil reinforcement such that, as pile load increases the maximum induced tensile force increases. Results also indicate that maximum tensile forces typically occurred in the soil reinforcement near the pile location. Past research results were combined with data from this study and a statistical regression analysis was performed using all data associated with welded-wire grid reinforcements. A regression equations was developed to predict the peak induced tensile force in welded-wire grids based on independent variables including lateral pile load, normalized pile distance (S/D), transverse distance (T/D), L/H ratio, and vertical stress. The equation has an R^2 value of 0.79, meaning it accounts for approximately 79% of variation for all welded-wire grid reinforcements tested to date.

Keywords: Kyle Rollins, lateral load, pile, p-multiplier, welded-wire grids, MSE wall

ACKNOWLEDGEMENTS

This study was funded through FHWA Transportation Pooled Fund program TPF-5(272) "Evaluation of Lateral Pile Resistance Near MSE Walls at a Dedicated Wall Site" and was supported by Departments of Transportation from Florida, Iowa, Kansas, Massachusetts, Minnesota, Montana, New York, Oregon, Texas and Utah. Utah served as the lead agency with Jason Richards as the project manager. This support is gratefully acknowledged; however, the opinions, conclusions and recommendations contained herein do not necessarily represent those of the sponsoring organizations.

Contributions from various companies also helped in accomplishing the main objectives of this research. A special thanks to the following individuals and companies: Chris Ragan at Atlas Tube for donating the square and pipe piles; Price Bethel at Spartan Steel for donating the H piles; Eric Hendricksen at Desert Deep Foundations, Inc. for providing pile driving services at cost; Geneva Rock, Inc. for providing site grading services and the test site location; Hadco Construction for providing their services in constructing the wall; Reinforced Earth Company and SSL for donating the steel strip and welded-wire grid wall systems; and to David Anderson and Rodney Mayo for their invaluable knowledge and assistance during testing. Thank you everyone for your contributions, services and expertise.

I would like to express my sincere gratitude to Dr. Kyle M. Rollins for the opportunity to study and perform research under him, and to Dr. Kevin W. Franke and Dr. Norman L. Jones for their advice and help on my committee.

Lastly, I would like to thank my beautiful wife and children for their patience, love and support for me throughout my research, education and career.

TABLE OF CONTENTS

LIST OF TABLES

LIST OF FIGURES

1 INTRODUCTION

Increasing right-of-way constraints have led to the increased popularity of Mechanically Stabilized Earth (MSE) walls near bridge abutments. Piles located within the reinforced zone of MSE walls that are used to support bridge abutments must resist both vertical loads from the bridge superstructure as well as lateral loads produced by earthquakes and thermal expansion and contraction. Currently, there is little guidance to design for the lateral resistance of piles behind MSE walls. Common methods employed at this time are spacing the piles far enough behind the wall (often 6 to 8 pile diameters) to negate the walls influence; assuming there is no lateral resistance from the wall; or placing the pile close to the wall and assuming a lateral resistance reduction factor based on engineering judgment. These methods are inefficient for the following reasons: (1) increasing the distance between the wall and the pile increases cost by increasing the bridge span; (2) assuming no lateral resistance increases foundation costs because the pile size and/or the number of piles required will increase; and (3) using engineering judgment gives no standard of design for reduction factors.

Research performed by Pierson et al (2008) on concrete shafts behind an MSE wall reinforced by geosynthetic reinforcement indicates that lateral resistance decreases as pile spacing from the wall decreases with significant wall distortion in the masonry block wall. Further research conducted by Rollins et al (2013) on steel piles with metallic reinforcement confirms the research by Pierson et al (2008) and also found that p-multipliers based on pile spacing behind an MSE wall may be used to account for the decreased lateral soil resistance near an MSE wall. Rollins et

al (2013) concluded that induced tensile forces in reinforcements from pile loading could be estimated using variables such as pile load, pile spacing behind the wall, and transverse distance of the pile from the reinforcement.

Although the research conducted to date is valuable, results are limited to a handful of tests with a significant number of variables with respect to soil density, reinforcement type, and reinforcement length to height ratios. Trends appear to be emerging but there is not enough information for developing design recommendations. Because of the limited data and the large number of variables, further testing is needed to provide better understanding of the MSE wall-pile interactions and to develop design recommendations.

Objectives

The main objectives of this research investigation are:

1. Measure reduced lateral pile resistance vs. displacement curves for pipe piles at different distances behind an MSE wall with welded-wire reinforcement
2. Measure the increase and distribution of tensile force in the welded-wire reinforcement induced by lateral pile loading.
3. Develop design rules (e.g. p-multipliers) to account for reduced pile resistance as a function of spacing behind the MSE wall
4. Develop a design approach to predict maximum reinforcement force induced by pile loading.

Scope of Work

To accomplish the research objectives, a full-scale MSE wall was constructed to conduct research on laterally loaded steel piles. The wall was constructed in two phases using welded-wire

grid and steel strip reinforcements so that the performance of the two reinforcement systems could be evaluated separately but with comparable backfill conditions. Because each reinforcement system develops resistance in different ways, this allows separate design approaches to be developed if necessary. During Phase I lateral pile load tests were performed at a wall height of 15 feet with a reinforcement length to height (L/H) ratio of about 0.9, which might be common for seismic design. During Phase II, tests were conducted at a wall height of 20 feet with an L/H ratio of about 0.7, which is more typical for static loading. The difference in reinforcement L/H ratios makes it possible to determine if reinforcement length has any effect on lateral pile resistance or induced force in the reinforcements.

Pile types consisted of pipe, square and H piles and were located behind the wall in the reinforced zone at distances of approximately 2, 3, 4 and 5 pile diameters from the back face of the wall. The variation in pile type makes it possible to determine if the p-multipliers or induced tensile force are affected by the shape of the piles.

This systematic examination of the interaction between piles and MSE walls has been the focus of four other theses, namely Hatch (2014), Han (2014), Besendorfer (2015) and Luna (2016). This thesis focuses on the behavior of the pipe piles located in the welded-wire grid reinforcement zone at a wall height of 20 feet with an L/H of about 0.70.

2 LITERATURE REVIEW

Currently, little guidance is given for designing the lateral resistance of loaded piles behind mechanically stabilized earth (MSE) walls. A review of MSE walls, soil reinforcement resistance to pullout, laterally loaded analysis of piles, and case histories of full-scale lateral load testing of piles is presented in this chapter.

2.1 MSE Walls

MSE walls are cost effective retaining structures that use reinforcing in the soil behind the wall to add strength and stability to the structure. Layers of reinforcing holds the facing system in place, which allows for construction of high vertical walls and prevents soil raveling from occurring. MSE walls were first built commercially in the early 1970's and are now widely used in practice. MSE walls are typically used on projects that have bridge abutments, wing walls or in areas where right-of-way is restricted. Advantages of MSE walls over conventional walls include: (Berg et al 2009)

- Simple and rapid construction procedures;
- Do not require large construction equipment or skilled laborers;
- Require less site preparation than alternative systems;
- Require less space in front of the structure for construction;

- Reduce right-of-way acquisition;
- Are technically feasible to heights greater than 100 feet; and
- Are more tolerant to deformations than alternative systems.

There are two general categories of reinforcing used in MSE walls: extensible and inextensible reinforcing. Extensible reinforcing is defined as a material that deforms with the surrounding soil and consists of any type of geosynthetic, such as geotextiles or geogrid, and is usually made of polyethylene or polyester. Inextensible reinforcing is defined as material that deforms considerably less than the surrounding soil and consists of steel or galvanized steel strips and welded-wire grids or mats (Berg et al 2009).

Typically, MSE walls have been designed using the Allowable Stress Design (ASD) method or the Load Resistance Factor Design (LRFD) method. Both methods evaluate the external and internal stability of the stabilized mass. The difference between the ASD and LRFD methods is how they design for uncertainty. ASD combines all load and material stress uncertainties into one factor of safety, regardless of the method used to estimate resistance. LRFD accounts for uncertainty in both material resistance and load and can provide more consistent levels of safety in the overall design by using resistance factors and load factors.

External and internal stability analyses are evaluated during the design process of MSE walls. External stability analysis of MSE walls assumes that the reinforced soil and wall act as one consistent mass. External failures include sliding, overturning, and bearing as shown in Figure 2-1.

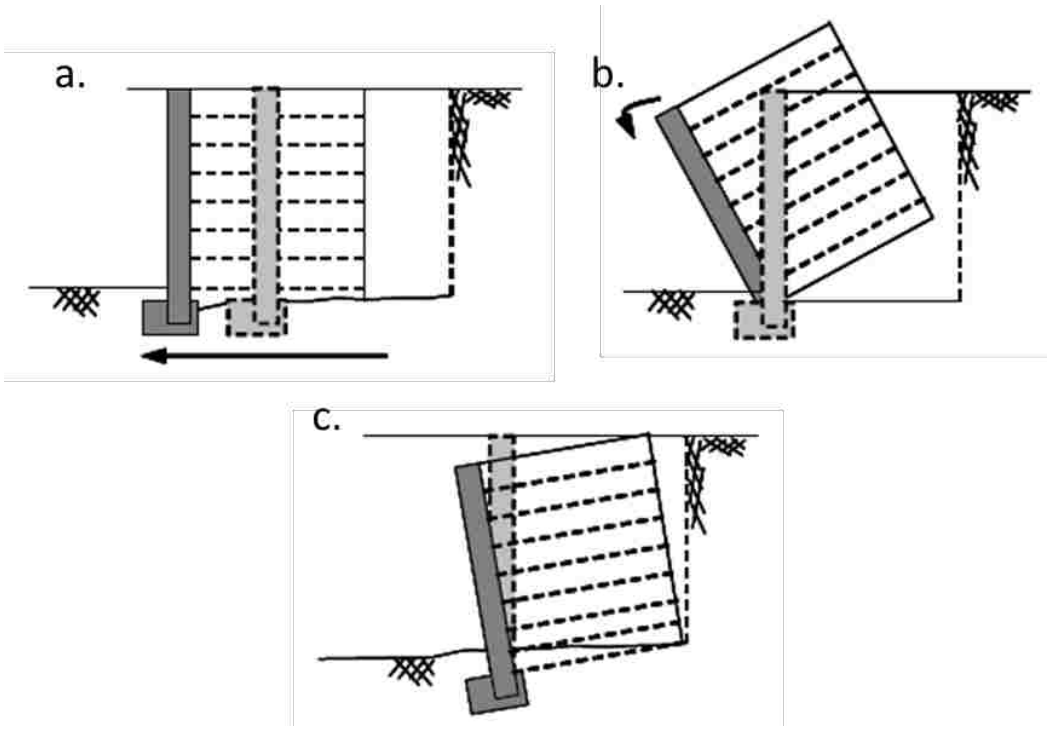

Figure 2-1: External stability failure cases: (a) sliding, (b) overturning, and (c) bearing.

Internal failure for an MSE wall can occur in two different ways: elongation and pullout of the reinforcement. Elongation occurs when tensile forces acting on the reinforcement are larger than yield strength of the reinforcing material and results in stretching or breaking of the reinforcement. Pullout occurs when tensile forces acting on the reinforcement are larger than the pullout resistance of the surrounding soil. In both cases, failure leads to large movement and possible collapse of the structure. The relevant steps for analyzing internal stability are as follows: (Berg et al 2009)

- Select the type of soil reinforcement;
- Define the critical failure surface (for selected reinforcement type);
- Define unfactored loads;

- Establish the vertical layout of soil reinforcements;
- Calculate factored horizontal stress and maximum tension for each reinforcement layer; and
- Calculate nominal and factored pullout resistance of soil reinforcements and check established layout.

Internal stability calculations vary depending on whether the reinforcing is extensible or inextensible. Inextensible welded wire grids were used on this project and will be the reinforcement discussed for the internal stability analysis.

The critical failure surface for inextensible reinforcing, as shown in Figure 2-2, is assumed to be bilinear, located at the zone of maximum tensile force in the reinforcement and passes through the toe of the wall. Maximum tensile forces for each reinforcement layer can be calculated using Equation 2-1 and are directly related to the type of reinforcement used (Berg et al 2009).

Figure 2-3 shows the relationship between reinforcing material used and the overburden stress. The coefficient of lateral stress, K_r, obtained from Figure 2-3 is used to calculate the horizontal stress as shown in Equation 2-2. Vertical spacing, S_v, of inextensible reinforcement with pre-cast concrete facings is generally constant. In order to increase resistance, the size of reinforcement or number of reinforcement members can be increased. In the case of welded wire grids, the diameter is increased and/or the number of longitudinal bars is increased.

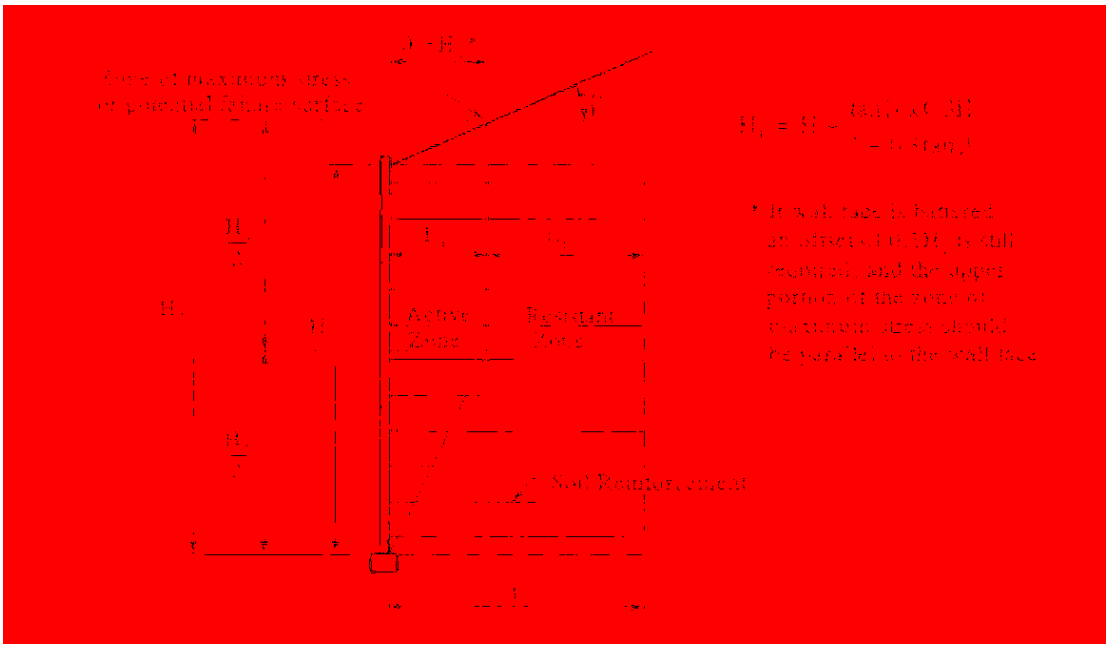

Figure 2-2: Potential failure surface location for MSE walls with inextensible reinforcement (Berg et al 2009).

Figure 2-3: Variation of the coefficient of lateral stress ratio with depth in an MSE wall (Berg et al 2009).

$$\boldsymbol{T_{max} = \sigma_H S_v} \quad \textbf{(2-1)}$$

where

T_{max} is the maximum tensile force in a reinforcement layer,

σ_H is the horizontal stress along the failure surface (see Equation 2-2), and

S_v is the vertical spacing between reinforcement layers.

$$\boldsymbol{\sigma_H = K_r \sigma_v + \Delta \sigma_h} \quad \textbf{(2-2)}$$

where

K_r is the coefficient of lateral stress (see Figure 2-3),

σ_v is the vertical stress (see Equation 2-3), and

$\Delta\sigma_h$ is horizontal stress due to external surcharges.

$$\boldsymbol{\sigma_v = \gamma_r Z + q} + \Delta\boldsymbol{\sigma_v} \quad \textbf{(2-3)}$$

where

γ_r is the moist unit weight of the reinforced soil,

Z is the depth to the reinforced layer from the top of wall,

q is a uniform surcharge load, and

$\Delta\sigma_v$ is a concentrated vertical surcharge load.

The pullout capacity, P_r, for each reinforcement is the force required to generate sliding of the reinforcement. Pullout capacity is dependent on the length, cross-sectional area and material

type of the reinforcements as well as surcharge loads and soil properties. Equation 2-4 shows how to calculate pullout capacity, P for a unit of welded wire grid reinforcement.

$$\boldsymbol{P_r = F^* \alpha \sigma'_v L_e C b} \quad \textbf{(2-4)}$$

where

P_r is the pullout capacity of the reinforcement per unit width,

F* is the pullout resistance factor (see Equation 2-5),

α is a scale effect correction factor equal to 1 for metallic reinforcements,

σ'_v is the vertical effective stress at the reinforcement layer,

L_e is the length of embedded reinforcement resisting the soil at a given point,

C is the reinforcement effective unit perimeter and is equal to 2 for grids, and

b is the width of the welded-wire grid reinforcement.

$$\boldsymbol{F^* = \begin{cases} 20(t/S_t), Z = 0 \\ 10(t/S_t), Z \geq 20\ ft \end{cases}} \quad \textbf{(2-5)}$$

where

t is the transverse bar thickness of the reinforcement,

S_t is the spacing between transverse bars, and

Z is the depth to the reinforcement layer below the top of the wall.

$$\boldsymbol{R_c = \frac{b}{S_h}} \quad \textbf{(2-6)}$$

where

b is the width of the reinforcement, and

S_h is the horizontal center to center spacing between grids on the same layer.

The horizontal spacing between grids, S_h, calculated in Equation 2-6 factors in the section of wall that is affected by the reinforcement. For this study, S_h was not used in the calculations because strain gauges measured the induced pile load directly, and the reinforcement was the prime focus of induced load, not the wall. Therefore, R_c was equal to b for this study.

2.2 Tests for Pullout Resistance Factors

A total of 402 full-scale pullout tests were performed on inextensible reinforcements at Texas Tech University. The primary purpose of the testing program was to evaluate pullout resistance factors (F*) for ribbed steel strips and welded wire grid reinforcements in sandy backfill (Lawson 2013). The backfill material was classified as a poorly graded sand with silt (SP-SM) with a maximum dry unit weight of 124.5 pcf, an optimum moisture content of 7.8 percent and an average relative compaction of 95.7 percent. A portion of the ribbed steel strips were tested in under-compacted soil with a relative compaction of approximately 91 percent. A comparison of the change in compaction to the change in F* values is found in Table 2-1 and provides valuable insight on how small changes in relative compaction can greatly affect the soil resistance on the reinforcement. In general, a change in relative compaction of 4 % affected the pullout resistance factor by 34% (Lawson 2013).

Table 2-1: Influence of relative compaction on pullout resistance factor, F* (Lawson 2013).

Degree of Compaction	Mean F*	Lower Confidence Interval	Upper Confidence Interval
Under-compacted backfill	1.77	1.50	2.09
Properly compacted	2.69	2.26	3.20

After creating a database, statistical analyses were performed on the data. The objective of the analyses was to identify key variables that affect the measured F* value and to develop F* prediction models and intervals based on the new data set (Lawson 2013). Results of the statistical analyses agree with AASHTO that depth of fill, transverse bar diameter and transverse bar spacing influence F* in welded-wire grids. Embedment length, longitudinal bar diameter and longitudinal bar spacing were significant variables affecting F* that the AASHTO equation does not take into account. This study shows that as longitudinal and transverse bar spacing decreases or the transverse bar diameter increases, F* increases.

A nonlinear regression was used to define the relationship between F* and the depth of fill, opposed to a bilinear regression line used by AASHTO (Lawson 2013). Figure 2-4 shows the measured F* values versus the depth of fill and includes the AASHTO bilinear equation as a solid black line for comparison. At depths shallower than ten feet, the data from this study produced F* values up to 2.5 times (near the surface) greater than those used by AASHTO. It is important to note that the scatter in the measured F* values is significant even in these tests where compaction was closely controlled. The scatter is greatest at the top of the wall presumably owing to differences in the potential for dilation associated with small changes in relative compaction. Therefore, scatter in the tensile force induced by lateral pile loading which occurs near the top of the wall should be expected to be significant.

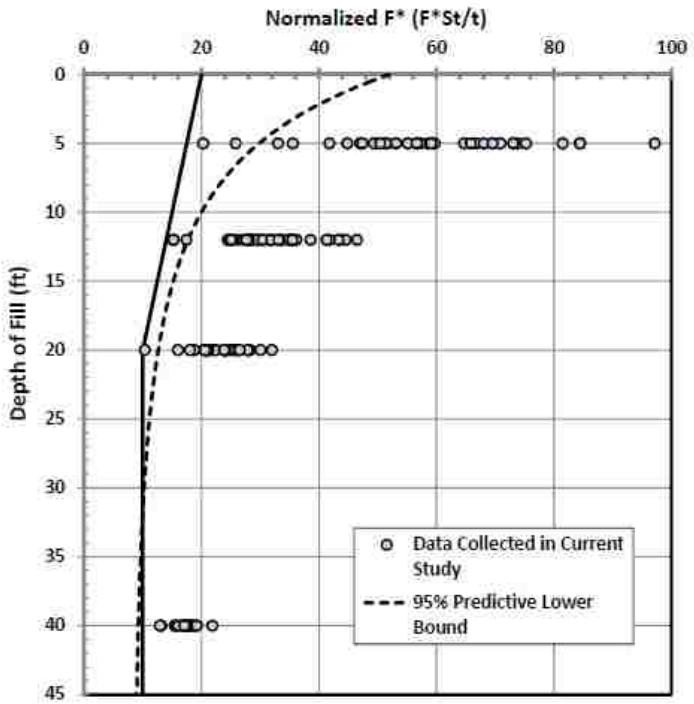

Figure 2-4: Normalized pullout resistance factor, F*, vs. depth of fill for welded-wire grid reinforcements in sandy backfill (Lawson 2013).

2.3 Laterally Loaded Analysis of Piles

A common way to analyze laterally loaded piles is by using the p-y method. The p-y method is based on modeling the soil-pile interaction as a nonlinear beam on an elastic foundation (BEF) where a series of springs are used to model soil behavior, as shown in Figure 2-5. Analysis of laterally loaded piles with the p-y method is generally performed by finite difference and finite element software including COM624, LPILE, FB-Pier, etc. LPILE is perhaps the most widely used program in the United States and was the software used for analysis on this project.

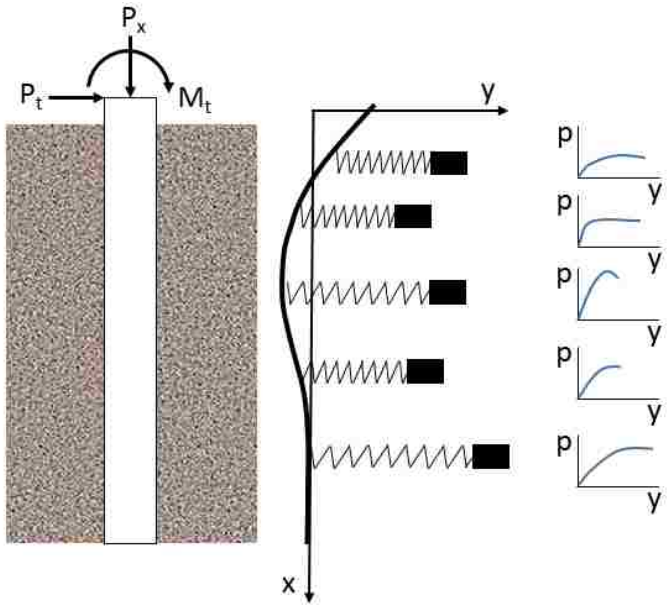

Figure 2-5: Conceptual model of the p-y method (Isenhower et al. 2015).

LPILE is a finite difference program that analyzes the lateral loading of driven piles and drilled shafts. LPILE is the commercial version of the computer program COM624 which was originally developed by Reese and Matlock at the University of Texas in the 1970s and is one of the most widely used programs for lateral pile load analysis. The program is capable of producing deflection, shear, bending moment and soil response of the pile to the maximum depth the pile is driven. LPILE also automatically generates p-y curves based on soils from full-scale load tests previously studied. Soil types programmed into LPILE include clay, sand, weak rock, and a number of specialty soils. The program also allows manual entry of soil parameters.

API sand and Reese sand are two of the sand types in LPILE with similar criteria and differ primarily in the initial modulus of subgrade reaction and the shape function of the curves. The API sand criteria uses a more convenient equation for computation and will be the soil criteria used for analysis on this project. The API procedure for computing p-y curves is as follows: obtain values for the angle of internal friction, soil unit weight, and pile diameter; compute the ultimate soil

resistance; and develop the load-deflection curve based on the smallest calculated ultimate bearing capacity value. Values for soil properties are either obtained through field testing, correlation, or empirical means and are used in LPILE as input parameters.

Two models are used for computing the ultimate bearing capacity, p_u, for piles in sand. The first model is a passive wedge-type failure for soil resistance near the ground surface and can be calculated using Equation 2-8. An example of wedge failure is demonstrated in Figure 2-6. The second model is for failure at deeper depths caused by lateral flow of soil around the pile and is calculated using Equation 2-9. At a given depth, x, the model giving the smallest value of P_u should be used as the ultimate bearing resistance when developing the p-y curve. The p-y relationships for sand are non-linear but may be approximated by using Equation 2-10.

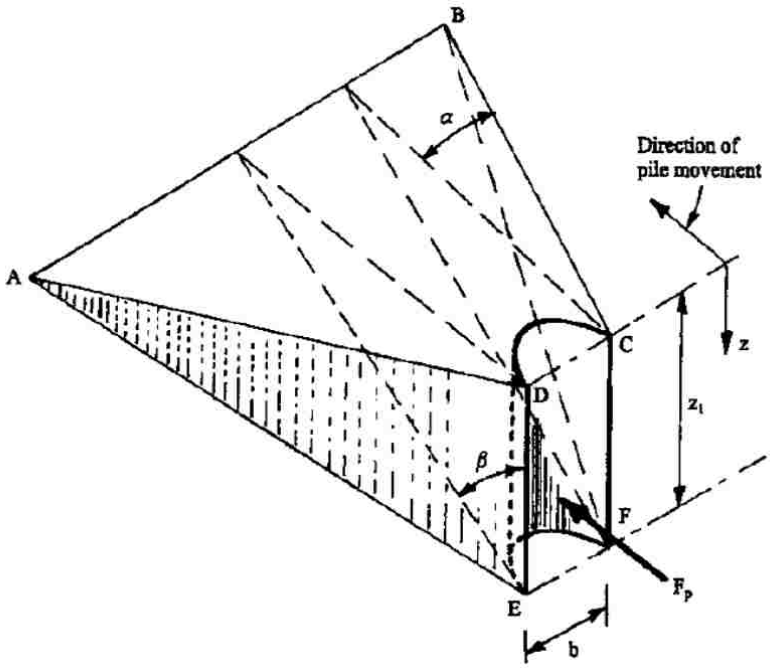

Figure 2-6: Passive wedge failure of laterally loaded piles in sand at shallow depths (Isenhower et al. 2015).

$$P_{us} = (C_1 x + C_2 b)\gamma' x \quad \textbf{(2-7)}$$

$$P_{ud} = C_3 b \gamma' x \quad \textbf{(2-8)}$$

where

P_u is the ultimate resistance in force per unit length (s = shallow, d = deep),

γ' is the effective unit weight of soil,

x is depth from ground surface,

ϕ' is the angle of internal friction of sand in degrees,

C_1, C_2, and C_3 are coefficients determined from Figure 2-7 as a function of ϕ', and

b is the average pile diameter from the ground surface to depth x.

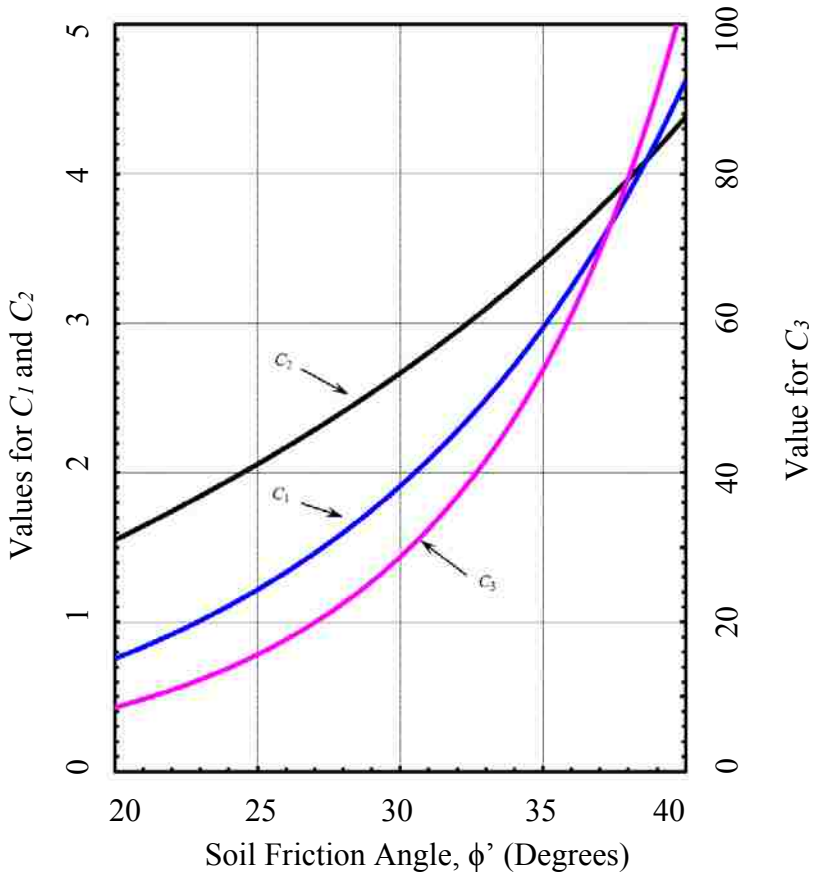

Figure 2-7: Ultimate bearing coefficients as a function of the internal angle of friction (API, 1982).

$$\boldsymbol{p = Ap_u \tanh\left(\frac{kx}{Ap_u} y\right)} \quad \textbf{(2-9)}$$

where

p is resistance on the p-y curve,

A is $\left(3.0 - 0.8\frac{x}{b}\right) \geq 0.9$ for static loading, 0.9 for cyclic loading,

p_u is computed from Equations 2-8 and 2-9, and is the smaller of the two values,

k is the initial modulus of subgrade reaction as determined from Figure 2-8,

x is depth from ground surface, and

y is deflection on the p-y curve.

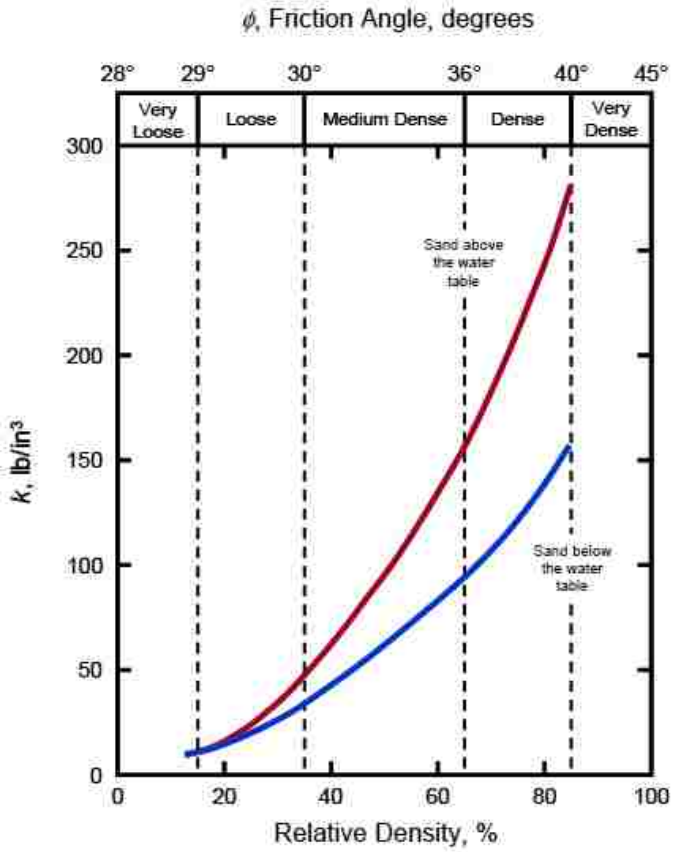

Figure 2-8: Soil modulus reaction based on friction angle or relative density of soil (API, 1982).

2.4 Full-Scale Load Tests

Several full-scale load tests have been performed on laterally loaded piles piles/shafts behind MSE walls over the last decade including work from Pierson (2009), Rollins et al (2013), Hatch (2014), Han (2014) and Besendorfer (2015). The following sections will discuss the full-scale load tests performed to date including the conclusions and limitations drawn from each test.

2.4.1 Laterally Loaded Shafts Behind an MSE Block Wall

The first full-scale lateral load test behind an MSE wall was performed by Pierson and Parsons in 2007. The project was located in Kansas DOT right-of-way near Kansas City, Kansas. The research consisted of laterally loading eight 36-inch diameter cast-in-place reinforced concrete shafts behind a 20 foot high masonry block retaining wall with Tensar UX1400 and UX1500 extensible geogrid reinforcements. The shafts were generally 20 feet long, and spaced a normalized distance of one shaft diameter (1D) to four shaft diameters (4D) behind the back face of the wall. Backfill consisted of crushed limestone gravel with an angle of friction of 51 degrees (Pierson et al 2009).

Instrumentation was used to monitor lateral load and displacement of shafts, wall displacements, pressures behind the wall facing, strain within the reinforcing and movement within the wall (Parsons et al 2009). Shaft data was obtained by monitoring hydraulic pressure, load cells and linear variable differential transformers (LVDTs). Inline load cells were used on all of the single pile tests. Each test shaft and reaction shaft were fitted with two LVDTs at different elevations to determine the change in elevation. The reaction and reference beams were also fitted with LVDTs to monitor movement. Inclinometers were placed inside the shafts to monitor shaft deflection and measurements were taken at different load steps. A pile head load vs. deflection plot presented in Figure 2-9 for four single shaft tests located at different distances behind the wall

indicates that lateral soil resistance decreases as the normalized distance decreases. However, it should be noted that the reduction does not appear to decrease uniformly with distance. For example, the lateral resistance of the pile at 3D decreases by about 30% on average relative to the pile at 4D; however, the lateral resistance for the pile at 2D is about the same as that for the 3D pile. This could be a result of non-uniform compaction between the pile and the wall face.

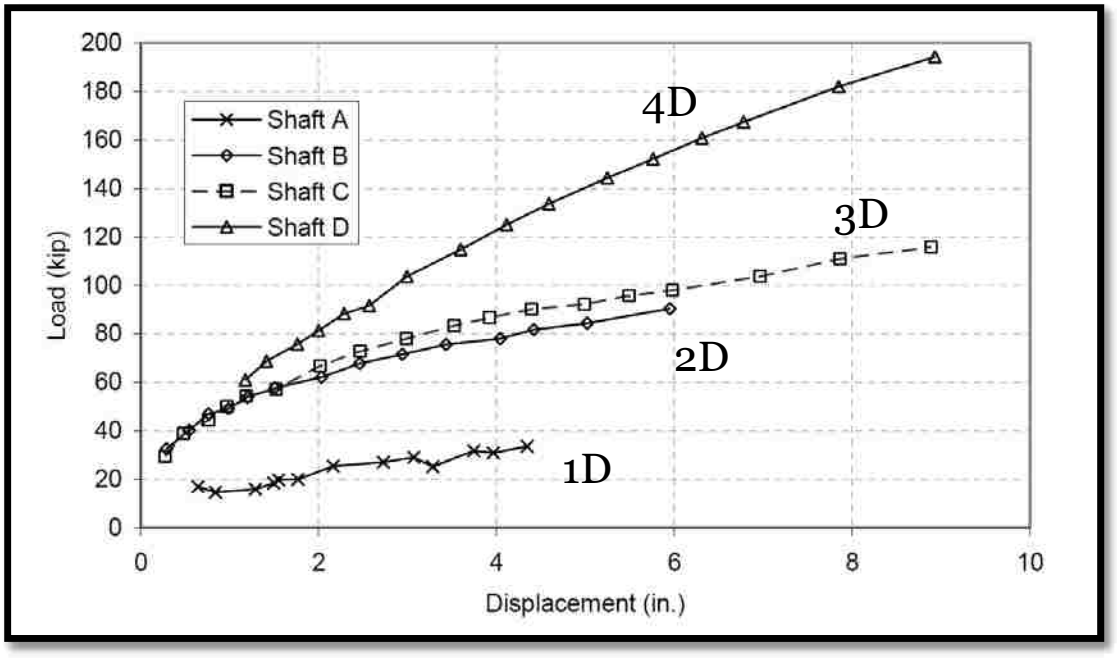

Figure 2-9: Load at 2.5 minutes vs. deflection of laterally loaded single shafts (Pierson et al 2009).

Geogrid was instrumented with strain gauges, located on the top and bottom of the reinforcement for redundancy. Data from the strain gauges was used to measure load transferred to the reinforcements. They found that as geogrid stiffness (strength) increased the wall deflection decreased and the area of wall displacement increased. (Pierson et al 2011). Post-test tension cracks were observed at the edge of the reinforced soil block indicating that failure of the wall was

external and that reinforcement length was critical on this project. In general, strain was highest near the pile and decreased as distance from the pile increased.

Pressure cells were placed behind the wall face and were used to measure pressure at multiple elevations directly in front of the loaded shafts. Wall deflection was measured by placing targets on the wall face and measuring target movements between each load with a digital camera on a fixed tripod. Movement measured from the targets and LVDTs were consistent with each other. Because the wall and shafts were built for research, wall deflections of over 6 inches were measured on some of the tests. Figure 2-10 shows that 9 inches of shaft movement deflects the wall 6 inches, indicating that the wall is not resisting the pile load very effectively. Further evidence of poor lateral resistance is that wall movement is reduced by approximately 60 percent when spaced two pile diameters from the deflection in line with the shaft.

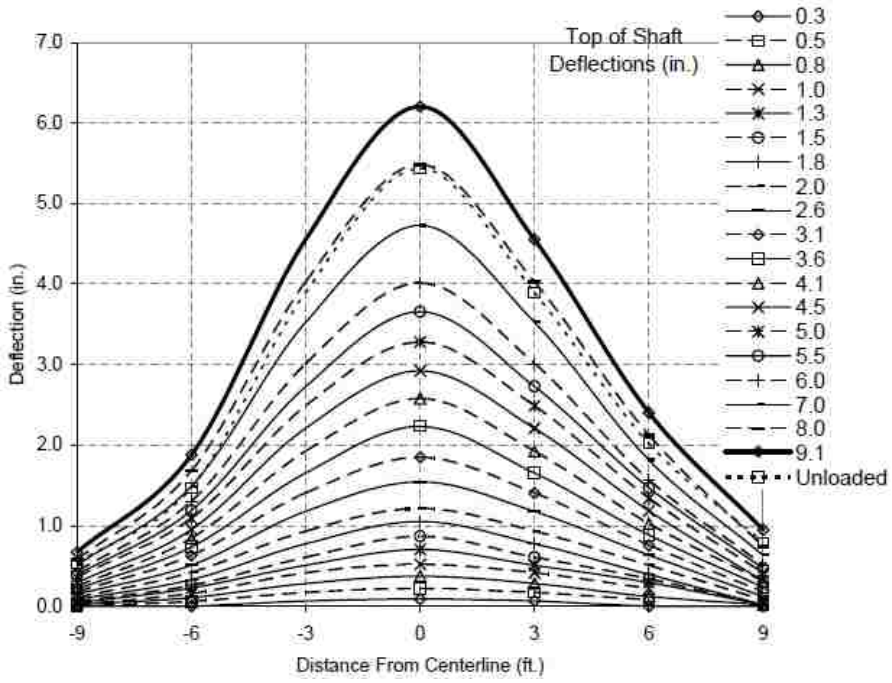

Figure 2-10: Wall deflection based on distance from centerline of Shaft C located 3D behind the wall face near the top of wall (Pierson et al 2009).

2.4.2 Full-Scale Load Testing Near UDOT Bridge Abutment Walls

Lateral load tests behind MSE walls were performed in Utah County, Utah at the following sites: Pioneer Crossing, U.S. Highway 89 and Provo Center Street (Price 2012, Nelson 2013, Rollins et al, 2013). Each site was located in Utah Department of Transportation (UDOT) right-of-way and where bridges were under construction. Testing was performed on a total of eight steel piles with diameters from 12.75 to 16 inches and at distances of 1.7D to 7.5D from the wall face. Reinforcement was all inextensible, but both welded-wire grid and ribbed strip reinforcements were employed along with one-stage and two stage walls. Wall heights ranged from about 20 to 40 ft. Four of the piles tested were production piles used to support the bridges and had set locations. The remaining four piles were installed specifically for testing purposes. The variables for each laterally loaded pile are shown in Table 2-2.

Test results from Rollins et al (2013) confirmed Pierson's conclusion that lateral resistance decreases as the normalized distance from the wall decreases. To account for the reduced lateral resistance due to proximity to the wall, Rollins et al (2013) computed p-multipliers for each test pile using the computer program LPILE. The p-multipliers were then plotted versus distance from the wall face and best-fit curves were developed as shown in Figure 2-11. According to Figure 2-11, the length to height (L/H) ratio and normalized distance behind the wall both play a role in determining p-multiplier values. The data suggest that with L/H ratios of 1.1 and 1.6, a p-multiplier of 1 can be used when the normalized distance from the back face of the wall is 5.2 and 3.8 pile diameters, respectively. It should be noted that the friction angle (ϕ) and/or the lateral stiffness factor (k) used to analyze many of the Price (2012) and Nelson (2013) tests were either much higher or lower than would be expected for the type of soil they were tested in. This is, in part, caused by not accounting for the surcharge loads when calculating p-multipliers. Surcharge loads

were later considered to increase the effective wall height changing the L/H ratios to be approximately 1.0 to 1.4. Figure 2-12 shows an alternative interpretation of the results which indicate that the p-multipliers are only affected by spacing less than approximately 3.8D.

Table 2-2: Test data and information from UDOT bridge tests (Price 2012, Nelson 2013).

	US Highway 89		Pioneer Crossing			Provo Center Street		
Test Pile	TP1	TP2	TP3	TP4	TP5	TP6	TP7	TP8
Outside Pile Diameter [in]	12.75	12.75	16	16	16	12.75	12.75	12.75
Pile Wall Thickness [in]	0.375	0.375	0.375	0.375	0.375	0.375	0.375	0.375
Wrapped with HDPE? If Yes, Thickness [mm]	No	No	Yes, 10	Yes, 10	Yes, 10	No	No	No
Distance from Back Wall Face to Center of Pile [ft]	7.7	4.0	3.8	6.9	2.2	1.3	2.8	6.7
Normalized Pile Spacing [pile diameters]	7.2D	3.8D	2.9D	5.2D	1.6D	1.3D	2.7D	6.3D
Wall Height at Time of Testing [ft]	20.5	20.5	29.8	37.7	34.7	23.25	23.25	23.25
Reinforcement Length [ft]	33	33	50	42	39	28	28	28
Reinforcement Length-to-Full Height of Wall (Surcharge included)	1.29	1.42	1.27	0.98	0.97	1.03	1.20	1.03
Wall Facing Type	Concrete Panel		Concrete Panel			Welded Wire		
Inextensible Reinforcement Type	Grids		Grids			Strips		
Vertical Spacing of Reinforcement [ft]	2.5		2.5			2		
Surcharge Load [psf]	708	383	1363	735	808	657	135	657
Wall Panel Dimensions [ft]	5x12		5x10			4.8x9.75		
Backfill Material	Sandy Gravel		Sandy Gravel			Sandy Gravel		
Moist Unit Weight of Soil [pcf]	141.8		142.0			134.9		

Price (2012) and Nelson (2013) also analyzed the normalized load in the reinforcement as a function of normalized distance from the pile for both types of reinforcement. The maximum tensile force is normalized by the maximum pile load and plotted against the transverse distance between the pile and reinforcement normalized by the longitudinal distance between the pile and the wall, as shown in Figure 2-13. They determined that the normalized force decreases exponentially as the normalized distance increases. They developed an envelope between the best fit curve of the data and conservative test data values, as shown in Figure 2-13.

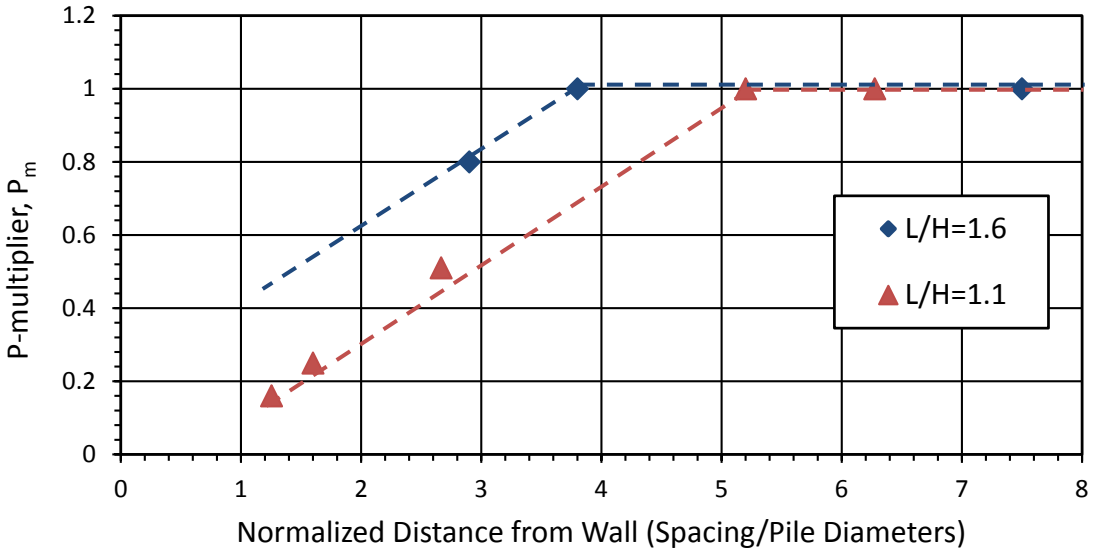

Figure 2-11: Tentative p-multiplier curves as a function of normalized distances for two reinforcement ratios (Rollins et al 2013).

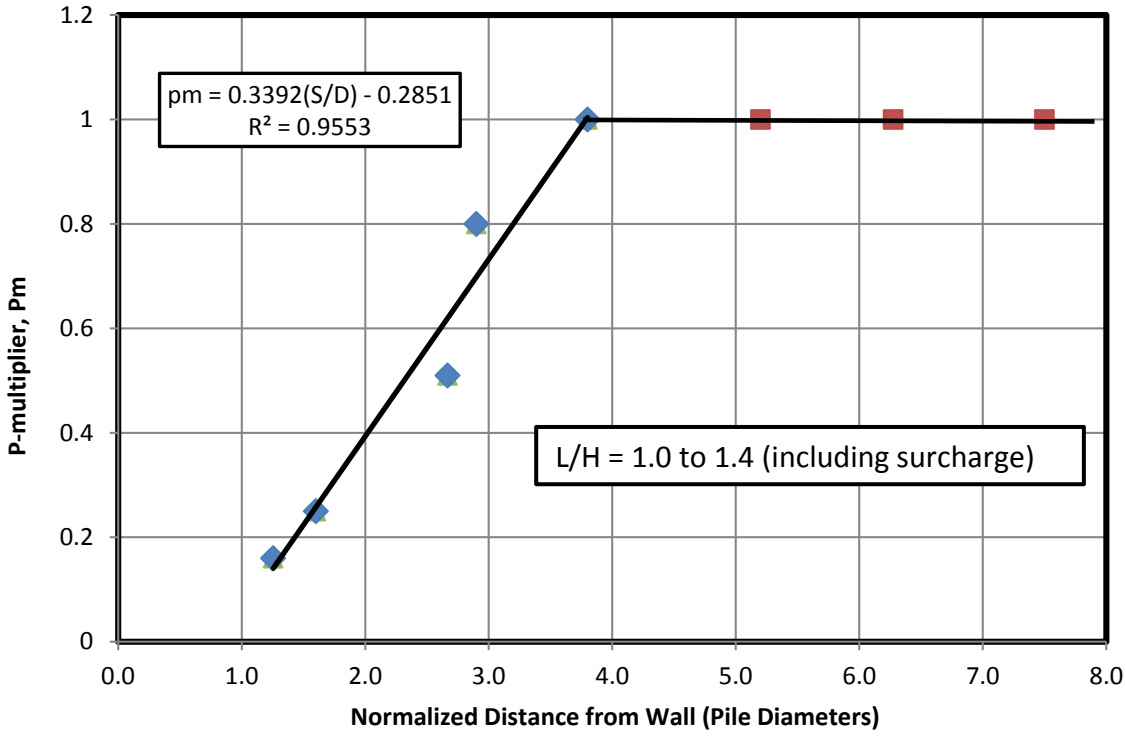

Figure 2-12: P-multiplier curves as a function of normalized distance with reinforcement ratios corrected for surcharge (Rollins et al 2013).

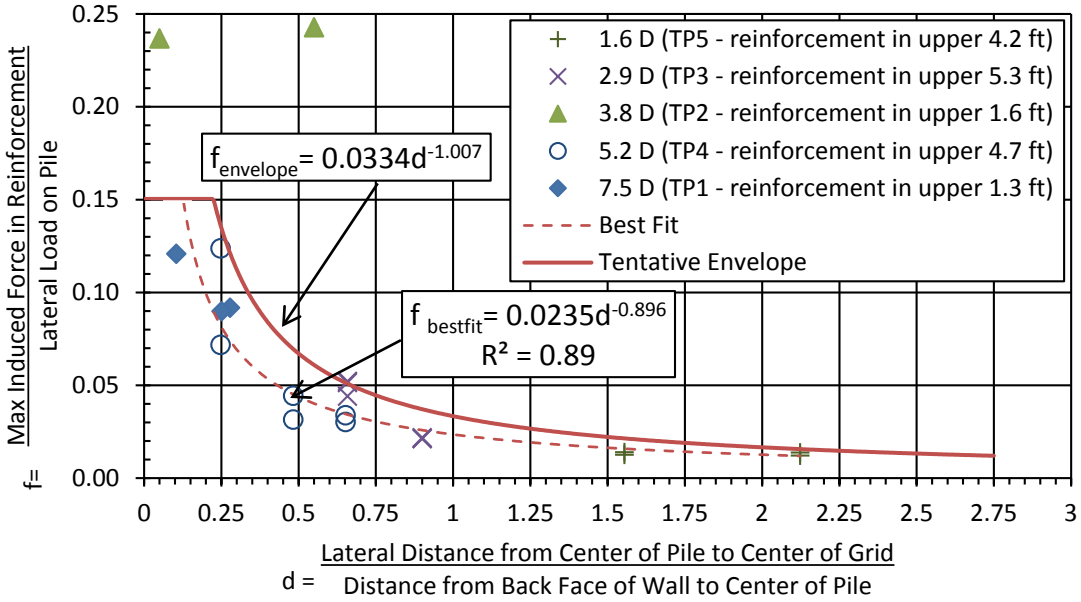

Figure 2-13: Plot of normalized induced force in wire grid reinforcement vs. normalized distance from pile (Rollins et al 2013).

2.4.3 Full-Scale Lateral Load Testing Behind an MSE Wall

Additional research has been completed on laterally loaded piles behind an MSE wall of which this report is a part. Tests were performed at wall heights of 15 feet and 20 feet with a constant reinforcement length to examine the influence of the reinforcement length to height (L/H) ratio on pile performance. Inextensible welded-wire grids and ribbed strips were each used on one half of the wall for soil reinforcement. Pipe, square and H-piles were used as test piles to determine if the pile shape of is a factor affecting the soil resistance. Further test layout and the instrumentation of piles, reinforcing, MSE wall, etc. will be discussed later in this report.

Reports for the 15-foot phase of the wall for both the ribbed strip and welded-wire grid sections of the wall using steel pipe piles were completed by Han (2014) and Hatch (2014), respectively. A report for the 20-foot phase of the wall for the ribbed strip section of the wall using steel pipe piles has been completed by Besendorfer (2015). Data from these studies confirm that

lateral pile resistance decreases as normalized distance between the pile and wall decreases. Their data also show that the L/H ratio does not influence the p-multiplier as previously suspected based on the limited set of test results available to Price (2012) and Nelson (2013). Figure 2-14 shows a best fit line representing the previous test data ran on steel pipe piles and omits the lines based on the L/H ratio. Data to this point indicates that if a pile is spaced 3.8 pile diameters or greater behind an MSE wall, it will not have reduced soil resistance due to its proximity to the wall and have a p-multiplier of 1. Furthermore, if a pile is closer than 3.8 pile diameters to the MSE wall, the p-multiplier will be reduced linearly as shown in Figure 2-14. Results from these tests also indicate that induced reinforcement load increases as pile load increases, and as pile spacing and transverse distance from reinforcement to the pile decreases. Maximum wall deflections of less than 0.5 inches were measured for pile head loads of more than 50 kips and pile head deflections of 3 inches or more. This indicates that inextensible reinforcement is ideal to resist laterally loaded piles.

2.5 Limitations of Existing Research and Need for Additional Research

As indicated previously, this study addresses lateral loading of steel pipe piles at the 20-ft phase of the MSE wall on the welded-wire grid portion of the wall. Similar analysis to that of Han (2014), Hatch (2014) and Besendorfer (2015) will be completed and results will be compared in the attempt to validate the p-multiplier chart in Figure 2-14 and check for different factors that affect the induced load on soil reinforcement. Additionally, lateral pile load tests have never before been performed near an MSE wall with an L/H ratio of about 0.7, which is typical of static loading conditions when welded-wire grid reinforcements have been used. This research will investigate the effects that an L/H ratio of 0.7 has on lateral resistance and p-multipliers when welded-wire grids are employed.

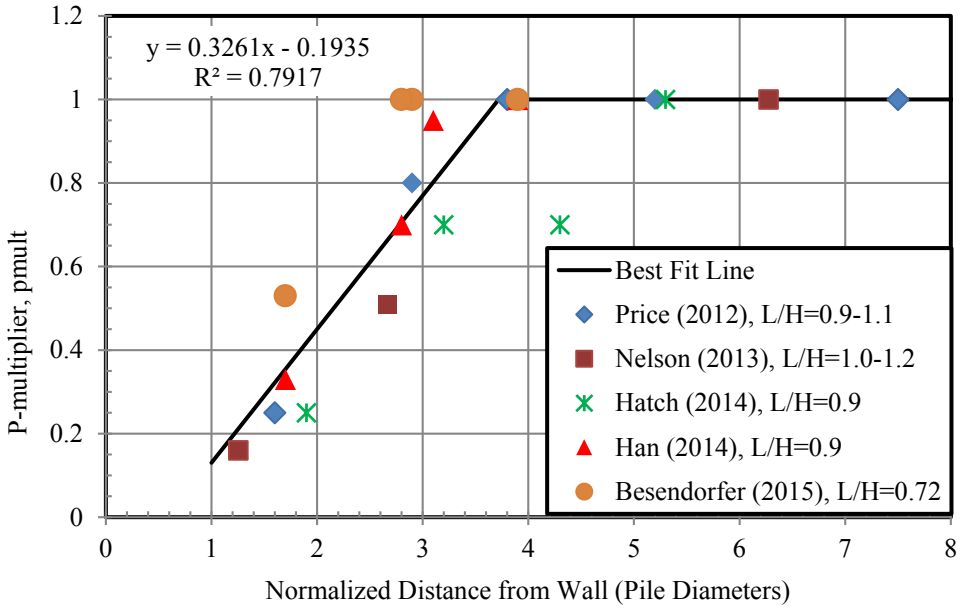

Figure 2-14: P-multiplier chart for steel pipe piles accounting for surcharge load (Besendorfer, 2015).

3 TEST LAYOUT

Testing for this project was conducted on Geneva Rock property located on the south side of Point of the Mountain in Utah County, near Lehi, Utah. Coordinates for the site are 40.453194, -111.899304. The general site location and a close-up view of the site are shown in Figure 3-1.

Figure 3-1: Location of the project site (Google earth, 2015).

3.1 Site Preparation

Prior to site grading and wall construction, the test location consisted of an existing slope ranging between 3:1 (horizontal to vertical) and 5:1 in steepness. Grading of the site was completed using a CAT D9T bulldozer with built-in automatic leveling and elevation instrumentation. After initial grading of the staging area and project site was completed, a 2-foot-deep cut was excavated along the length of the wall face location to provide minimum embedment for the leveling pad and MSE wall. The cut was extended 25 feet back from the wall location with approximate cuts of 5 to 7 feet deep into the hillside near the reaction pile locations. Excess fill from the cuts was stored east of the site for later use. Site grading and cuts are shown in Figure 3-2.

Figure 3-2: Project site after completion of site grading.

3.2 Piles

Test piles for this site consisted of round A252-Grade 3 12.75x0.375 pipe piles, HSS 12x¼ square piles and HP 12x74 H-piles. All piles had a yield strength of approximately 57,000 psi. Round and square piles were donated by Atlas Steel and H-piles were donated by Skyline Steel and Spartan Steel.

A total of twenty-five 40-foot long steel piles were driven to a depth of 18 feet below grade prior to wall construction. A summary of the blow counts for the piles used in this study are located in Table 3-1. The piles were driven by Desert Deep Foundations using an ICE I-30V2 diesel hammer. The hammer was installed on tracks inside of a steel cage tower, aligned with the pile and held in place by a crane. Figure 3-3 shows the pile driving set up. All pipe and square piles were driven open ended and were plugged with soil during installation. Plugs ranged between 10.3 and 10.9 feet above the pile toe for the pipe piles used in this study. For the purposes of this research, the test piles were considered hollow.

Pile locations were designed and laid out to normalized distances of 2 pile diameters/widths (2D), 3D, 4D and 5D from the back of the wall panel with a horizontal spacing of 5 feet on center from each other. This report covers the pipe piles tested at the 20 foot wall level on the east side of the retaining wall using steel welded-wire grid reinforcing. The actual normalized distances for piles 2D, 3D, 4D and 5D for this report are 1.8D, 3.4D, 4.3D and 5.2D, respectively. The actual horizontal spacing between piles 2D, 3D, 4D and 5D are 5’5”, 4’7” and 4’7”, respectively. Normalized spacing varied from design values owing to construction tolerances when driving piles.

Additional test piles were driven behind the designed reinforced soil mass and used as control tests since they were not influenced by the proximity of the retaining wall. The control

piles were also used to support the reaction beam during testing. Pile locations are shown in Figure 3-4.

Table 3-1: Blow counts (N) of driven pipe piles behind the SSL portion of the wall.

Depth (ft)	N (blow counts)			
	1.8D	3.4D	4.3D	5.2D
1				
2	1	1		
3	1	1		
4	1		2	1
5	1	1		
6	1	1		
7	3	1	2	2
8	3			
9	3			2
10	5		7	2
11	5		6	6
12	5		7	6
13	3		5	5
14	3	25	4	3
15	3	3		2
16	3		3	2
17	3		4	3
18	3	5	3	4
Total	47	38	43	38

Figure 3-3: Installation of piles using a diesel hammer.

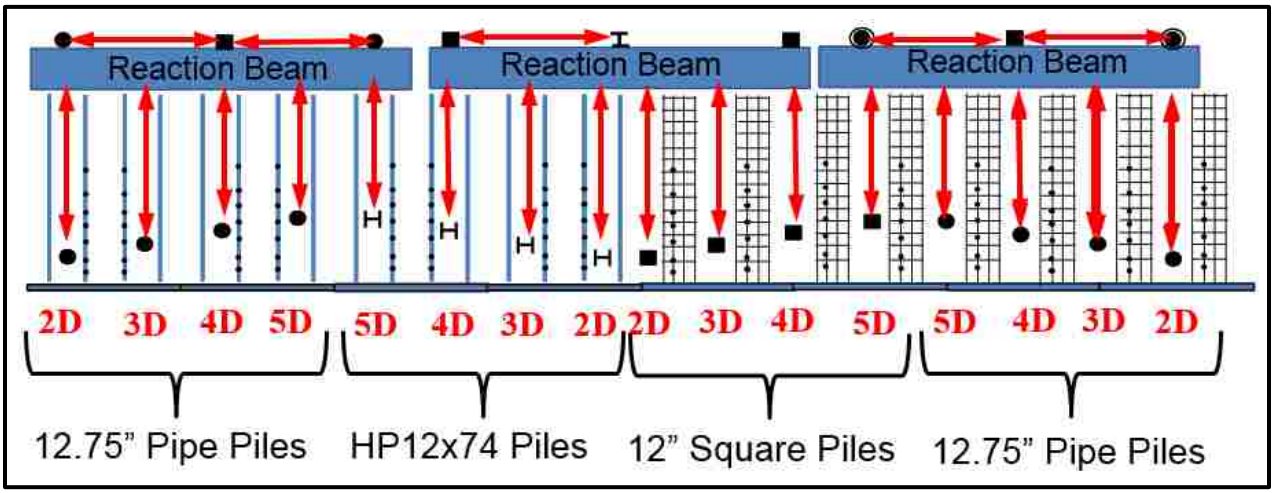

Figure 3-4: Plan view of pile locations.

3.3 MSE Wall

The MSE wall was designed according to the AASHTO 2012 LRFD code and completed in two phases. Phase 1 consisted of constructing the MSE wall to a height of 15 feet and testing select piles. At the completion of testing, Phase 2 began by resuming the wall construction to a final height of 20 feet and running similar testing as that in phase one. The elevation view for both phases is shown in Figure 3-5.

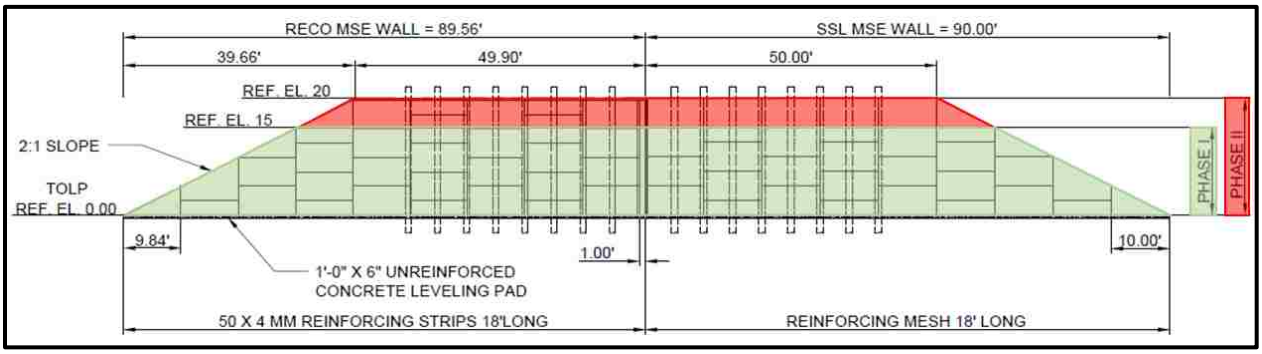

Figure 3-5: Elevation view of the MSE wall highlighting different phases of construction.

The MSE wall was constructed by Hadco, Inc. using two different wall systems. The eastern half of the wall consists of 50 feet of main wall and 40 feet of wing wall and was built using the SSL wall system. The SSL wall system consists of 5'x10' reinforced concrete panels with textured facings (see Figure 3-7) and 18-foot long galvanized steel welded-wire grid soil reinforcements. Reinforcements are attached to 0.75-inch loops in the wall by two W30 connector pins as shown in Figure 3-6. Reinforcements are spaced every 30 inches vertically and approximately every 60 inches horizontally. The number of longitudinal wires and horizontal spacing in the reinforcement changes based on the reinforcement layer as shown in Table 3-2.

Table 3-2: Design details for the welded-wire grid reinforcement based on location from top of wall.

Grid Layer (From Top of Wall)	Depth From Top of Wall (in)	Longitudinal Wire			Horizontal Wire	
		Number	Size	Spacing (in)	Size	Spacing (in)
1	15	6	W11	8	W11	6
2	45	5	W11	8	W11	12
3	75	5	W11	8	W11	12
4	105	5	W11	8	W11	12
5	135	5	W11	8	W11	12
6	165	6	W11	8	W11	12
7	195	6	W11	8	W11	12
8	225	6	W11	8	W11	12

*W11 wire has a diameter of 0.374 in.

Figure 3-6: Welded-wire grid reinforcement connected to wall loops by W30 pin connectors.

The western half of the wall entails 50 feet of main wall and 40 feet of wing wall and was built using the Reinforced Earth Company (RECO) wall system. The RECO wall system is comprised of 5'x10' reinforced concrete panels with smooth facings (see Figure 3-7) and 18-foot galvanized steel ribbed strip soil reinforcements connected to the wall panel with bolts, as shown in Figure 3-9. Plan views for both wall systems are shown in Figure 3-10. A complete set of the SSL wall plans are included in Appendix B for reference.

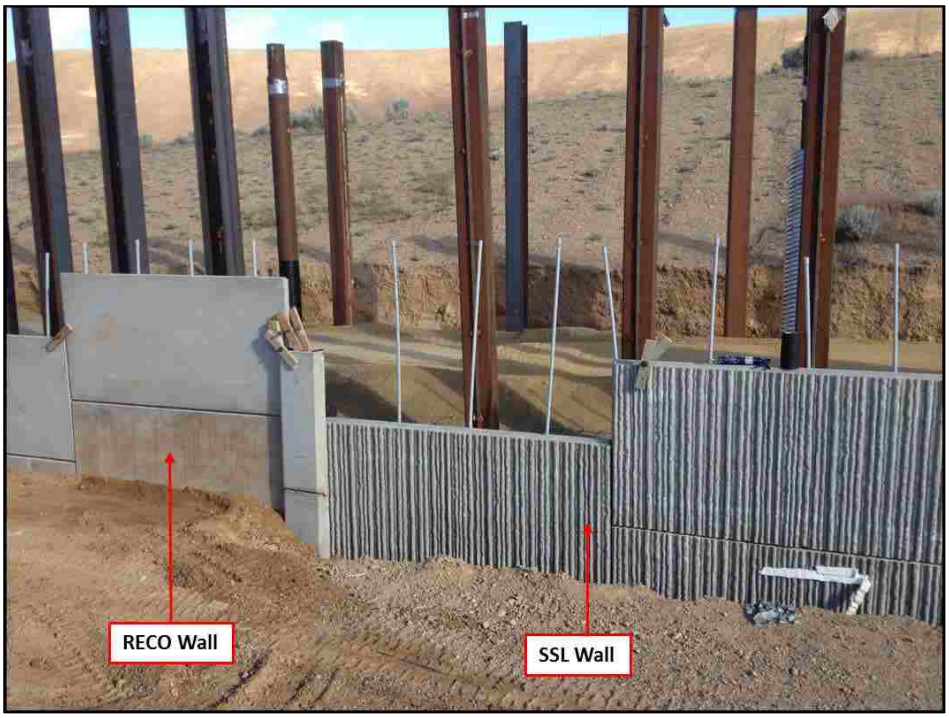

Figure 3-7: Different wall systems used for this project.

Figure 3-8: SSL galvanized steel welded-wire grid soil reinforcing layout with test piles.

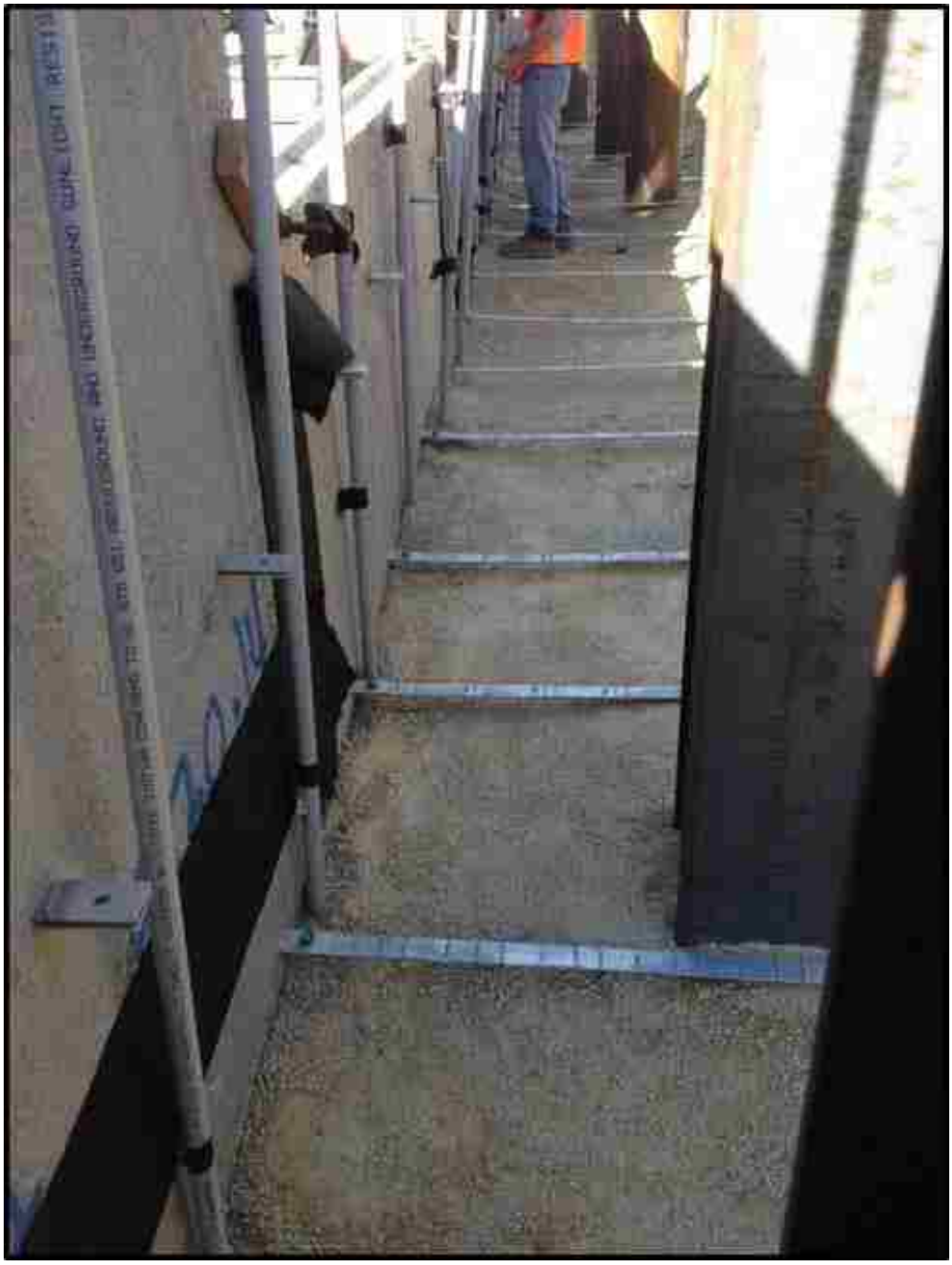

Figure 3-9: RECO steel ribbed strip soil reinforcing set up.

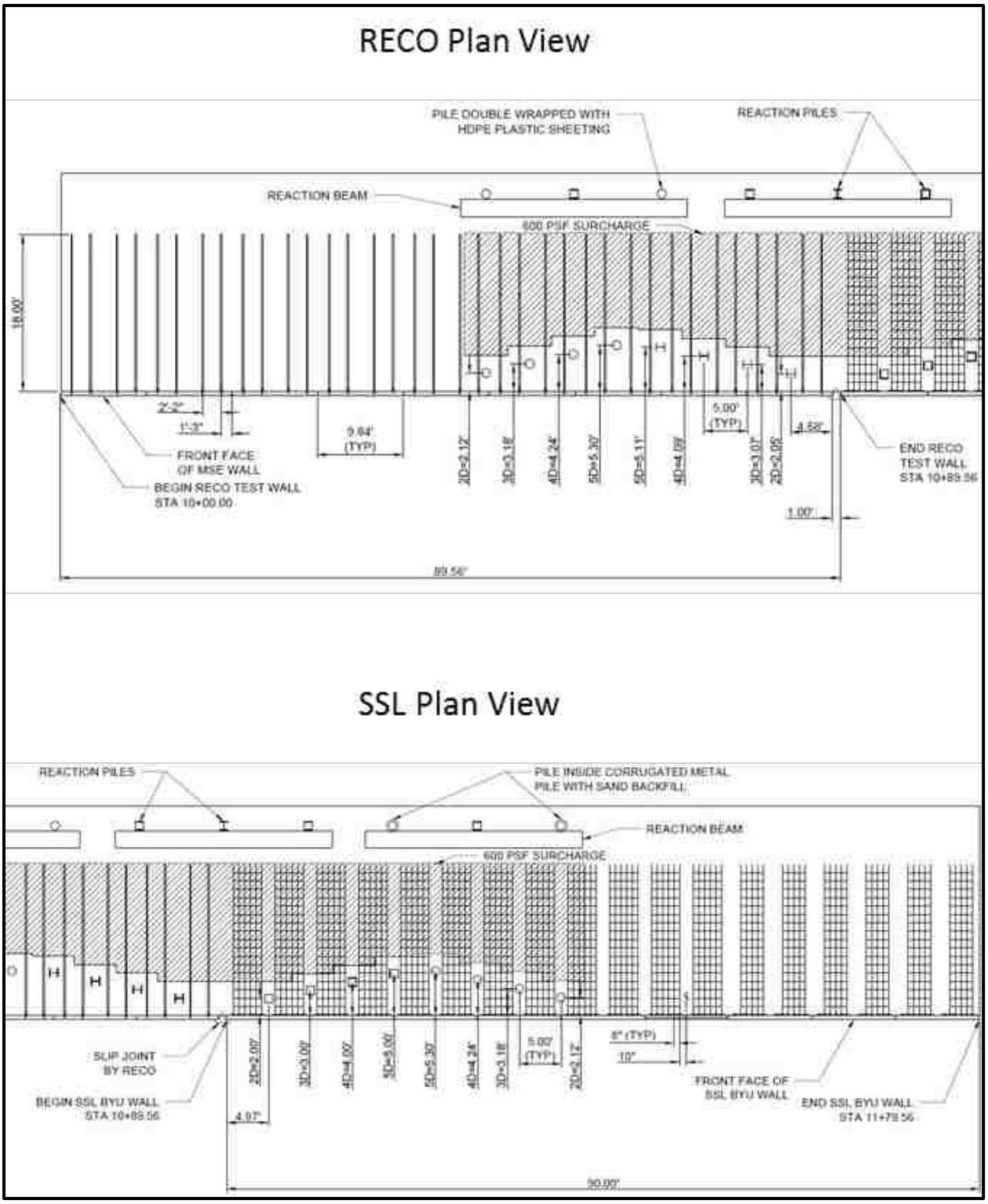

Figure 3-10: Plan view of the project.

3.3.1 Backfill

After the initial row of wall panels were leveled and installed, backfill was placed in 12-inch lifts behind the test piles as shown in Figure 3-11, and in 6-inch lifts between the test piles and the back of the wall. Prior to compaction, the backfill was moisture conditioned (see Figure 3-11) within 2 percent of optimum as determined by the Standard Proctor test.

Figure 3-11: (a) Backfill lifts behind test piles; (b) moisture conditioning of backfill.

Each lift was compacted using a vibratory roller compactor behind the test piles (see Figure 3-12), a vibratory plate compactor between the test piles and the back of wall, and a jumping jack compactor directly around test piles behind the reinforced zone as shown in Figure 3-13. After compaction of each lift, a nuclear density gauge, as shown in Figure 3-14, was used to obtain unit weights and moisture contents of the backfill to ensure consistent compaction.

Figure 3-12: Compaction of backfill behind the test piles using a vibratory roller compactor.

Figure 3-13: Compaction of backfill between the test piles and the back of wall using jumping jack and vibratory plate compactors.

Figure 3-14: Density and moisture testing of backfill using a nuclear density gauge.

Geneva Rock provided the backfill, which was classified as AASHTO A-1-a material and as a silty sand with gravel (SP-SM) according to the Unified Soil Classification System (USCS). The backfill for Phase 1 had a standard proctor density of 128.0 pcf and an optimum moisture content of 7.8%. The backfill for Phase 2 had a standard proctor density of 126.7 pcf and a calculated optimum moisture content of 9.7%. Test results of the backfill properties are included in Appendix C. The target density for the compacted backfill was 95% of standard proctor. Actual average moisture contents were 6.0% behind the test piles and 5.2% between the test piles and the back of wall, as shown in Figure 3-15. The actual average relative compaction of the backfill was approximately 96% in the fill behind the test piles and approximately 92% between the test piles and back of wall, as shown in Figure 3-16. Lower compaction between the wall and piles is typical in normal MSE wall construction because it is difficult to get compaction in small or confined areas and heavy compaction is likely to displace the wall panels laterally. Compacted backfill properties are shown in Table 3-3 and Table 3-4 and also include the standard deviation and coefficient of variation for each data set.

Table 3-3: Backfill properties between test piles and back of MSE wall.

	Moisture Content [%]	Dry Unit Weight [pcf]	Moist Unit Weight [pcf]	Relative Compaction [%]
Average	5.2	116.7	122.8	91.8
Standard Deviation	1.58	3.22	3.76	2.78
Coefficient of Variation	0.303	0.028	0.031	0.030

Table 3-4: Backfill properties behind the test piles.

	Moisture Content [%]	Dry Unit Weight [pcf]	Moist Unit Weight [pcf]	Relative Compaction [%]
Average	6.0	122.8	130.1	96.4
Standard Deviation	1.66	2.64	3.14	2.32
Coefficient of Variation	0.276	0.021	0.024	0.024

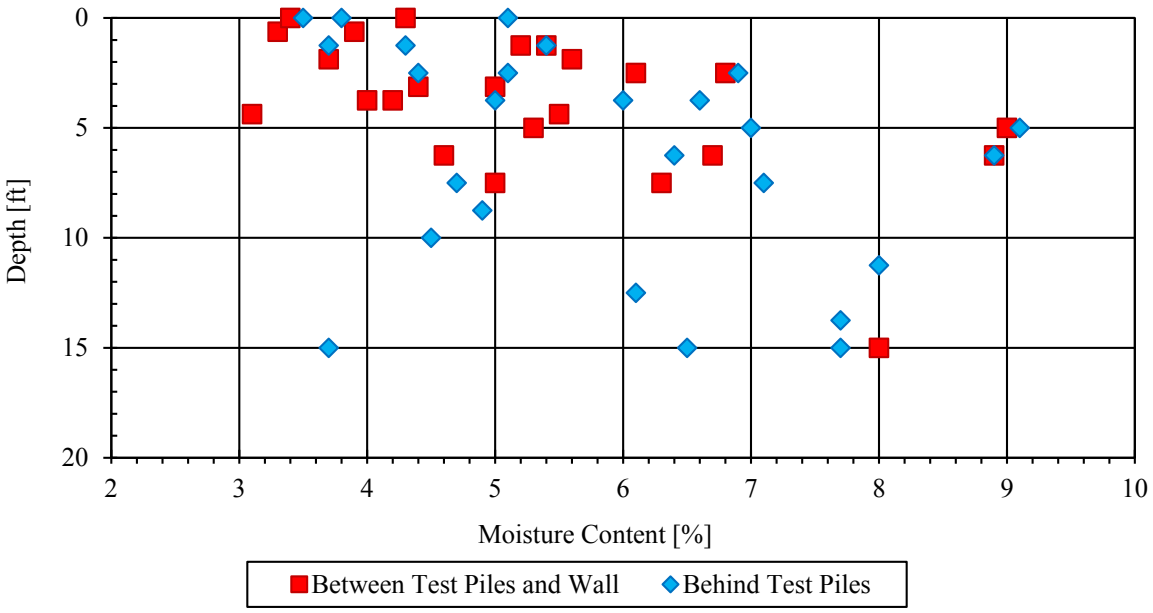

Figure 3-15: Measured moisture content of backfill.

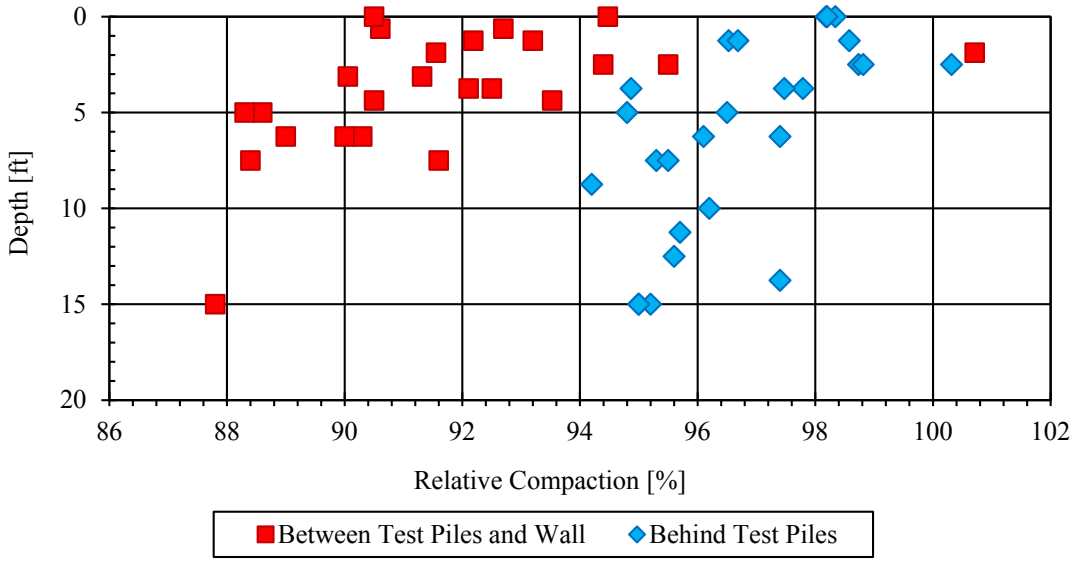

Figure 3-16: Measured relative compaction of backfill.

3.3.2 Surcharge

Prior to pile load testing, concrete blocks with dimensions of 2'x2'x6' were placed on either side of the test pile and load apparatus to induce a surcharge load representative of the weight of the abutment and approach fill at a typical bridge abutment. The concrete blocks were typically placed 3 blocks wide, 2 blocks high and 2 blocks deep as shown in Figure 3-17. The area of surcharge covered approximately 12 feet directly behind the pile and approximately 6 feet to either side perpendicular to the load apparatus with a gap approximately one foot wide to accommodate the loading strut. The surcharge created by the concrete blocks simulates a portion of the abutment wall and backfill about 5 ft high with an overall unit weight of 120 pcf.

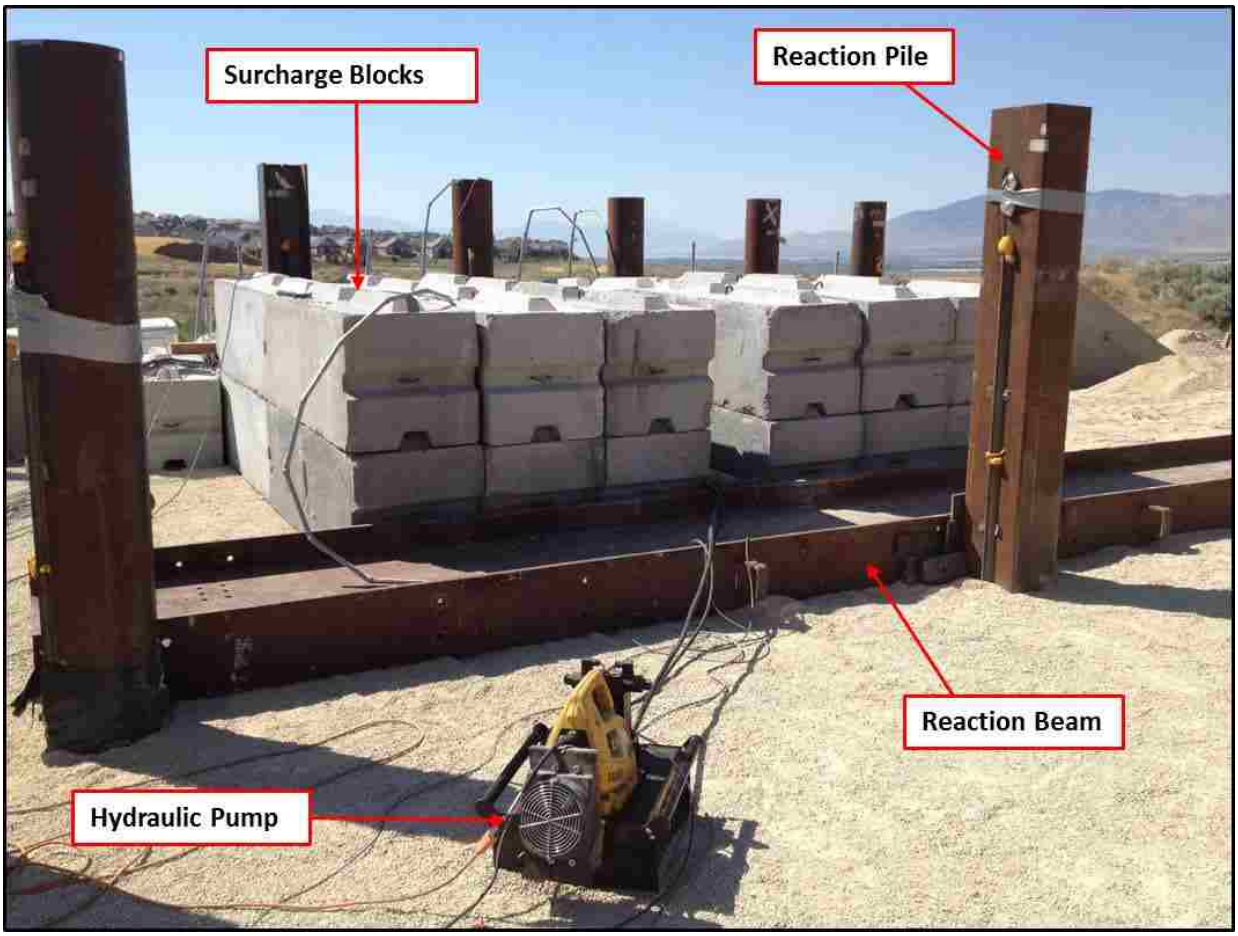

Figure 3-17: Typical set up for pile load testing.

3.4 Loading System

As mentioned in section 3.2, piles were installed behind the reinforced earth mass to support the reaction beam during load testing of the piles as shown in Figure 3-17. Therefore, the load applied to the test pile did not influence the load in the reinforcements. A load apparatus was then set in place to connect the test pile with the reaction beam. The apparatus, beginning closest to the test pile, consisted of an inline load cell, a hydraulic jack and steel strut as shown in Figure 3-18.

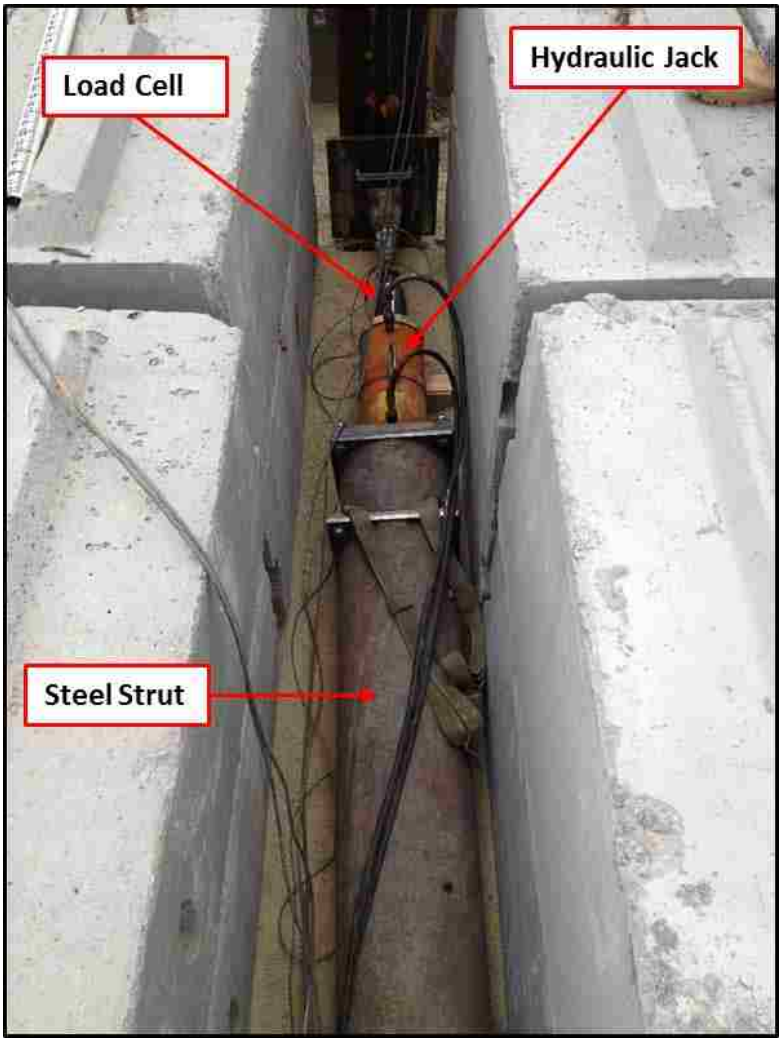

Figure 3-18: Load apparatus configuration.

Each test pile had a steel C-channel welded to the pile at approximately one foot above the ground surface which allowed for a flat surface to apply the load. The C-channel was connected with an inline load cell, which was attached to the hydraulic jack. A hydraulic pump, as seen in Figure 3-17, was also attached to the hydraulic jack via hydraulic hoses to regulate load pressures. Both a pressure transducer on the hydraulic pump and inline load cell were used to measure loading throughout the testing of the pile. Any remaining space between the hydraulic jack and the reaction beam was filled with steel struts and steel plates.

4 INSTRUMENTATION

A variety of instruments were used at each test pile to measure the applied load, deflection, strain and rotation on the pile as well as wall deflection, ground displacement and strain in the soil reinforcements. This chapter discusses the layout and instruments used to obtain data on this project.

4.1 Load Cell and Pressure Transducers

An in-inline load cell and pressure transducer were used to measure the applied load on the pile. The load cell was located between the pile and the hydraulic jack. The pressure transducer was attached to the hydraulic pump. Readings for the pressure transducer and load cell were collected at a rate of 2 readings per second by an Optima Electronics Corp. MEGADAC 5414AC (MEGADAC) data collector. Although loads from both instruments were recorded, they did not correlate with one another. Lab testing verified that the load cell was giving erroneous readings, most likely due to eccentric loading. As a result, the data collected from the pressure transducer was used for the data analyses for each pile discussed in this report.

4.2 String Potentiometers

String potentiometers were used to measure pile head displacement and rotation, wall displacement and horizontal ground displacement. Data from the string potentiometers was collected at a rate of 2 readings per second and stored in the MEGADAC data collector.

As shown in Figure 4-1, string potentiometers were attached to a 2x4 that was clamped to a wooden 4x4 independent reference beam. The reference beam was strapped on each end to stationary concrete blocks that were located outside of the testing area of influence (typically > 6 feet from the test pile). Pile head deflection was measured by connecting a string potentiometer to an eyebolt that was magnetically attached to the side of the pile at the same elevation as the applied load. Another string potentiometer was connected to an eyebolt 3 feet above the first by clamping a 2x4 to the side of the pile. Pile head rotation was calculated by taking the difference of the pile head deflections at the load point and 3 feet above the load point and using trigonometry to find the angle at which the pile head was rotated.

Horizontal ground displacement was measured by connecting string potentiometers to steel stakes that were driven into the ground as shown in Figure 4-2. Stakes were typically spaced at 1-foot intervals from the front face of the pile. Horizontal displacement was measured by taking the difference of the initial and measured values recorded from the string potentiometers. Wall displacement was measured by installing an eyehook into the top of the concrete wall panel directly in front of the pile and connecting a string potentiometer to the eyehook. The difference of the initial and measured values were taken to find the wall displacement at any given load.

Vertical ground displacement was measured using a survey level and rod. Elevation measurements of the ground surface were taken before and after the pile load tests at 1-foot intervals from the pile face.

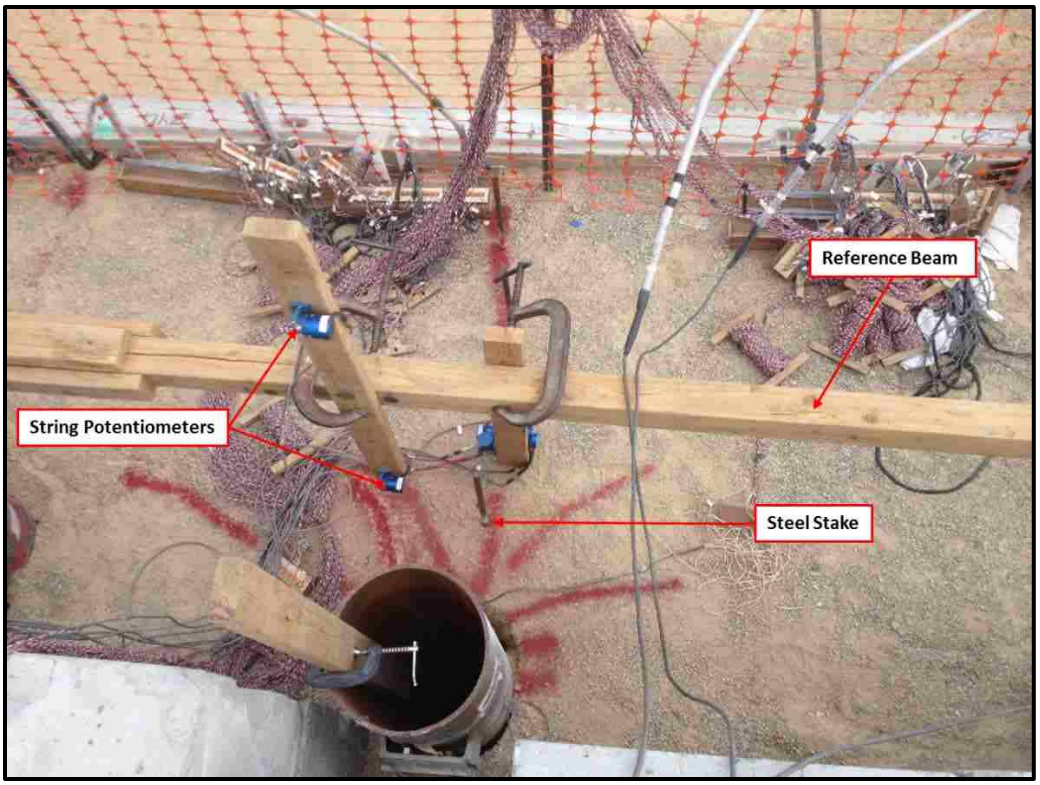

Figure 4-1: Instrumentation setup of a typical pile load test.

Figure 4-2: Horizontal ground displacement setup.

4.3 Strain Gauges

Strain gauges were installed on the soil reinforcing and test piles to determine tensile force and bending moment, respectively. The following two sections discuss the installation and configuration of the strain gauges to the soil reinforcement and piles, respectively.

4.3.1 Soil Reinforcement Strain Gauges

Electrical resistance strain gauges were installed on the welded-wire grids at BYU facilities prior to shipping them to the project site. Strain gauges were placed on the second longitudinal wire from the right, as shown in Figure 4-3, at increments of 0.5, 2, 3, 5, 8, 11, and 14 feet from the back of the wall face. To minimize bending effects, a strain gauge was placed on the top and bottom of the longitudinal bar at each distance interval. The strain gauges were attached with epoxy and protected by wrapping the lead wires in electrical tape and securing them to the sides of the longitudinal bar as shown in Figure 4-3. To minimize damage, the lead wires were run through a PVC conduit attached vertically to the back face of the wall panel and connected to terminal strips at the ground surface, as shown in Figure 4-4. The terminal strips were directly connected to the MEGADAC data collector during pile testing.

The top 4 layers of soil reinforcing were instrumented with strain gauges. Each layer had one grid on each side of the test pile that was connected to the data collector during pile load testing. Table 4-1 shows the soil reinforcement configuration for each test pile.

Figure 4-3: Typical strain gauge setup for a welded-wire grid layer.

Figure 4-4: Strain gauge connections to terminal strips.

Table 4-1: Transverse distance from pile center to instrumented longitudinal bar on the reinforcing (looking in the direction of loading (South).

	Layer Depth (in)							
	15		45		75		105	
Test	Left	Right	Left	Right	Left	Right	Left	Right
1.8D	17.5	42	-	43	22	43	17	35
3.4D	24.5	43	23	37.5	23	38	31	38
4.3D	17.5	40.5	18.5	33.5	17.5	34.5	19	34
5.2D	15	46.5	22.5	38.5	21.5	46	23	39

* The grid left of the 1.81D pile in Layer 2 was not instrumented.

4.3.2 Pile Strain Gauges

Waterproof electrical resistance strain gauges were installed on the test piles prior to shipping them to the project site. Strain gauges were placed on each side of the pile for redundancy at depths of 4, 6, 8, 11, 14, 17 and 20 feet below the top of the pile, or 2, 4, 6, 9, 12, 15 and 18 feet below the load point. The strain gauges were attached with epoxy and further protected from the elements by spraying foam insulation around the gauges and wires, then covering them with angle iron. The angle iron was tack welded onto the pile between strain gauge locations and acted as protection during pile driving (see Figure 4-5). Lead wires were bundled in bags and taped near the top of the pile for transportation and pile driving. Wires that were sheared or damaged prior to testing were repaired to the extent possible. However, some strain gauges were inevitably bad or malfunctioning and were removed from calculations during the data analyses. The pile strain gauges were connected to terminal strips, as shown in Figure 4-5, which directly connected to the MEGADAC data collector during testing of the piles.

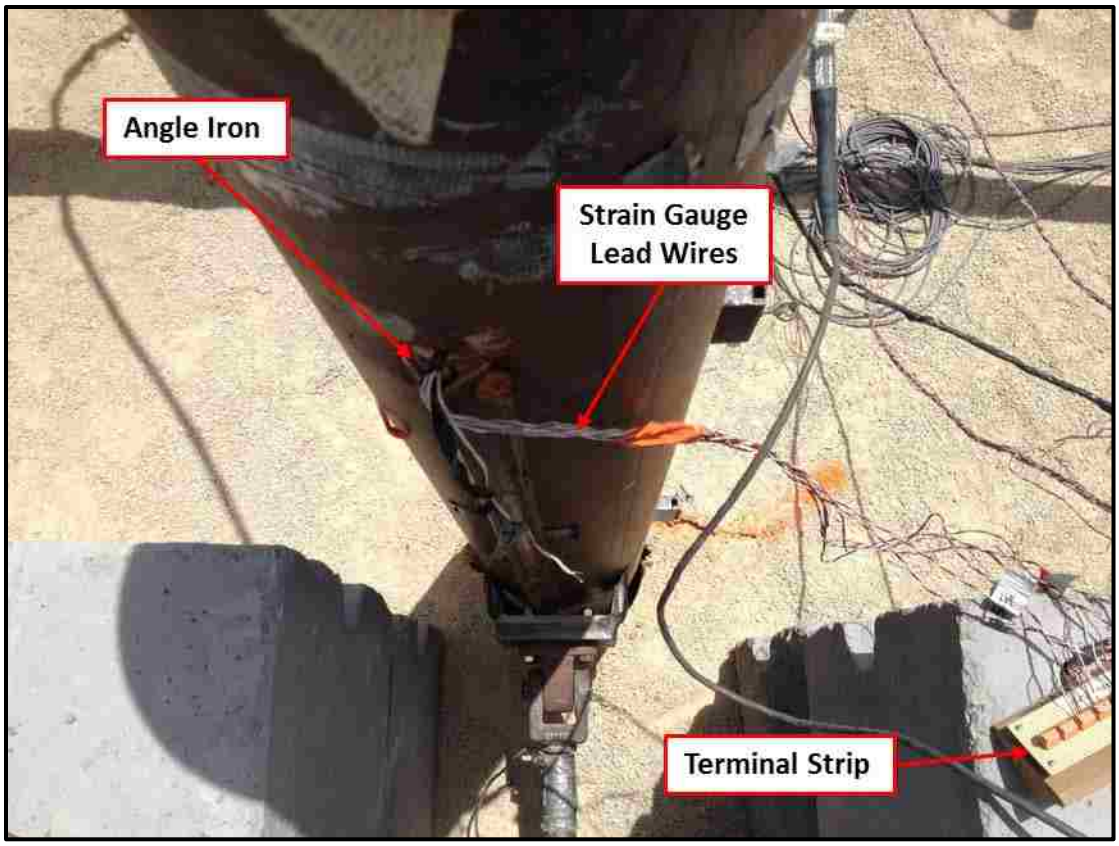

Figure 4-5: Typical pile instrumentation setup.

4.4 Shape Arrays

Four high-bandwidth Measurand® Shape Accel Arrays (Shape Arrays) were used on this project to measure horizontal wall deflection. Shape Arrays are similar to inclinometers but can measure much larger deformations and have the ability to be placed horizontally to measure vertical deformation. They are designed to collect high frequency data from all sensors continuously. The outer shell of a Shape Array consists of two layers of braided stainless steel which provide twist resistance and pull strength.

Prior to testing, the Shape Arrays were calibrated at BYU and transported to the test site. The Shape Arrays were placed inside 1.05-inch inside-diameter PVC conduit which had previously been installed vertically on the back of the wall panels. Generally, four vertical arrays were

installed for each test. One array was installed approximately in front of the test pile while the others were spaced at varying distances to the side, as shown in Table 4-2. Each Shape Array consists of 24 segments that are each 1-foot long. Each foot-long segment is connected by joints and contains 3 MEMS accelerometers which measure tilt along the x, y and z axes. During testing, the accelerometers continuously send signals to the computer running Measurand SAA Recorder software. Typically, two sets of data were collected at each load deflection interval.

Table 4-2: Transverse distance (in inches) from the center of pile to the Shape Array.

	Array Number			
Test	**45104**	**45112**	**45115**	**45134**
1.8D	32.5	5	38	56.5
3.4D	34	72	105	10
4.3D	51	26	11	7
5.2D	92	6	34	62

4.5 Digital Imagery Correlation

Digital Image Correlation (DIC) is a 3D, full-field optical system that can measure deformation and strain on most materials. DIC was proposed in the early 1980s for solid mechanics applications and many of the procedures used today are direct results of early development in fluid mechanics (Hild). Tests can be applied to large or small areas and can be compared with other testing methods for accuracy (Measurement Principles of DIC). Hundreds to thousands of visible points are placed on an object and allow cameras to identify specific locations throughout the test period. During image evaluation, the images are divided into small local facets as shown in Figure 4-6. The position of the cameras in relation to one another is calculated when the system is calibrated and pixels within each facet are tracked. This information allows a correlation algorithm to be used to calculate the three dimensional position of each point from which contours of

displacement, deformation, and strain on the wall can be determined. The system is sensitive to measurements down to 1/100,000 of the field of view (Measurement Principles of DIC).

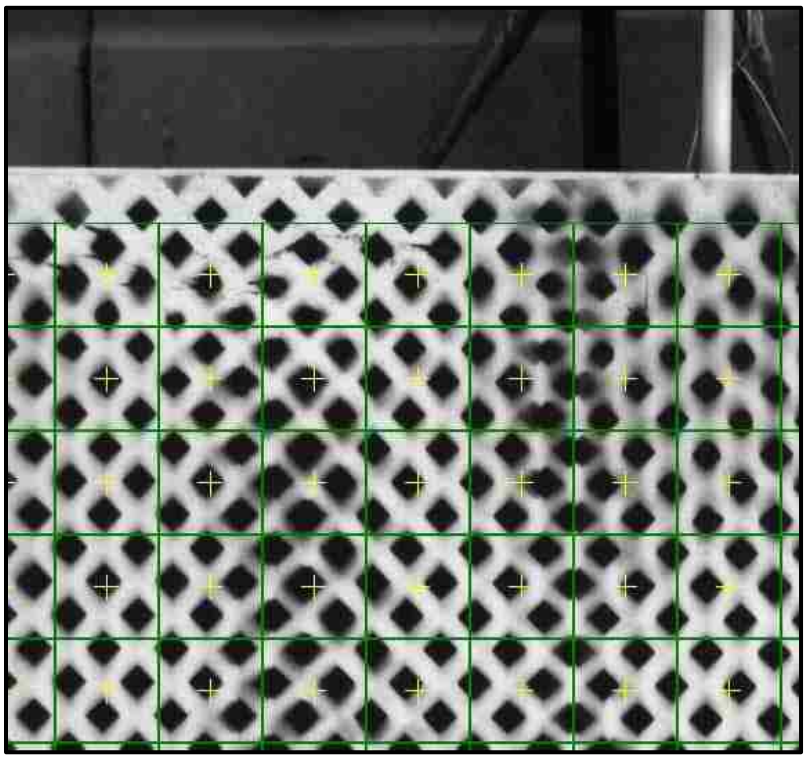

Figure 4-6: Example of facets in the DIC evaluation process.

The system setup for this project was the Q-400 DIC Standard 3D manufactured by Dantec Dynamics and included two cameras on a tripod connected to a computer running ISTRA-4D software, version 4.4.1, as shown in Figure 4-7. A black and white grid pattern was painted onto the wall surface to increase contrast and to make up the visible points required by the DIC system. Prior to load testing, the system was calibrated using a black and white checkered board. This required taking multiple images of the board at different angles at a distance similar to that during testing. Camera angle, shutter speed and focus were all adjusted during the calibration process.

Cameras were spaced approximately 25 feet from the wall face and centered on the test pile. Video images were typically focused on a 10-ft-high by 12-ft-wide area near the top of the wall.

During pile load testing, images were captured directly after and 5 minutes after each pile load increment. A total of 25 to 30 images were taken for each pile load test. Images were later evaluated using the ISTRA-4D software to determine wall deflection and provide contours of deflection.

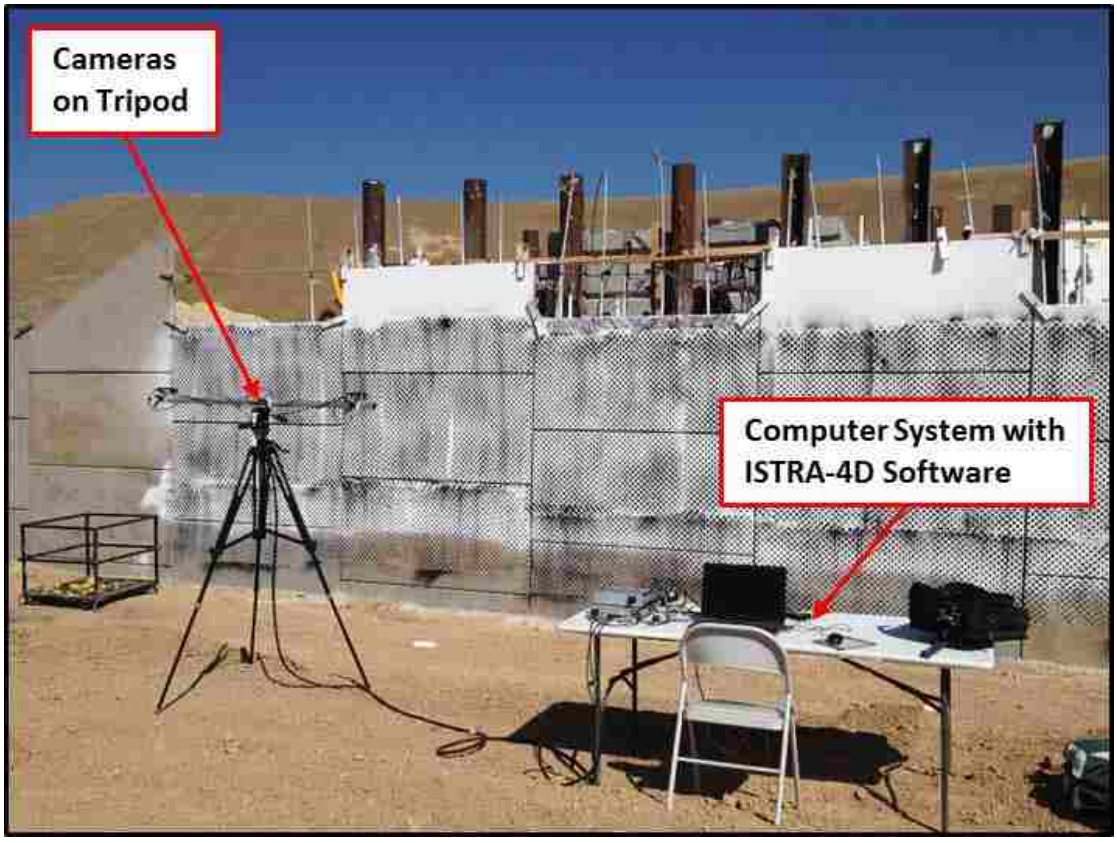

Figure 4-7: Typical DIC test setup.

5 LATERAL LOAD TESTING

Lateral load testing of the round piles adjacent to the 20-foot tall MSE wall with welded-wire reinforcement took place between August 7 and August 11, 2014. Prior to loading the four test piles, a reaction pile located outside of the reinforced mass but still within the compacted backfill was tested parallel to the MSE wall and used as a reference for the 5D pile. Testing was performed on all piles using a displacement control method in which load was applied to induce pile head deflection in 0.25-inch increments. Load was applied at a height of one foot above the ground surface and each pile was loaded up to a maximum of 3 inches of displacement. At each displacement increment fluid flow into the jack was locked off for 5 minutes while the pile load and deflection came to equilibrium. Readings were taken at the peak load, the 1-minute hold and the 5-minute hold. Typically, pile head load decreased rapidly from the peak load to the 1-minute hold then decreased very slowly to the 5-minute hold while deflection remained relatively constant. The peak load is most likely to simulate rapid loading such as that produced by earthquakes while the 1-minute and 5-minute holds are more demonstrative of static loading conditions.

5.1 Load Displacement Curves

Load displacement curves for the four test piles near the MSE wall and the companion test pile or “reaction pile” away from the wall are shown in Figure 5-1 through Figure 5-3 for the peak

load, the 1-minute hold and the 5-minute hold, respectively. Loads were measured using a pressure gauge on the hydraulic pump. Deflections were measured using the string potentiometer attached to the pile at the load elevation and connected to an independent reference frame. The measured load-deflection curve for the 1-minute and 5-minute holds were obtained by averaging the 30 seconds of load right after the hold interval. Load-deflection curves for individual test piles of the average peak, 1-minute hold and 5-minute hold are located in Appendix D for reference.

The load-deflection curves shown in these figures indicate that the lateral resistance generally decreases as the distance between the pile and wall decreases. The reaction pile and the 5.2D pile should in theory have similar load-deflection curves. However, the 5.2D pile has approximately 73% of the resistance of the reaction pile. This is most likely due to the compaction differences between the two piles. The backfill around the reaction pile was compacted with a roller compacter and had an average relative compaction of 96.4%, whereas the backfill between the 5.2D pile and the wall was compacted with a vibratory plate compacter and had an average relative compaction of 91.8% (see Table 3-3 and Table 3-4). Lower pile loads on the 4.3D test were likely caused because the hydraulic pump was malfunctioning for the first half of the test. Once the pump was fixed, the pile was reloaded to 1.5 inches of deflection because it is difficult to reapply load and get virgin load-deflection responses. Loads from 0 to 1.5 inches of deflection were recorded much lower than what was actually produced. Therefore, load points between 1.0 to 1.5 inches of deflection were interpolated and manually adjusted, but all points between 0 and 1.5 inches of deflection are likely still lower than actual loads induced on the pile. Corrections to 4.3D are addressed further in Chapter 6.

Generally, the 5.2D and 4.3D piles develop very similar lateral resistance for a given deflection suggesting that neither pile is significantly affected by the presence of the wall or that the reinforcements are retaining the soil sufficiently so that lateral resistance is not reduced at these larger pile spacings. However, for the piles spaced at 3.4D and 1.8D the lateral resistance typically decreases by 21% and 51%, respectively, relative to the pile at 5.2D spacing. In general, the average decrease in lateral resistance at 3 inches of deflection from peak load to 1-minute and 5-minute holds is 7% and 10%, respectively.

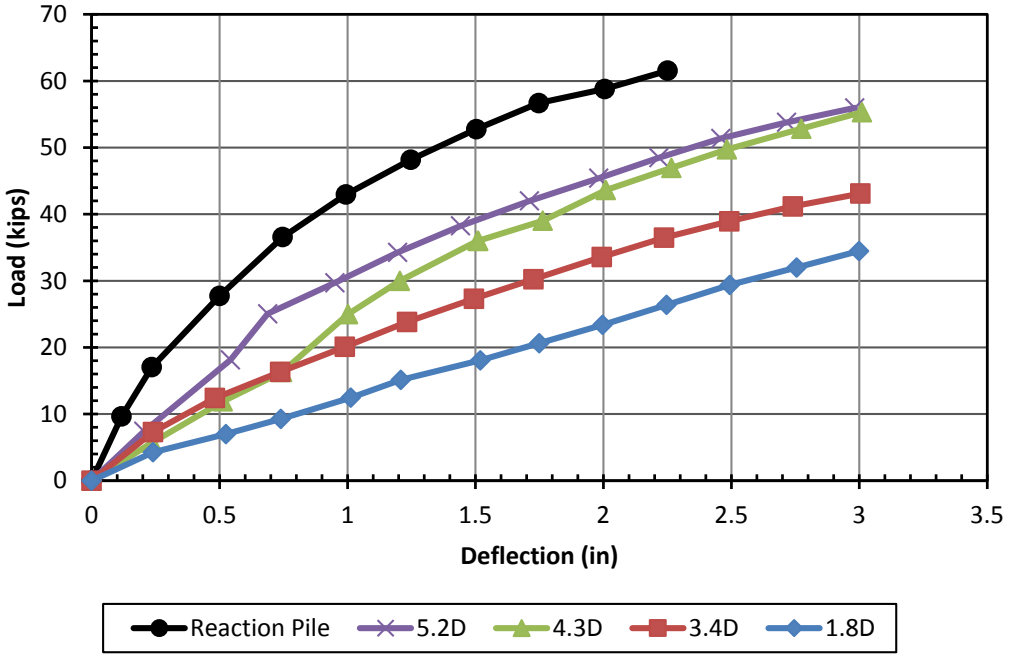

Figure 5-1: Pile head load versus pile head deflection for the average peak load.

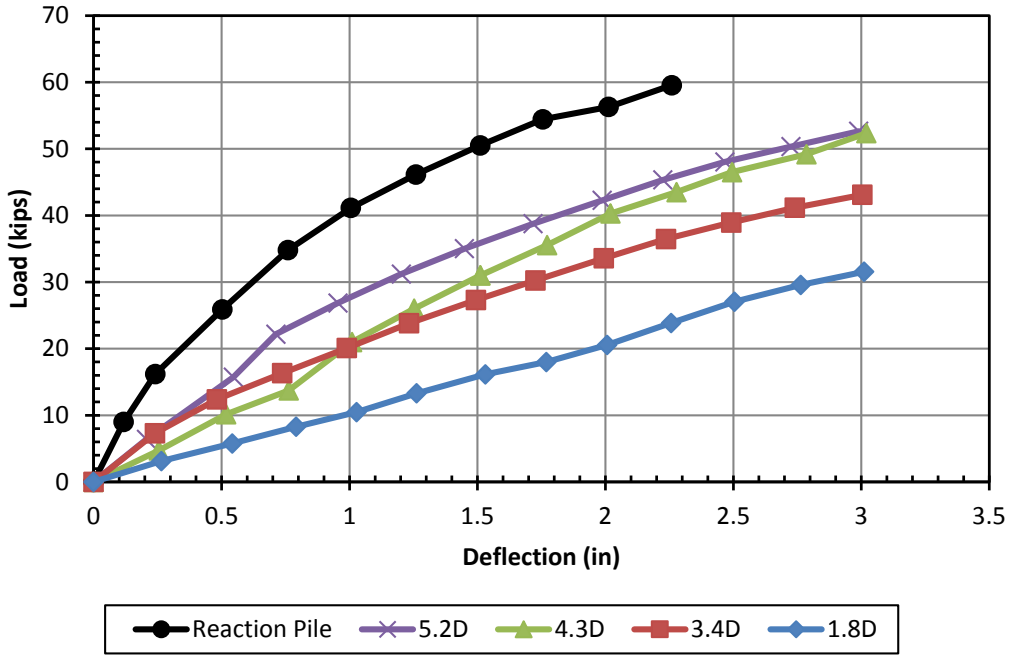

Figure 5-2: Pile head load versus pile head deflection for the 1-minute hold.

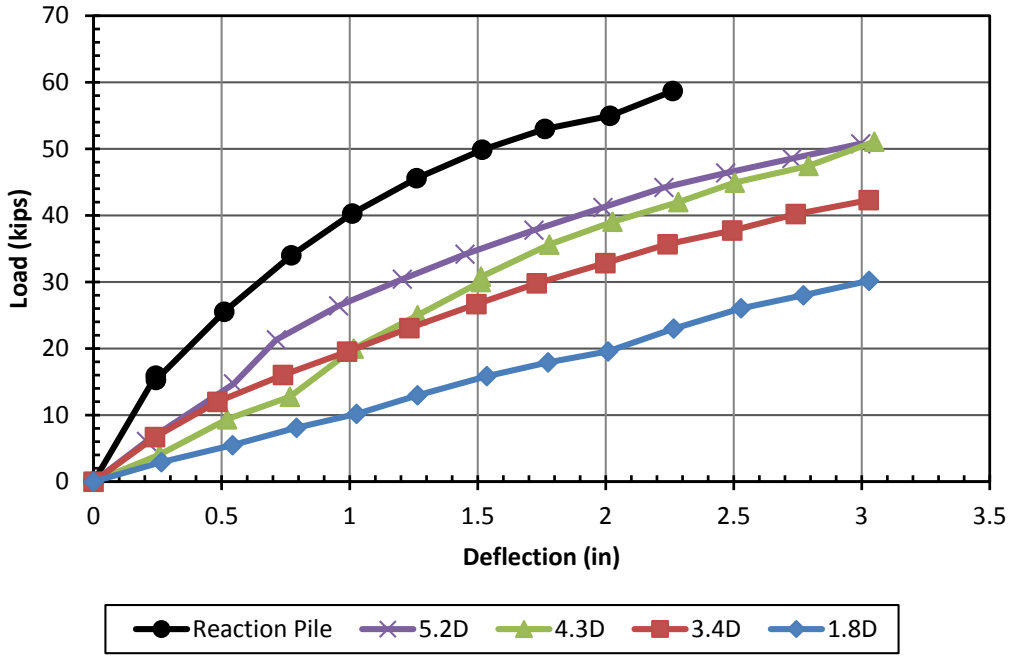

Figure 5-3: Pile head load versus pile head deflection for the 5-minute hold.

5.2 Pile Head Rotation

Pile head load versus pile head rotation for each test pile is shown in Figure 5-4. Pile head rotation, θ, in degrees was calculated using the equation:

$$\boldsymbol{\theta = sin^{-1}\left(\frac{d_{3ft} - d_{lp}}{36\ in}\right)} \quad \textbf{(5-5)}$$

where

θ is the pile head rotation,

d_{3ft} is the pile displacement 3 feet above the load point, and

d_{lp} is the pile displacement at the load point.

String potentiometer measurements and pile head loads were taken at the one-minute hold reading for each pile. As would be expected, the pile head rotation increases as the pile head load increases for each test pile. Typically, for a given load, the pile head rotation increases as the pile spacing decreases. This is most likely because the soil resistance decreases as the pile spacing decreases allowing the pile greater resistance to bending. As discussed previously, the 4.3D pile test experienced a loss of power to the hydraulic jack during testing and certain data points read very low and were adjusted based on other data points for that test and the typical curve from other test piles. At larger deflections, the load-rotation curves for the 4.3D pile is similar to that for the 5.2D pile as was the case for the load-deflection curves discussed previously. This result again suggests that there is little variation in lateral soil resistance for these two piles.

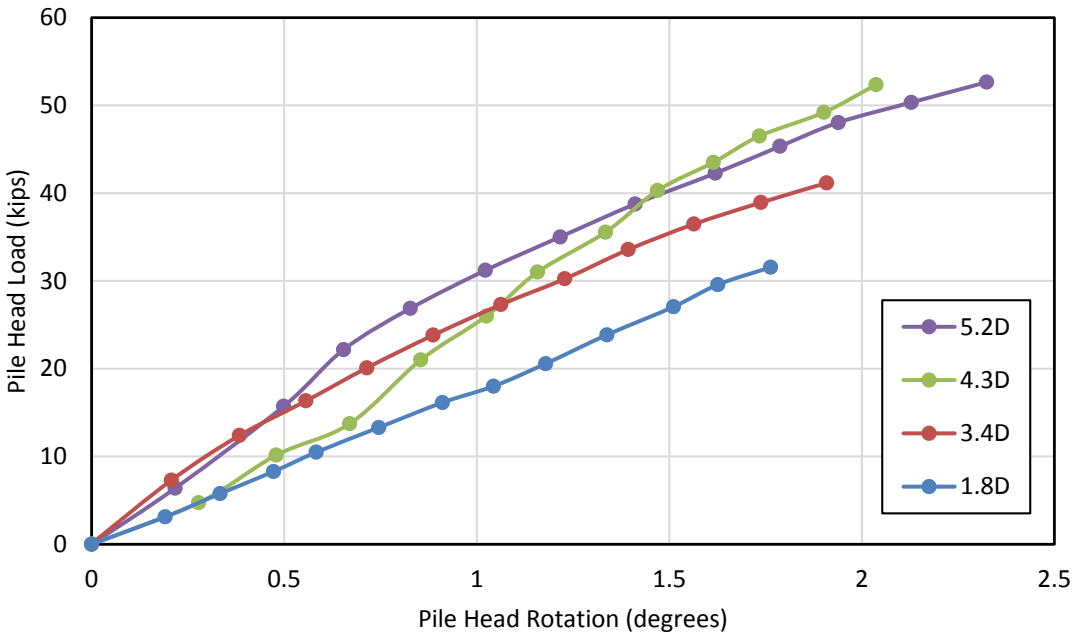

Figure 5-4: Pile head load versus pile head rotation for each test pile.

5.3 Soil Reinforcement Performance

As described previously, strain gauges were attached to the top and bottom of the welded-wire grid reinforcements and placed at intervals of 0.5, 2, 3, 5, 8, 11 and 14 feet from the back face of the wall (see section 4.3.1). The data collected from the strain gauges at each interval were averaged and used to calculate the load induced in the reinforcement. At certain intervals, one or sometimes both strain gauges were damaged or not working properly. For instances where only one gauge was working, that strain value was generally used in the calculations. When both strain gauges were damaged, the interval was omitted. Equation 5-1 was used to calculate the induced reinforcement load as follows:

$$T_i = EA(\mu\varepsilon_i - \mu\varepsilon_0)(10^{-6})B \quad \textbf{(5-1)}$$

where

T_i is the induced tension in kips for the entire welded-wire grid at the i^{th} data point,

E is the modulus of elasticity of the steel (29,000 ksi),

A is the cross-sectional area ($in.^2$) of the instrumented wire,

$\mu\varepsilon_i$ is the average micro strain for the i^{th} data point,

$\mu\varepsilon_0$ is the average initial micro strain, and

B = n-1 where n is the number of longitudinal bars on the reinforcement grid.

An example of the load distribution induced in the soil reinforcement behind the back of the MSE wall is shown in Figure 5-5 through Figure 5-8. Figure 5-5 and Figure 5-6 show tensile force distributions in layer L4 (approximately 105 inches below ground surface) during the lateral load test on the pile at 3.4D. These figures illustrate the similarities in the induced reinforcement loads when the transverse spacings (38 and 31 inches) are similar. Figure 5-7 and Figure 5-8 are of the 5.2D pile at layer L3 (approximately 75 inches below ground surface) measuring strain from a near and far transverse distance and illustrate the differences in the induced reinforcement loads when the transverse spacings (46 and 21.5 inches) vary. Typically, peak reinforcement loads increase as transverse spacings decrease. Figure 5-7 and Figure 5-8 also show that peak loads occur nearer to the pile face as transverse distance to the pile decreases, and farther in front of the pile face as the transverse distance increases. Because shear forces act to the side and front of the pile during loading, it makes sense that peak loads occur farther in front of the pile with increased transverse spacing of the reinforcement.

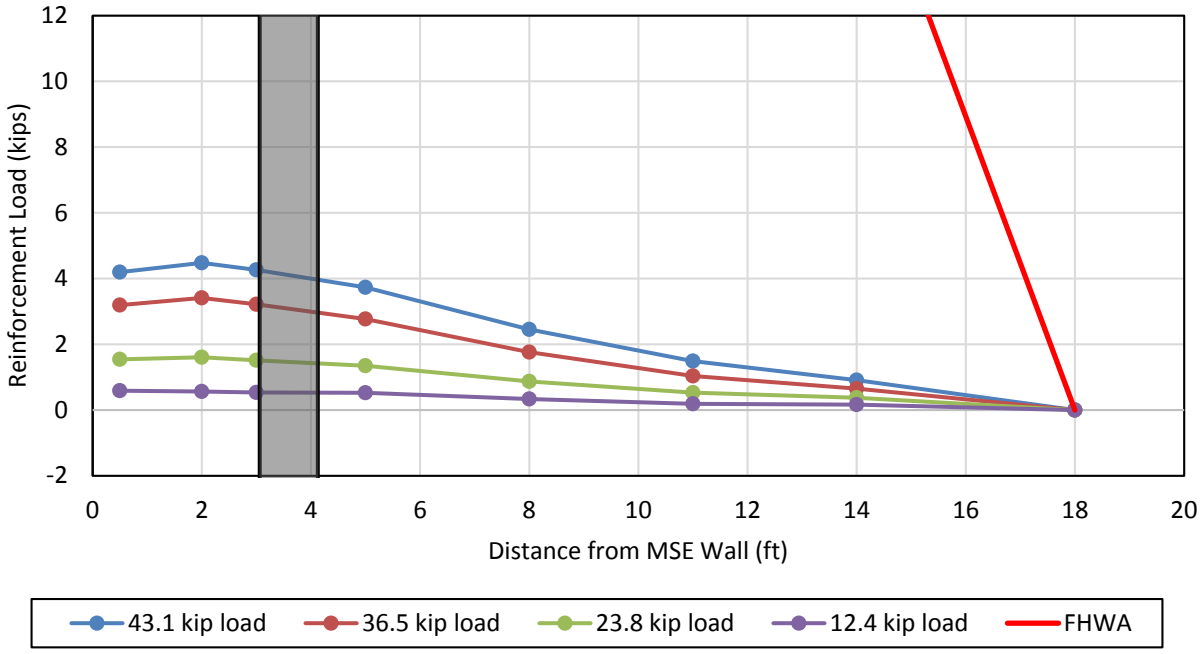

Figure 5-5: Induced loads in the soil reinforcement at different pile head loads relative to distance from the back of the MSE wall (3.4D pile, layer L4, 38 in. transverse spacing).

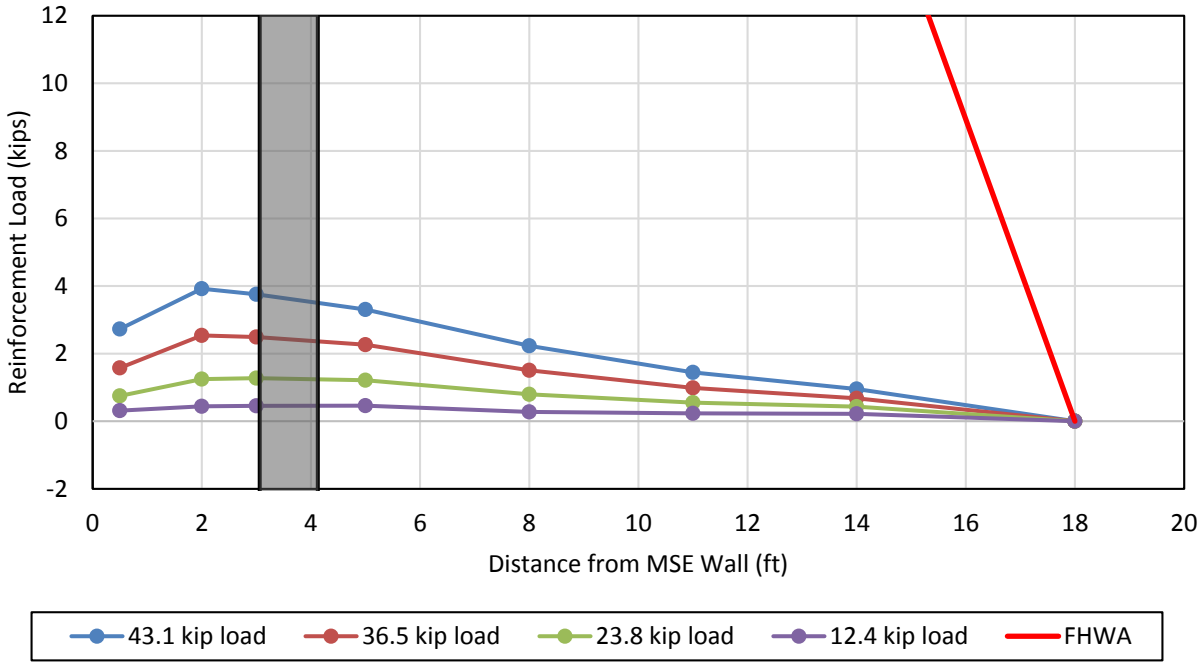

Figure 5-6: Induced loads in the soil reinforcement at different pile head loads relative to distance from the back of the MSE wall (3.4D pile, layer L4, 31 in. transverse spacing).

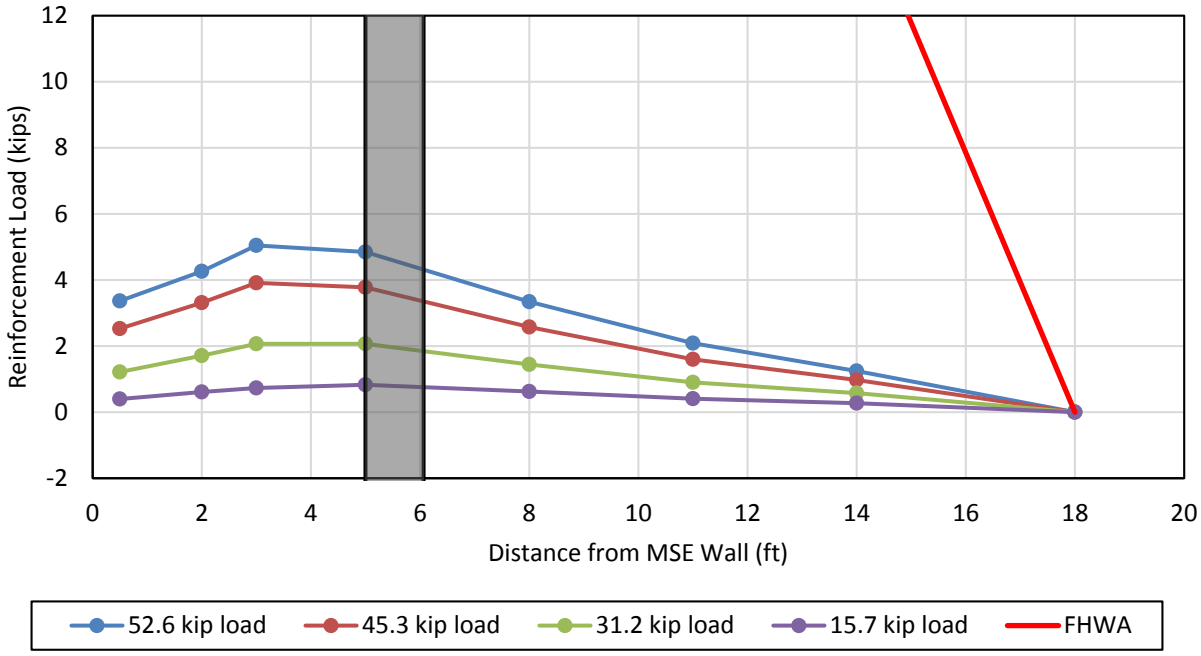

Figure 5-7: Induced loads in the soil reinforcement at different pile head loads relative to distance from the back of the MSE wall (5.2D pile, layer L3, 46 in. transverse spacing).

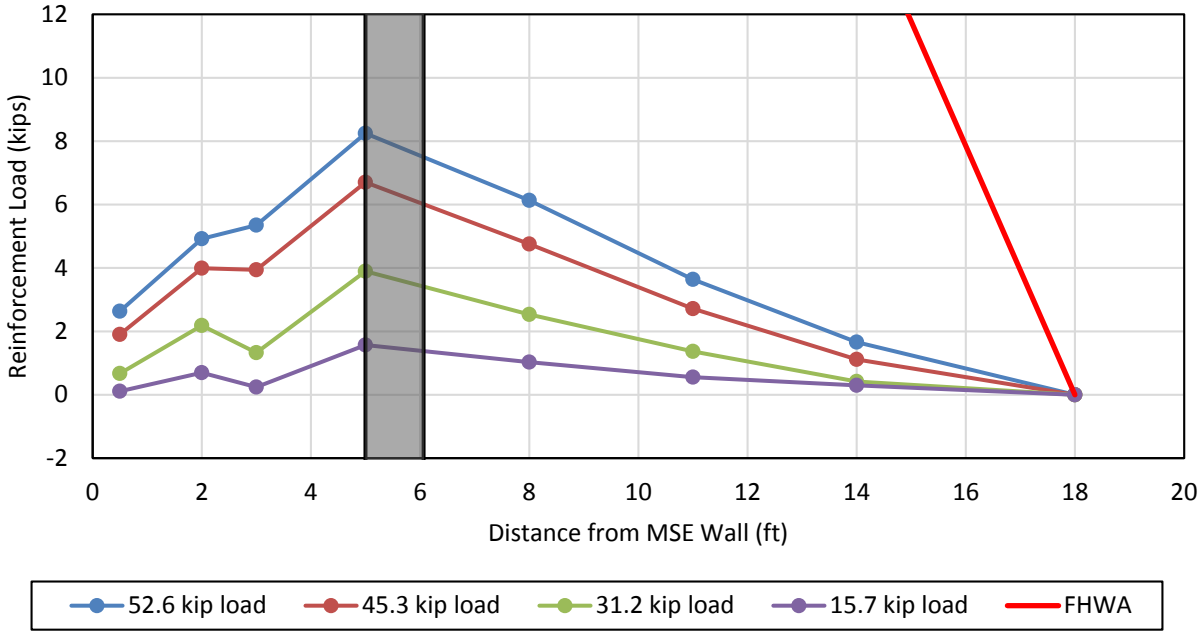

Figure 5-8: Induced loads in the soil reinforcement at different pile head loads relative to distance from the back of the MSE wall (5.2D pile, layer L3, 21.5 in. transverse spacing).

Each figure contains a red line defining the ultimate pull-out resistance from the FHWA equation (see section 2.1, Equation 2-4). It should also be noted that the pullout capacity of the welded-wire grids were designed for live surcharge loads, which increases the load factor on the demand, while no additional resistance is included from vertical stress. Calculating in this way increases the pullout resistance of the measured values. The calculated FHWA pullout resistance is much higher than the measured resistance, as shown in Figure 5-5 through Figure 5-8, which indicates that the pullout resistance of the reinforcement was nowhere near capacity. Induced reinforcement load plots for layers L1 through L4 for each test are located in Appendix F for reference.

Figure 5-9 depicts an idealized model of what is most likely occurring in the reinforcement. The model indicates that as the pile is loaded, the soil in front of the pile is being pushed toward the wall relative to the grid reinforcement causing skin friction on the reinforcement. The soil movement increases tension on the grid as the load is transferred from the soil to the reinforcement by skin friction. As the pile is loaded, the reinforcement behind the pile acts as an anchor as the grid moves toward the wall relative to the soil. Skin friction develops in the opposite direction leading to a decrease in tension in the reinforcement behind the pile as load is transferred to the surrounding soil by skin friction. This would cause the maximum tensile force to develop at or near the pile as observed in the measured distributions. However, at greater transverse distances away from the pile, the shear zone would move closer to the wall so the maximum tensile force would occur closer to the wall. Positive tensile force in the reinforcement at the wall face is likely caused from active earth pressure resulting from the pile head load. Negative tension (compression) near the wall face during testing is likely a result of the reinforcement bending due to uneven soil movement.

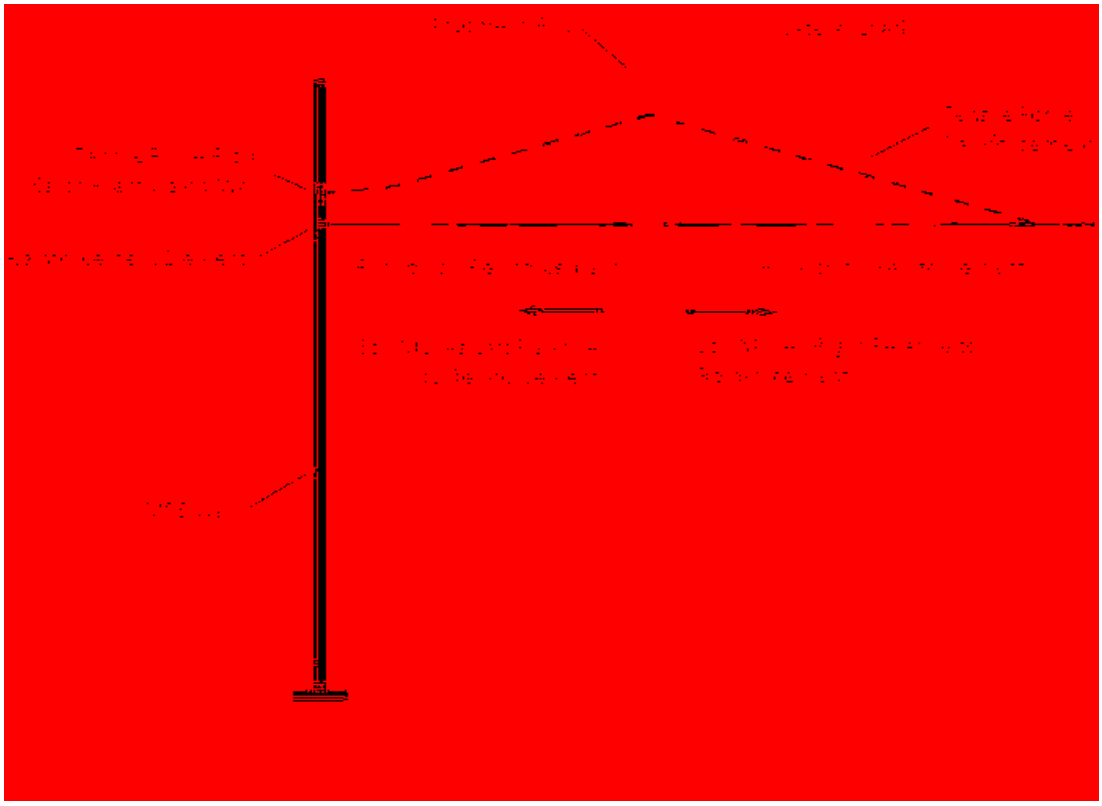

Figure 5-9: Interaction of soil and wall reinforcement for a laterally loaded pile behind an MSE wall (Hatch 2014).

The maximum induced load in the reinforcement at each pile head load increment is shown in Figure 5-10 through Figure 5-17 for each reinforcement layer during load tests on the 1.8D, 3.4D, 4.3D and 5.2D test piles. Each test pile consists of a near and far reinforcement based on the transverse distance of the pile center and the longitudinal bar of the reinforcement where the strain gauge is located. Exact distances of the strain gauges to the center of pile can be found in Table 4-1 with the smaller and larger distances representing the near and far locations, respectively. Because of previous testing at the 15-foot level, some reinforcements occasionally had residual strain in the readings, which were zeroed out at applied loads of zero. The figures show that as pile load increases, max induced tensile force in the reinforcement for each layer increases.

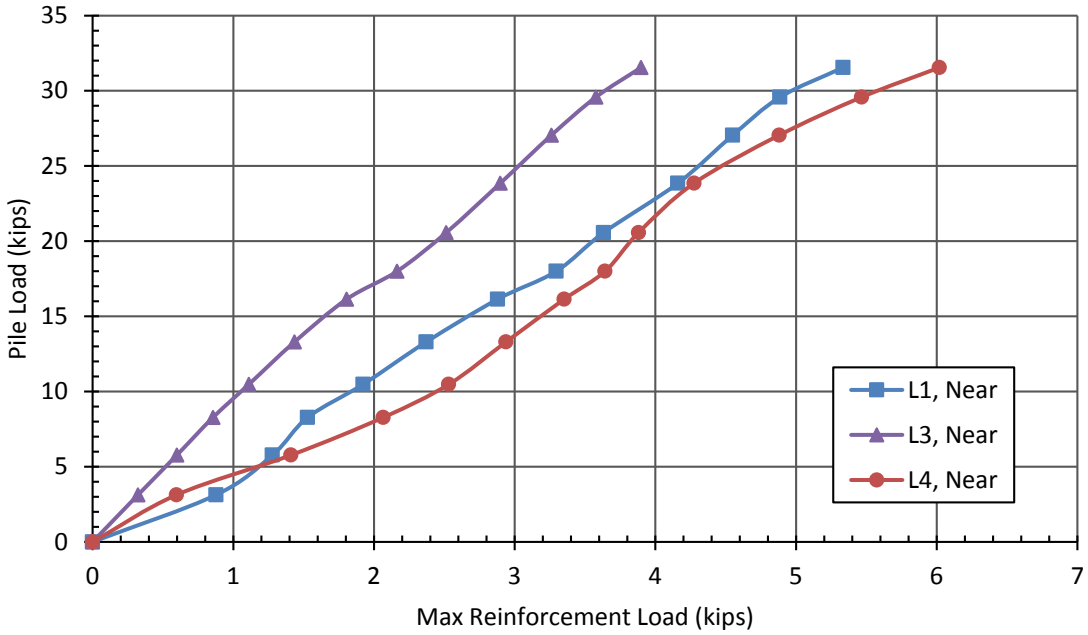

Figure 5-10: Relationship between the pile head load and the maximum reinforcement tensile force nearest to the 1.8D pile.

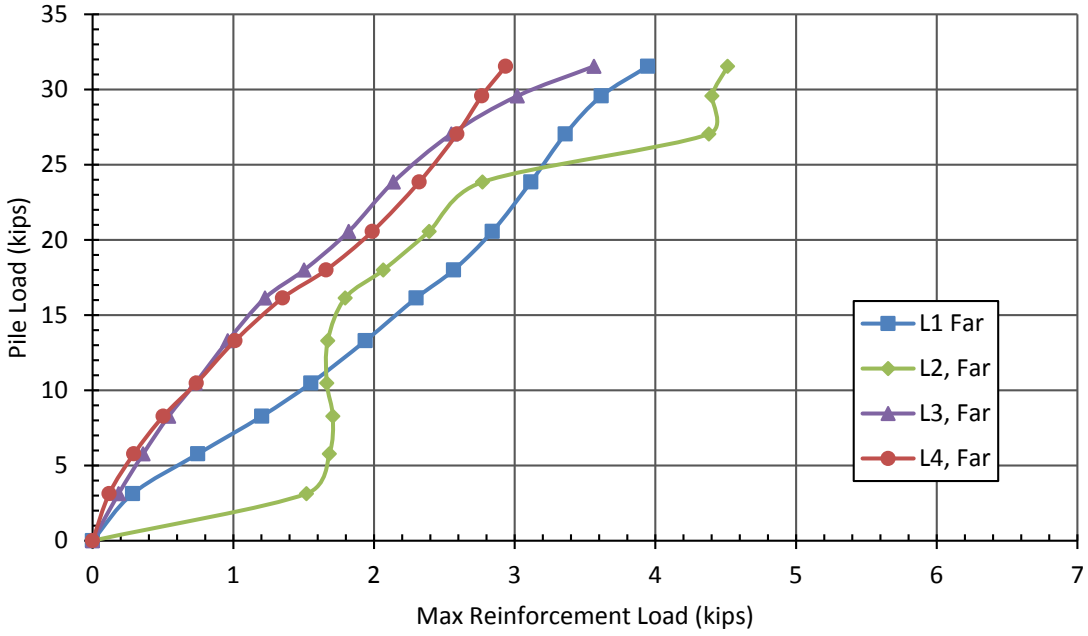

Figure 5-11: Relationship between the pile head load and the maximum reinforcement tensile force farthest from the 1.8D pile.

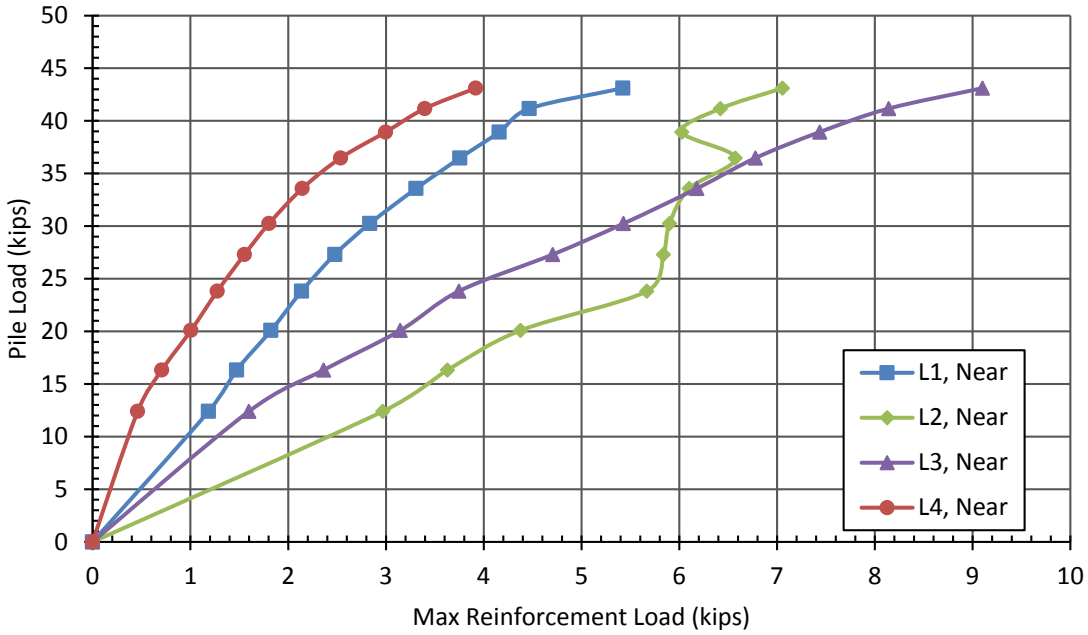

Figure 5-12: Relationship between the pile head load and the maximum reinforcement tensile force nearest to the 3.4D pile.

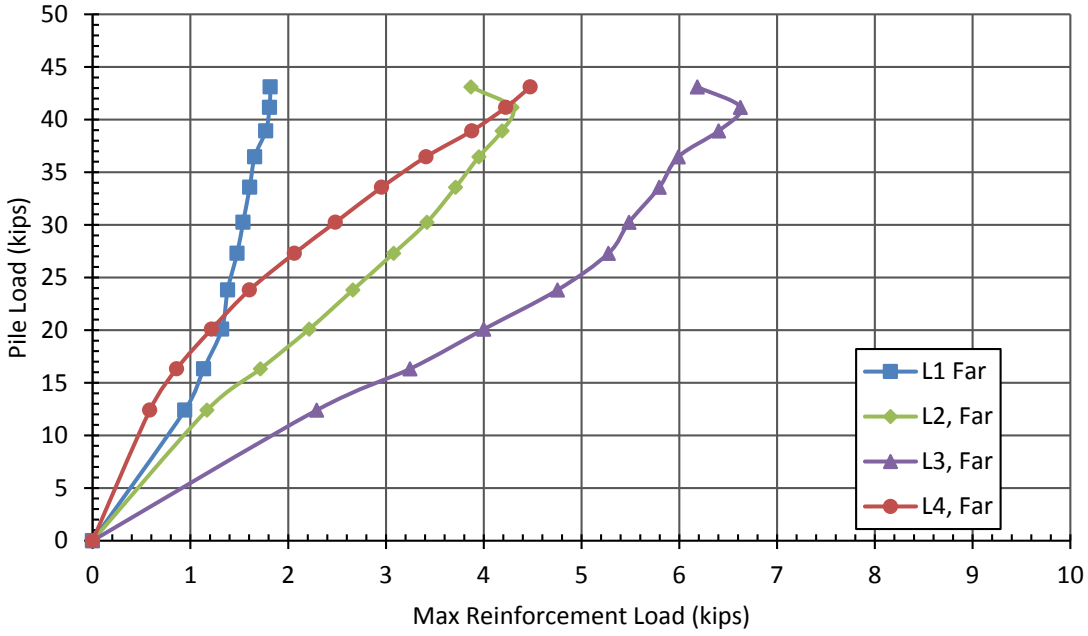

Figure 5-13: Relationship between the pile head load and the maximum reinforcement tensile force farthest from the 3.4D pile.

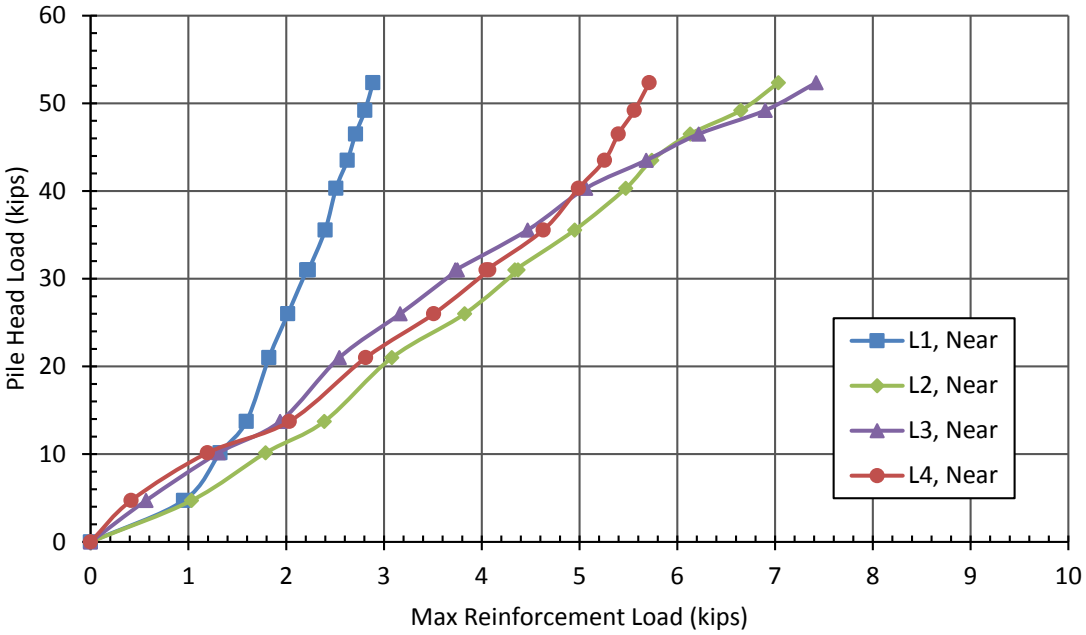

Figure 5-14: Relationship between the pile head load and the maximum reinforcement tensile force nearest to the 4.3D pile.

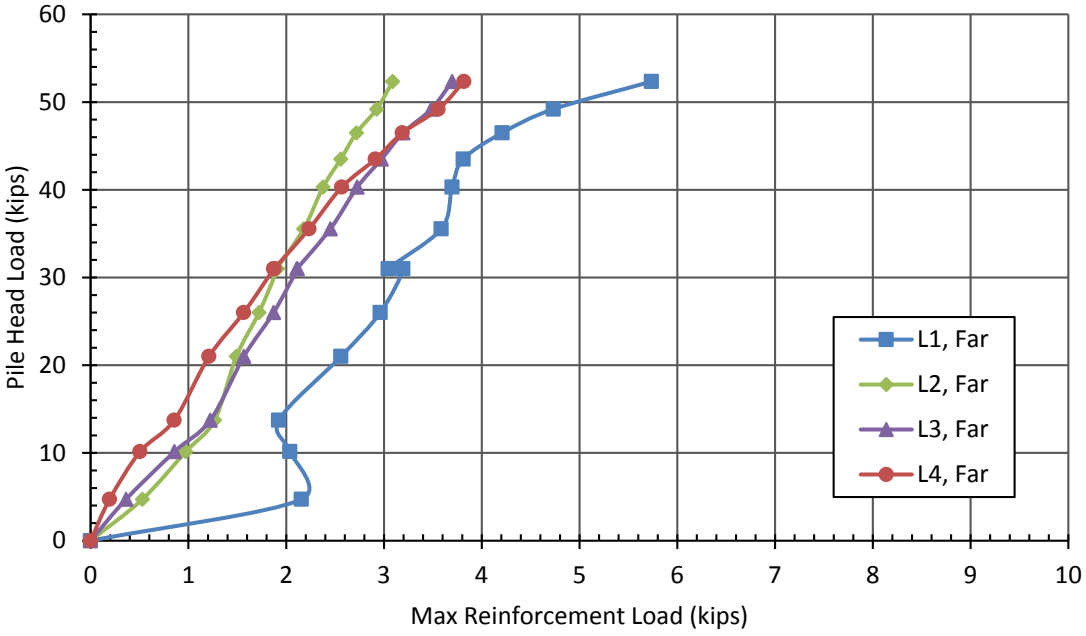

Figure 5-15: Relationship between the pile head load and the maximum reinforcement tensile force farthest from the 4.3D pile.

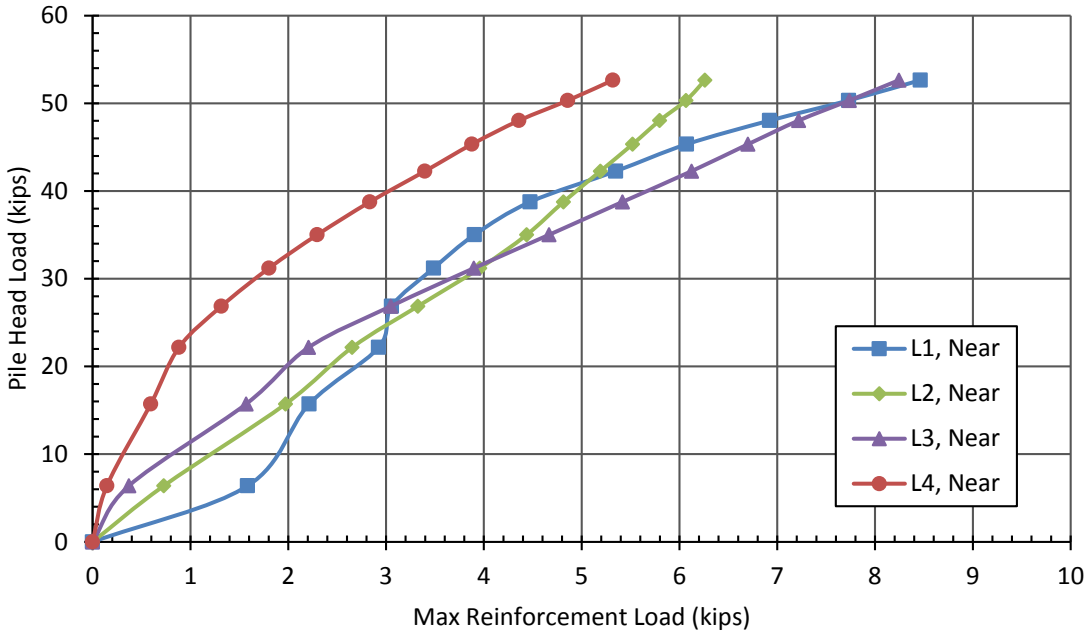

Figure 5-16: Relationship between the pile head load and the maximum reinforcement tensile force nearest to the 5.2D pile.

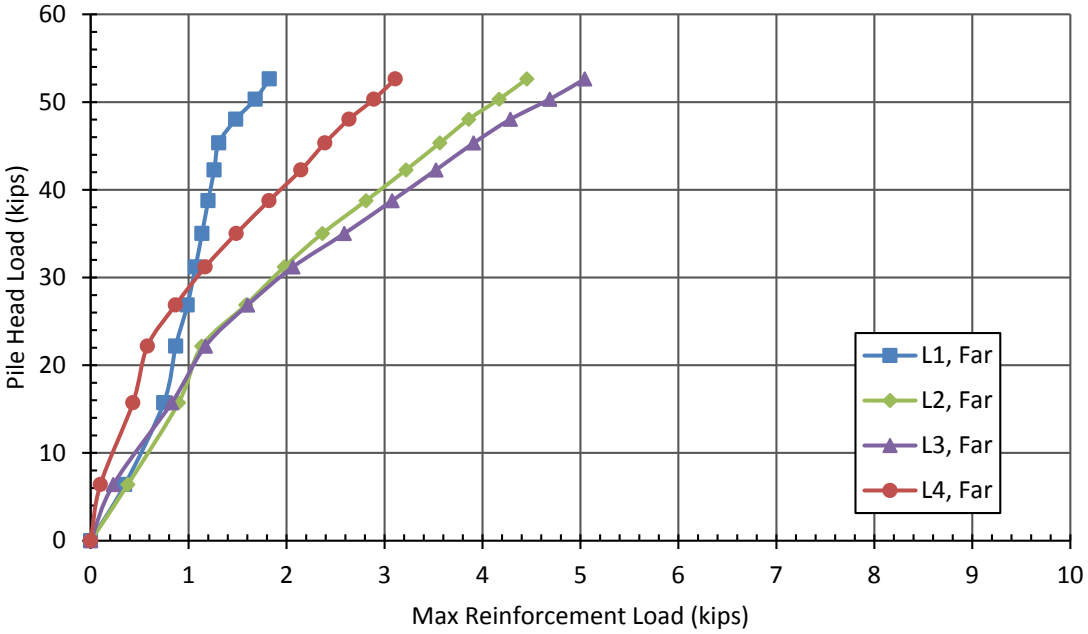

Figure 5-17: Relationship between the pile head load and the maximum reinforcement tensile force farthest from the 5.2D pile.

Max tensile forces for the 1.8D test were measured in Layers 1, 2 and 4 as shown in Figure 5-10 and Figure 5-11. The near reinforcement for Layer 2 of the 1.8D pile was not instrumented with strain gauges and, therefore, did not have any data as shown in Figure 5-10. It is likely that Layer 2 for the near reinforcement would have had a tensile force similar to that of Layer 1 had it been recorded. Figure 5-12 and Figure 5-13 indicate that Layers 2 and 3 have the highest max induced tensile forces in the reinforcement for the 3.4D test. The 4.3D test shows that Layers 2, 3 and 4 all have similar induced forces while Layer 1 is highest in one reinforcement (Figure 5-15) and lowest in the other (Figure 5-14). Layers 2 and 3 have the highest induced tensile force for the 5.2D test with the exception of Layer 1 on the near layer. Typically, the max induced tensile force in the layers increases with depth as pile spacing from the wall increases.

In general, the reinforcement data agree with Hatch (2014), Han (2014) and Besendorfer (2015) in the following ways: the peak induced load in the reinforcement is located at the pile or between the wall and the pile; as transverse distance from the pile increases, the induced reinforcement load decreases; as pile head load increases the induced reinforcement load increases; and as the pile spacing increases, the depth of the max induced load on the reinforcement typically increases.

5.4 Statistical Analysis of Load in Reinforcement

The development of tensile force owing to lateral pile loading adjacent to an MSE wall is a relatively complicated soil structure interaction problem. The pile is interacting with the soil, soil is interacting with the reinforcements, and the reinforcements are interacting with the wall. As a result, it was not possible to develop any meaningful simple models to describe the observed behavior. With the help of Dr. Dennis Eggett (BYU Statistics Department), a multiple regression statistical analysis was performed using data from Phase II (this study), Phase I (Hatch 2014), and

data previously collected from UDOT bridge construction (Nelson 2012). The Statistical Analysis System (SAS) software program was used to run the regression analysis using the general linear modeling (GLM) procedure. SAS was used to determine the statistically significant parameters in the model, after which the Data Analysis pack for Microsoft® Excel was used to fine tune the model by eliminating parameters and thereby simplifying the model without decreasing the R^2 value significant.

The regression analysis was performed by assigning the maximum tensile stress on the soil reinforcement as the dependent variable. Data was obtained for each load increment for each pile load test. The independent variables tested in this analysis were pile head load, normalized transverse distance from the pile center (T/D) where D is the pile diameter, vertical stress (σ_v) in lbs/ft^2, normalized spacing of the pile behind the MSE wall (S/D), and the reinforcement length to height ratio (L/H). In computing the vertical stress, the weight of the surcharge was considered and the surcharge height was also considered to increase the effective wall height H in accordance with AASHTO code requirements.

After the SAS analysis was completed, the relevant parameters were all of the independent variables and the following two-way interactions: vertical stress by L/H ratio, load by load, vertical stress by transverse distance, and load by transverse distance. Table 5-1 presents the R^2 value after the SAS analysis, and subsequent R^2 values after removing the next least significant term. Terms were removed from top to bottom in order of least significance to most significance, where the final R^2 value is the result of load as the final parameter. As seen in Table 5-2, two terms could be eliminated without markedly decreasing the R^2 value; however, removing additional terms would reduce the R^2 value by 3 to 5% for each term eliminated. Therefore, a somewhat more complicated equation was accepted to maintain a higher R^2 value.

Table 5-1: Effect of term elimination on R^2 values.

Term Removed	Resulting R^2 value	Decrease in R^2 value
None	79.7%	-
$\sigma^*(T/D)^+$	79.4%	0.3%
$P^*(T/D)^+$	78.9%	0.5%
P^2	75.5%	3.4%
$\sigma^*(L/H)$	70.6%	4.9%
L/H	67.3%	3.3%
S/D	63.7%	3.6%
σ	56.6%	7.1%
T/D	47.9%	8.7%

+Terms removed before computing the prediction equation.

Table 5-2: Final results of the statistical analysis with tensile force as the dependent variable.

Parameter	Coefficient	Standard Error	t-stat	P-value	Lower 95%	Upper 95%
Intercept	0.071797	0.0621477	1.155	2.48E-01	-0.050195	0.193789
P	0.025643	0.0010456	24.525	1.96E-99	0.023591	0.027696
T	-0.075961	0.0041800	-18.172	5.10E-62	-0.084166	-0.067756
σ	0.000372	0.0000452	8.230	7.61E-16	0.000283	0.000460
S/D	-0.045289	0.0035865	-12.628	1.86E-33	-0.052329	-0.038249
P^2	-0.000226	0.0000197	-11.454	3.15E-28	-0.000265	-0.000187
L/H	0.526285	0.0622950	8.448	1.39E-16	0.404004	0.648566
$\sigma^*(L/H)$	-0.000575	0.0000452	-12.724	6.71E-34	-0.000663	-0.000486

Data for the measured maximum tensile force and computed maximum tensile force were not normally distributed but were log normally distributed. Therefore, a base 10 log transformation was applied to the tensile force before running the analysis to account better for scatter in the data. A total of 806 data observations were used in the regression analysis resulting in an R^2 value of 0.789. An R^2 of 0.79 indicates that the equation accounts for approximately 79 percent of the

observed variation in the tensile force for the welded-wire grid reinforcements. P values are used to understand the statistical significance of a variable, with lower values being more significant. P values for this regression analysis were all less than 0.001 as shown in Table 5-2 indicating that all of the terms in the final equation are statistically significant. The final results of the log form regression analysis are presented in Table 5-2.

Based on the regression analysis, the maximum tensile force, F, in kips is given by the equation:

$$\boldsymbol{F=10\text{^}\left(0.072+0.026P-0.076\left(\frac{T}{D}\right)+3.7x10^{-4}\sigma_v-0.045\left(\frac{S}{D}\right)+\right.}$$

$$\boldsymbol{\left.0.53\left(\frac{L}{H}\right)-5.7x10^{-4}\sigma_v\left(\frac{L}{H}\right)-2.3x10^{-4}P^2\right)-1} \qquad \textbf{(5-2)}$$

where

P is the pile head load (kips),

T is the transverse distance from the reinforcement to the pile center (in.),

D is the outside pile diameter (in.),

σ_v is the vertical stress (psf),

S is the spacing from the pile center to the back face of the wall (in.),

L is the length of the reinforcement (ft.), and

H is the combined height of the wall and equivalent height of surcharge (ft.).

Parameter coefficients from Table 5-2 were limited to two significant figures in Equation 5-2. Note that reducing the coefficients to two significant figures simplifies the statistical regression equation without any significant loss in accuracy or change in R^2.

Predicted maximum tensile forces were then computed by taking the field data for the above parameters and plugging them into Equation 5-2. A comparison of the predicted and measured

maximum tensile forces in log form is shown in Figure 5-18. Data on the red 1:1 line indicates that the measured and predicted values are equal. The red dashed lines are associated with plus or minus one standard deviation which encloses approximately 68% of the data points. The black dashed lines indicate plus or minus two standard deviations which enclose approximately 95% of the data points. For convenience in showing measured and computed tensile forces directly, the data was transformed out of log form and is shown in Figure 5-19.

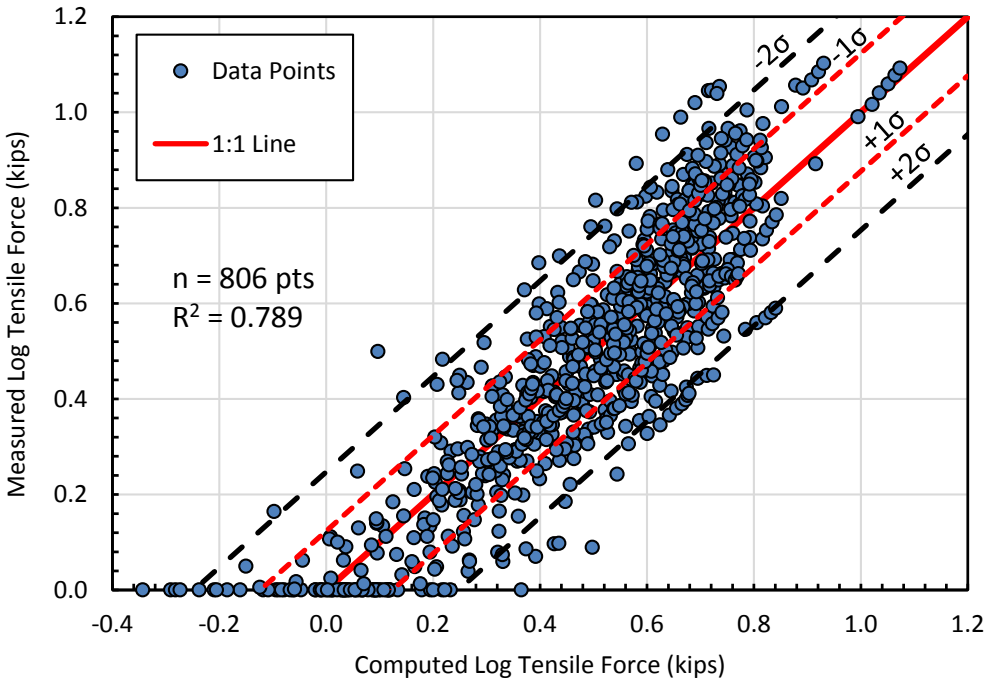

Figure 5-18: Measured versus computed logarithmic tensile force results.

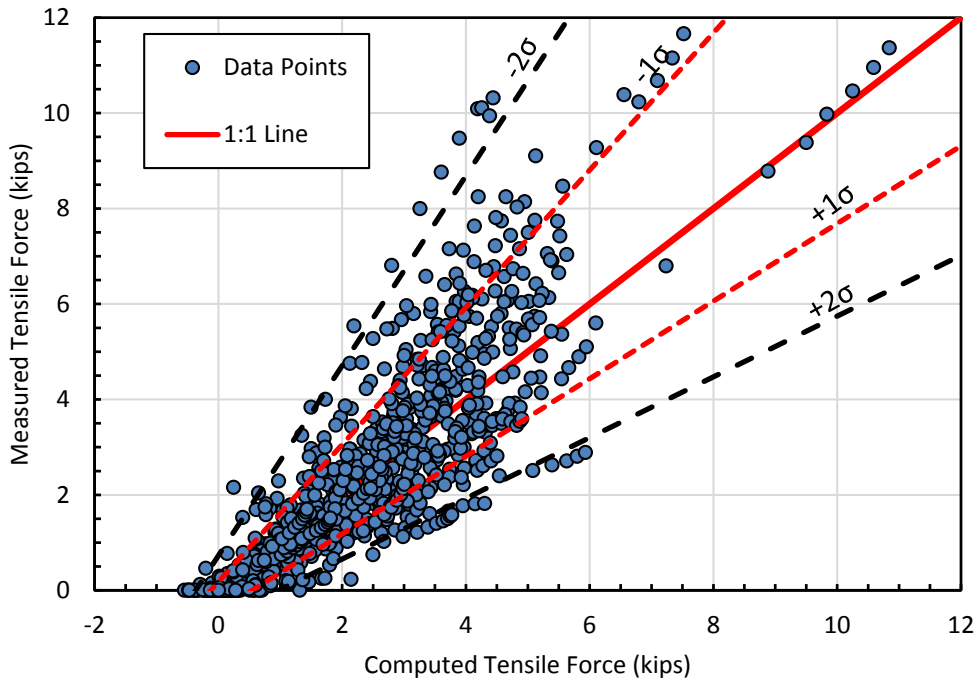

Figure 5-19: Measured versus computed tensile force results.

Data that is not located on the 1:1 red line in Figure 5-18 and Figure 5-19 demonstrates the difference (or residual) of the predicted data from the measured data. The residual for the data was calculated by using the following equation:

$$\boldsymbol{R = log(F_{measured} + 1) - log(F_{predicted} + 1)} \qquad \textbf{(5-3)}$$

where

R is the residual,

$F_{measured}$ is the measured maximum tensile force, and

$F_{predicted}$ is the predicted maximum tensile force.

The log residual is plotted against each independent variable in Figure 5-20 through Figure 5-24. If the regression equation is adequately capturing the influence of a variable, then the residuals will be uniformly distributed about zero with respect to the independent value. However,

if the residuals trend upwards or downwards as the independent value increases, then the regression equation may need to be revised over some data range. In general, the residuals fall within the range of -0.3 to 0.4 and appear to be uniformly scattered with respect to zero for all the independent variables. Generally, these results indicate that the regression equation is adequately accounting for the influence of the variables in the equation. However, there is a slightly upward trend towards positive residuals at greater stress levels in Figure 5-24. To further illustrate the uniformity of the scatter about zero and the validity of the equation, residuals were plotted as a function of computed log force as shown in Figure 5-25. The linear regression line from Figure 5-25 is centered on zero along the x-axis, demonstrating there is no bias in the regression equation based on residuals.

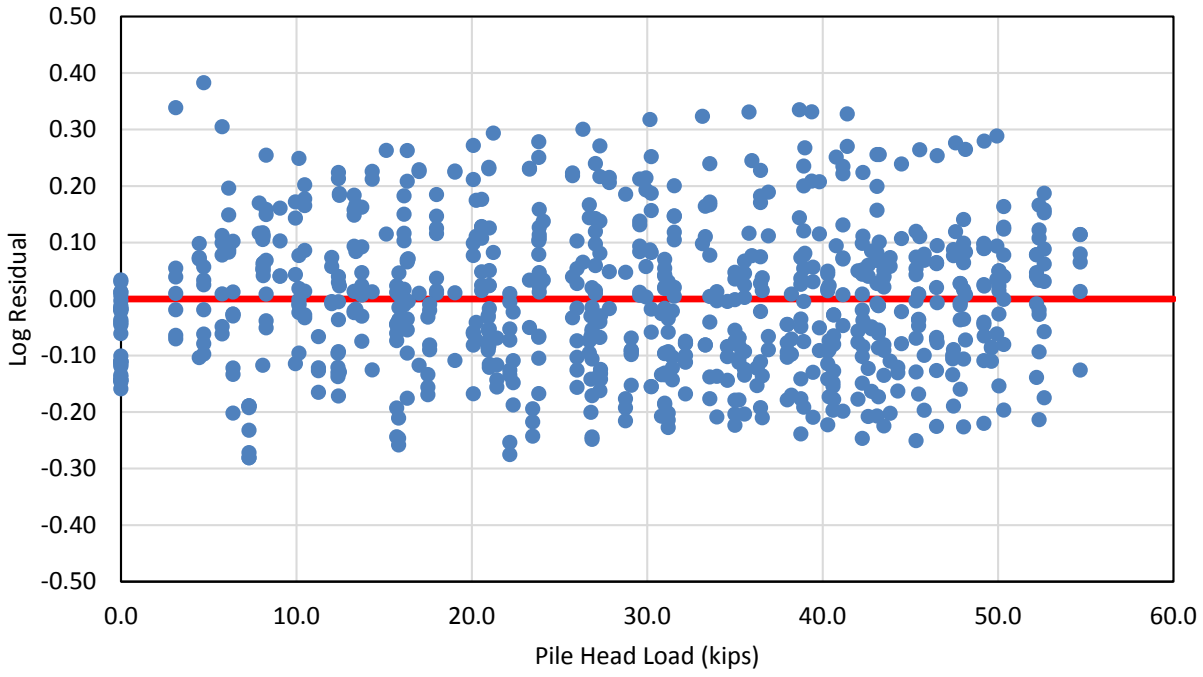

Figure 5-20: Log residual of the pile head load variable for the multiple regression analysis.

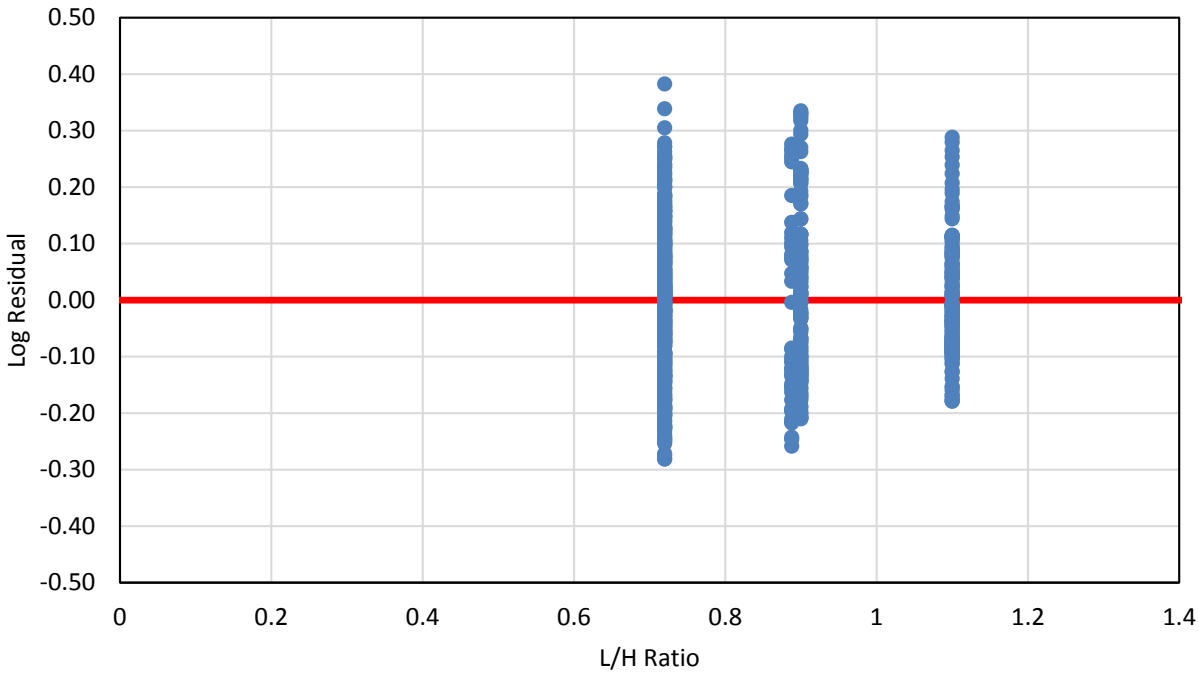

Figure 5-21: Log residual of the L/H ratio variable for the multiple regression analysis.

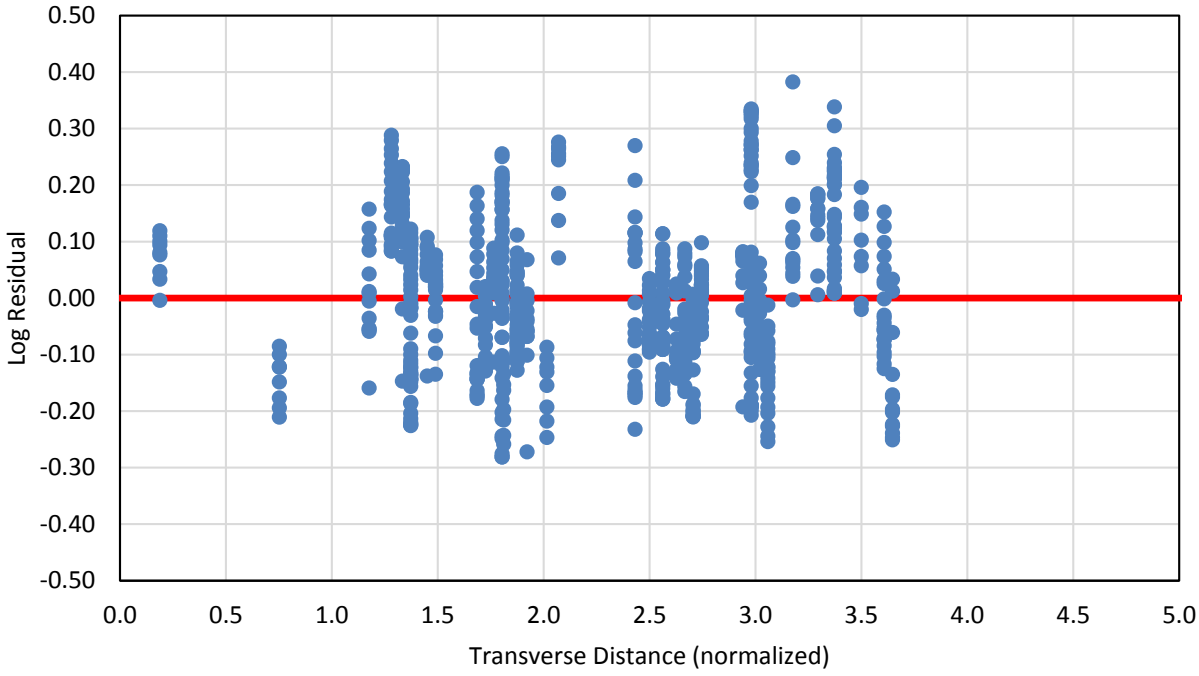

Figure 5-22: Log residual of the normalized transverse distance variable for the multiple regression analysis.

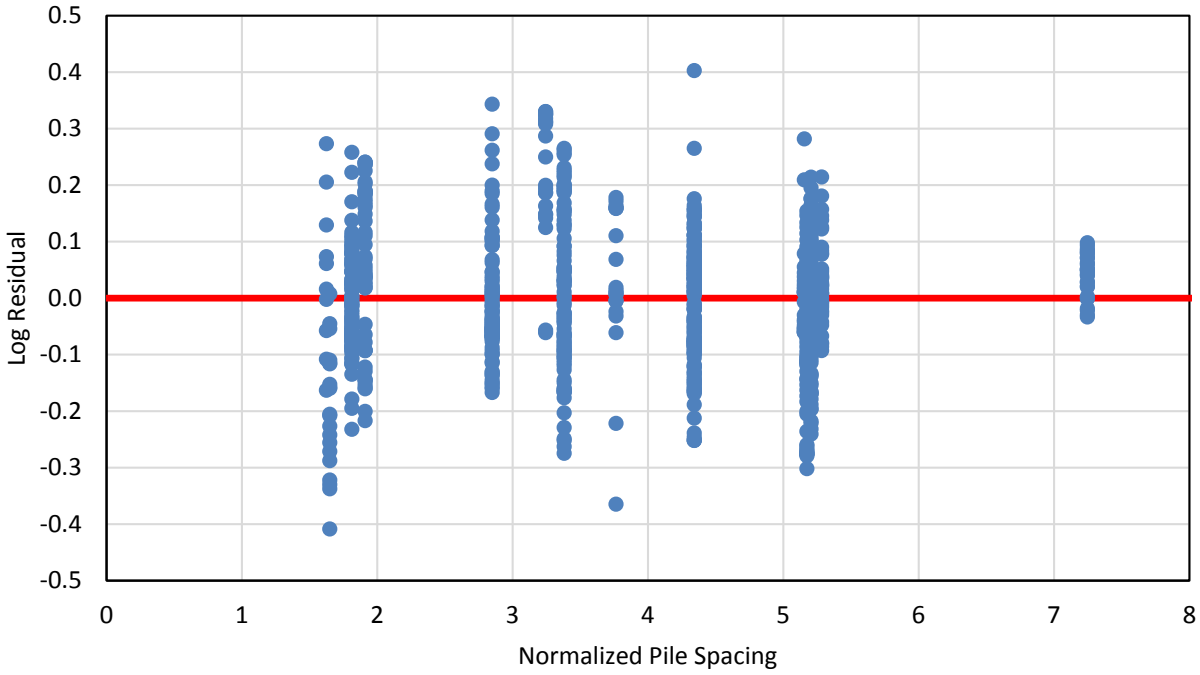

Figure 5-23: Log residual of the normalized pile spacing variable for the multiple regression analysis.

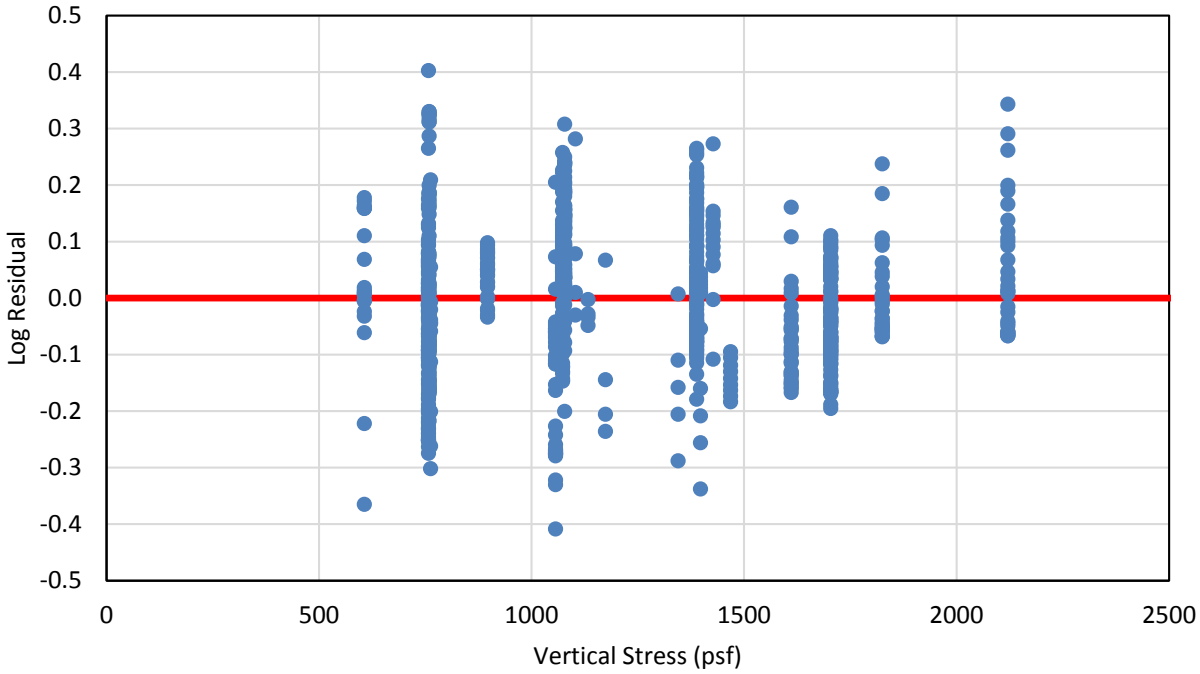

Figure 5-24: Log residual of the vertical stress variable for the multiple regression analysis.

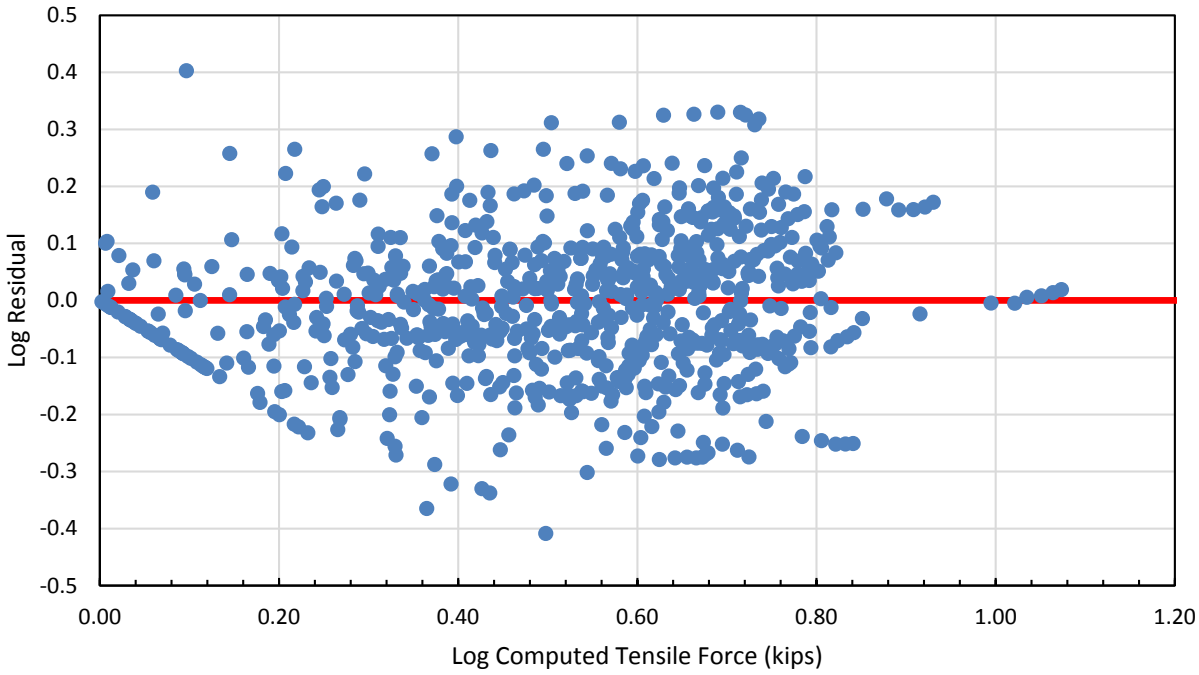

Figure 5-25: Log residual versus computed log tensile force.

5.5 Ground Displacement

Vertical and horizontal ground movement occurred during each of the laterally loaded pile tests. Vertical displacement was measured using an optical survey level. Because of safety concerns during testing, vertical displacement measurements were taken before and after testing of the pile. Horizontal displacement was measured using string potentiometers attached to a stationary reference beam and connected to steel stakes driven into the ground between the pile and back face of the wall. Horizontal displacement measurements were taken at the rate of two readings per second.

Vertical ground displacement at 3 inches of pile head displacement and along 1-foot intervals for each test pile is shown in Figure 5-26. In general, vertical displacement is greatest directly in front of the test pile and tapers off to almost no heave near the wall face. The 1.8D and 3.4D tests

are similar in their vertical displacement from the pile face to 1 foot in front of the pile. The 4.3D and 5.2D tests are similar in vertical displacement from the pile face to 2 feet in front of the pile. These similarities at different pile spacings could have occurred due to higher forces needed to achieve similar pile head deflection for farther spaced piles. In general, as pile spacing increases the vertical displacement increases when pile head deflection remains constant.

Horizontal ground displacement for the 3.4D pile test at various load increments is shown in Figure 5-27. Ground displacement figures for all test piles are located in Appendix E. Ground displacements for the 3.4D test increases as the pile load increases. In general, the following is true for horizontal ground displacement for each test pile: as pile load increases the horizontal ground displacement increases; horizontal displacement is greatest at the pile face; and horizontal displacement decreases as distance from the pile face increases. Results from this test are in agreement with other pile load tests behind an MSE wall (Besendorfer 2015).

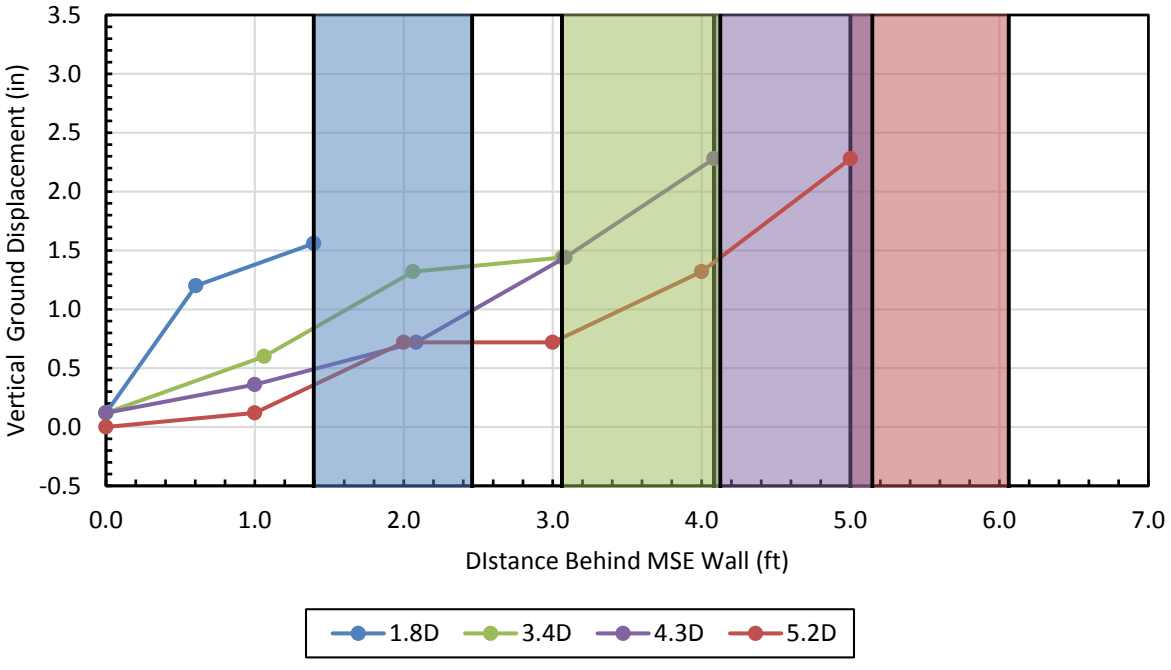

Figure 5-26: Vertical ground displacement for each test pile.

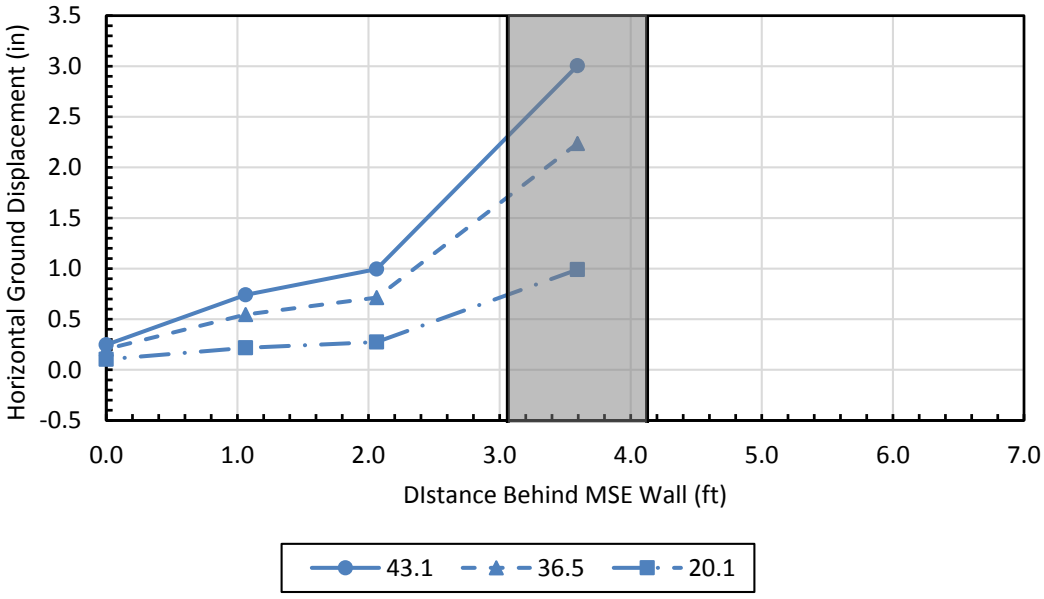

Figure 5-27: Horizontal ground displacement of 3.4D test pile at different loads.

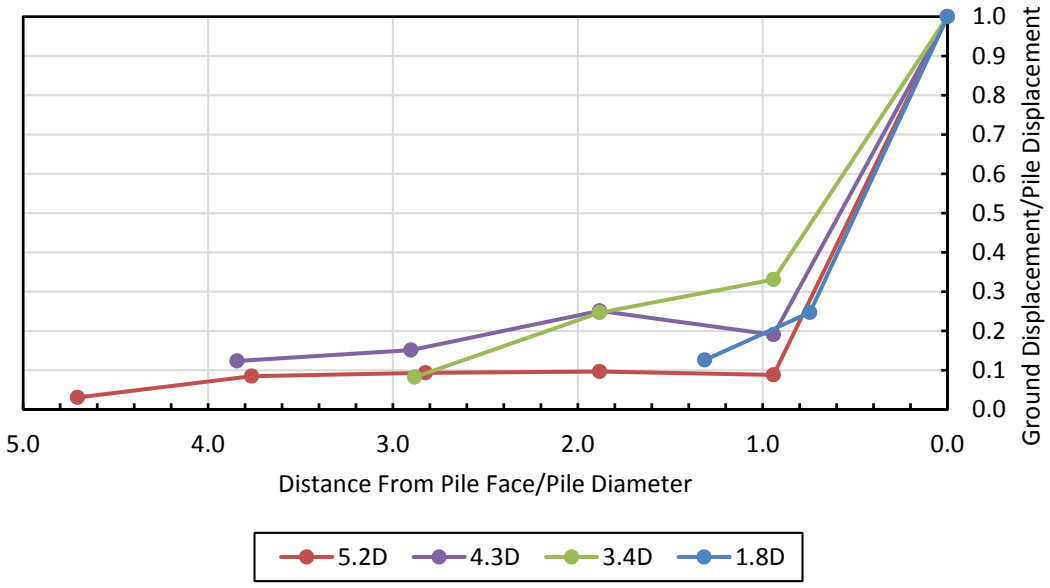

Figure 5-28: Normalized horizontal ground displacement for each pile test.

Figure 5-28 shows the normalized distance intervals and normalized ground displacement at 3 inches of pile head deflection for each test. The pile spacing was normalized by the pile diameter

while the ground displacement measurements were normalized by pile head displacement. Typically, as the normalized distance from the pile face increases, the normalized ground displacement decreases. The figure also indicates that the ratio of ground displacement to pile displacement drops dramatically within a normalized distance of 1D from the pile face and thereafter decreases from 0.35 to 0.

5.6 Wall Panel Displacement

Wall panel displacement was measured primarily by digital imagery correlation (DIC). Secondary measurements were obtained using a string potentiometer and shape arrays. The DIC cameras were placed approximately 25 feet in front of the test section of wall, the string potentiometer was attached to the top of the wall, and the four shape arrays were attached to the back face of the wall.

Figure 5-29 and Figure 5-30 show the wall deflection for each load test at 0.5 and 3 inches of pile head deflection. As seen in the figures, very little wall deflection occurred at 0.5 inches of pile head deflection. 5.2D shows more deflection than the other test piles, which is likely caused by camera movement or anomalies and will be discussed later in this section. At 3 inches of pile head displacement for DIC measurements, maximum wall deflections of 0.34 and 0.27 occurred in the 1.8D and 4.3D piles, respectively. In general, the test piles located at a wall joint experienced roughly two times the deflection as the test piles located in the center of the wall panel as shown in Figure 5-30. However, the area of wall panel that experienced large deflection was much smaller on the tests behind joints than the tests in the center of the panel. The tests at the center of the panel had smaller deflections that were more evenly distributed across the panel. Figure 5-30 also shows that as the pile spacing increases, the depth to maximum wall deflection typically increases.

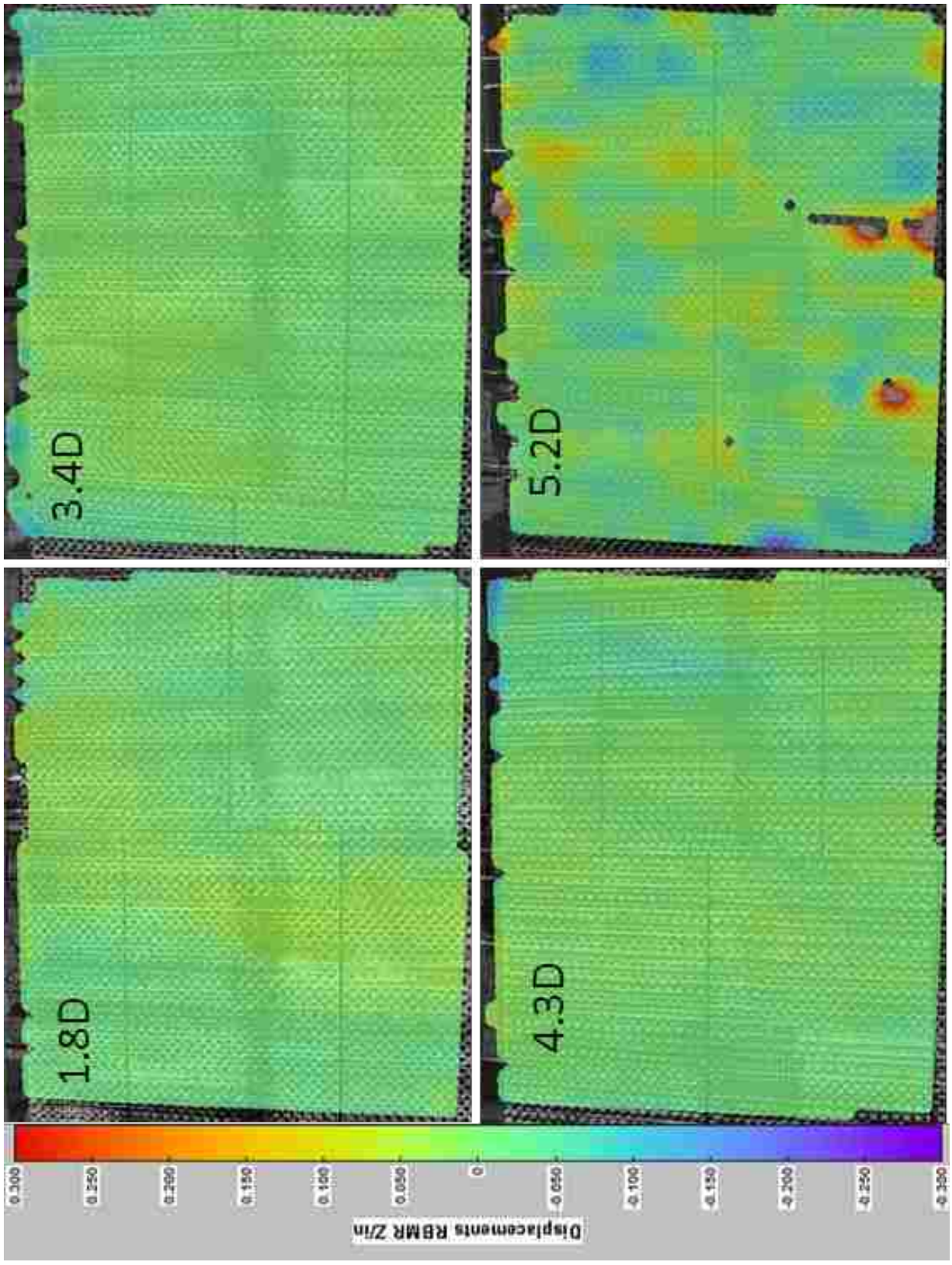

Figure 5-29: Wall panel displacement at 0.5” of pile head deflection.

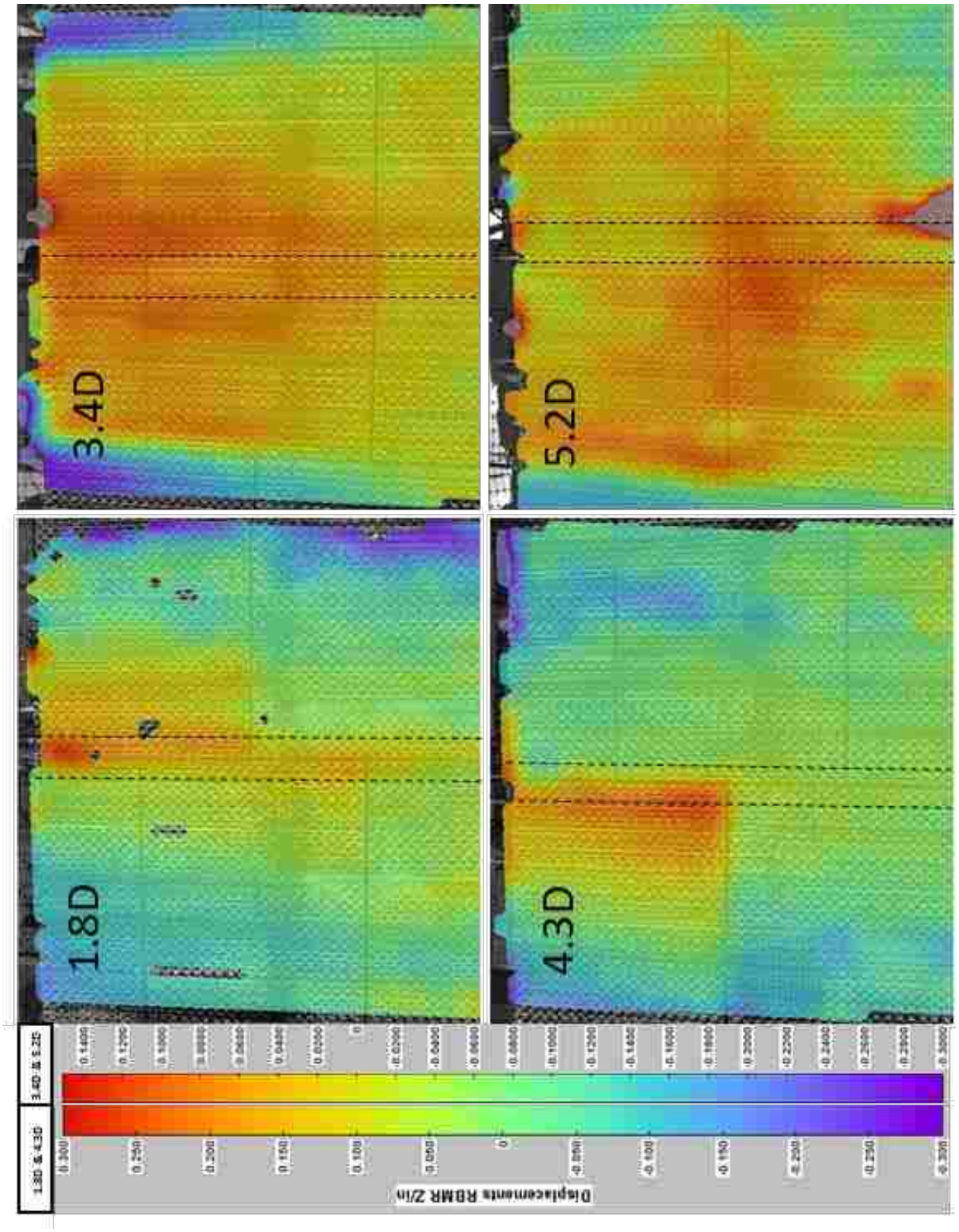

Figure 5-30: Wall panel displacement at 3" of pile head deflection. Note the different scales used for different pile distances.

The data shown in the figures were based on a Z-direction Rigid Body Motion Removed (RBMR) analysis, which only calculates displacements based on the bending or distortion of the wall in the Z (out-of-plane) direction. The regular Z displacement option accounts for all movement in the Z direction that the cameras detect, regardless if the movement is from the wall moving or from the cameras moving. Because of camera movement during testing, caused by wind or other external forces, the RBMR option was chosen for the analyses. However, for the RBMR option to be completely effective, a large area of wall needs to be used for the software to accurately remove rigid body motion. Ideally, wall panels that aren't affected by the testing should be included in the masked portion of the DIC analyses in order to test the accuracy of the RBMR option. The area of the wall that the DIC setup covered for each test was roughly 10'x12' and was likely not sufficient for the RBMR option to be completely accurate. For this project, points at the two bottom corners of each test pile picture at a given deflection were averaged and added to the RBMR deflection to account for any error that was left over in the original RBMR data. The displacements were then compared to the string potentiometer data as shown in Figure 5-31 through Figure 5-34.

In general, the data from the DIC and string potentiometers agree fairly well with the exception of the 4.3D test pile. The 4.3D pile has a deflection of approximately 0.2 inches near the top of the wall, whereas the string potentiometer measured a deflection of approximately 0.37 inches. A possible explanation for the large difference in deflection could be that the RBMR option for the 4.3D pile may not be accurate since all of the panels in the masked section of the wall (see Figure 5-30) were in movement from the pile loading.

Three of the four shape arrays were malfunctioning at the time of testing for this portion of the project. The working shape array was not always installed in front of the pile and so the data

collected cannot accurately be correlated with the displacement data. Typically, the shape array data showed much larger deflections than the DIC or string potentiometer data. This is most likely caused from the shape array conduit detaching from the back of the wall panel creating a gap that was filled with backfill during wall construction. The shape array conduit would deflect much more with soil between it and the wall by pushing the soil out of the way as the pile load increased. It is likely that, had the conduit been firmly attached to the wall throughout the whole construction process, the measured deflection from the working shape array would have been much closer to the values from the DIC and string potentiometer.

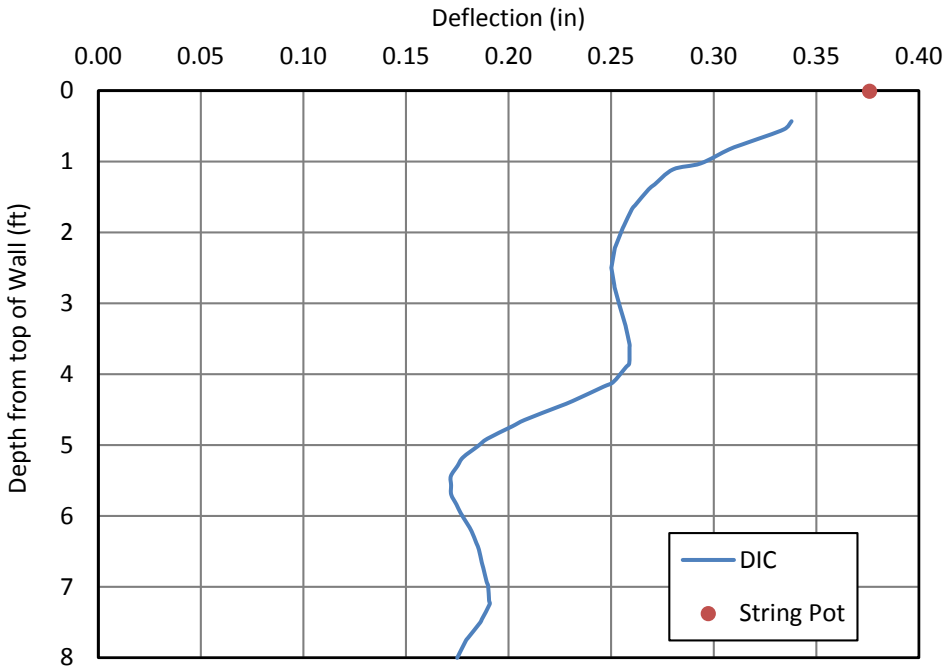

Figure 5-31: Wall displacement profile at 3 inches of pile head displacement for the 1.8D test pile.

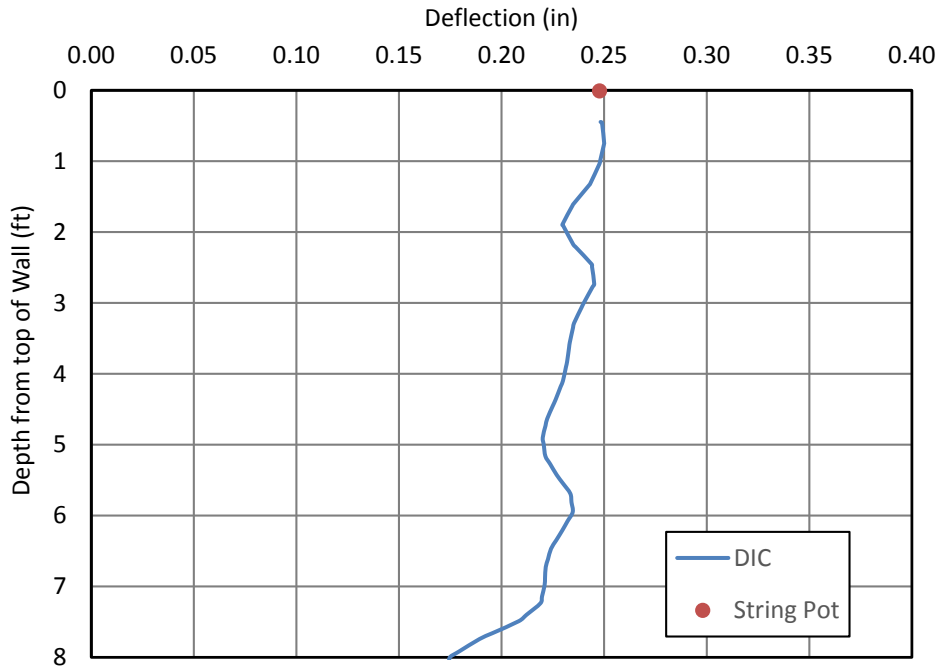

Figure 5-32: Wall displacement profile at 3 inches of pile head displacement for the 3.4D test pile.

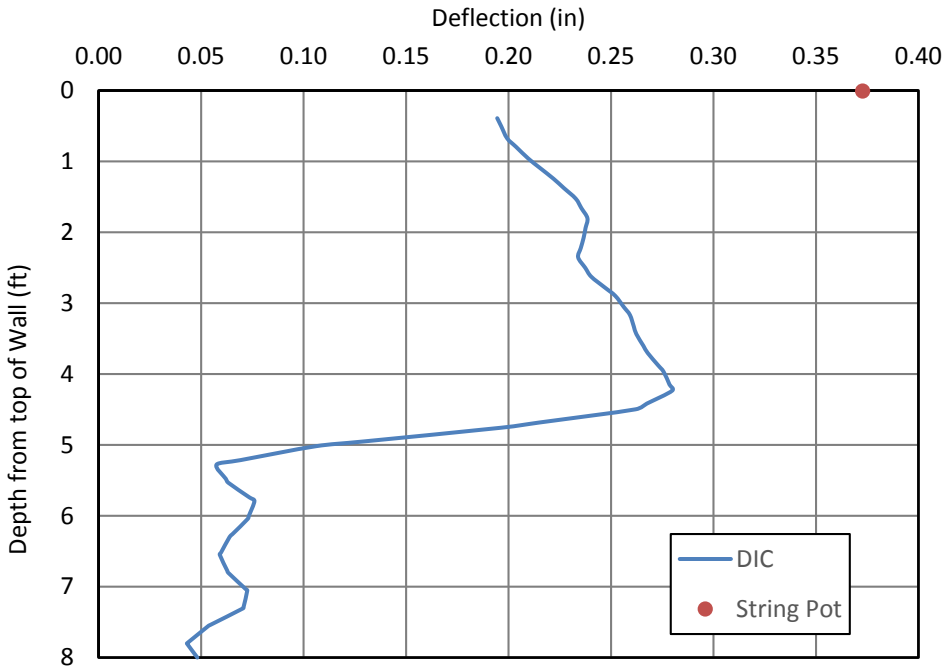

Figure 5-33: Wall displacement profile at 3 inches of pile head displacement for the 4.3D test pile.

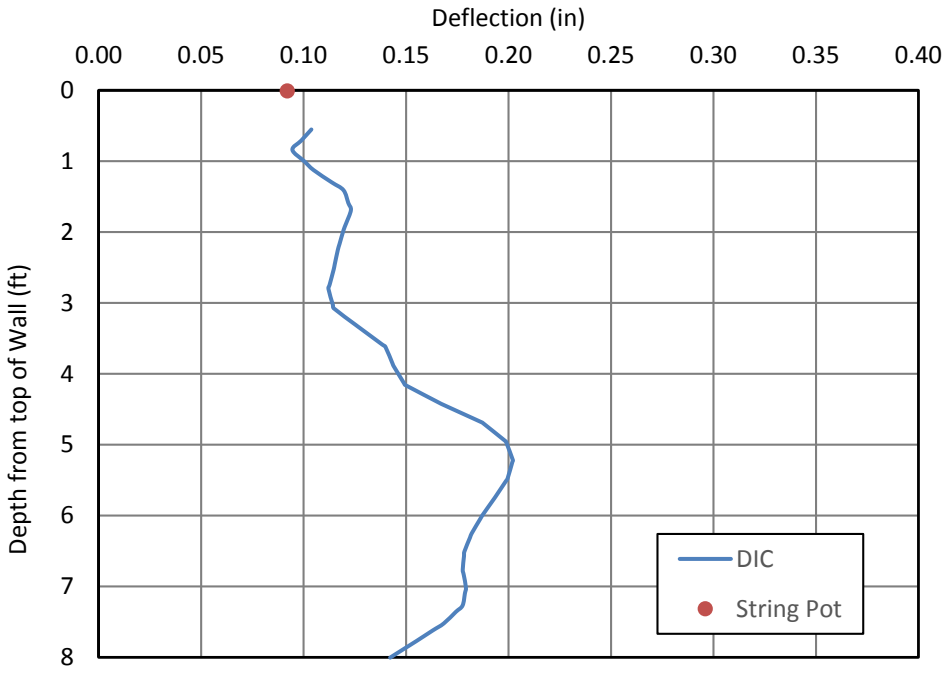

Figure 5-34: Wall displacement profile at 3 inches of pile head displacement for the 5.2D test pile.

5.7 Pile Performance

As indicated previously, strain data for each pile was measured using strain gauges that were placed on opposite sides of the pile at distances of 2, 4, 6, 9, 12, 15 and 18 feet below the ground surface. The strain data was used to find the bending moment, M, in inch-kips for each test pile using the equation:

$$\boldsymbol{M_i = \frac{EI}{2y}((\mu\varepsilon_{it} - \mu\varepsilon_{0t}) - (\mu\varepsilon_{ic} - \mu\varepsilon_{0c}))(10^{-6})} \qquad \textbf{(5-4)}$$

where

E is the pile modulus of elasticity (29,000 ksi),

I is the moment of inertia of the pile (including angle iron) in in^3,

$\mu\varepsilon_{it}$ is the micro strain for the i^{th} data due to tension,

$\mu\varepsilon_{ic}$ is the micro strain for the i^{th} data due to compression,

$\mu\varepsilon_{ot}$ is the initial micro strain caused by tension,

$\mu\varepsilon_{oc}$ is the initial micro strain caused by compression, and

y is the distance in inches separating the two strain gauges along the line of loading.

It should be noted that after testing in the field was completed, further laboratory testing indicated that the strain gauges used on the test piles were installed with the incorrect surface attached to the piles. Ten laboratory tests were performed on plate steel to verify the correct strain gauge surface by applying strain gauges with the correct and incorrect sides adhered to the steel. The measured strain values were compared with the data from the laboratory compression equipment and the appropriate strain gauge side was determined. Correction factors were determined by dividing the measured values of the correctly placed strain gauges by the incorrectly placed strain gauges. Laboratory testing showed that the correction factor for the strain gauges was approximately 3. This correction factor was then applied to Equation 5-4 before plotting the results.

The test piles were driven with the intention of having the strain gauges perpendicular to the wall face. However, all of the piles used on this portion of the project rotated somewhat during installation. Pile rotation was measured by taking the distance of the strain gauges to the center of the pile where the load was applied and using geometry to find the change in y, as shown in Figure 5-35. The corrected y value was used in calculating the bending moment in Equation 5-4.

In locations where one strain gauge was damaged during construction the other strain gauge value was doubled in Equation 5-4. If both strain gauges at a given depth were damaged or faulty the data point was omitted from the chart, as mentioned in section 4.3.2.

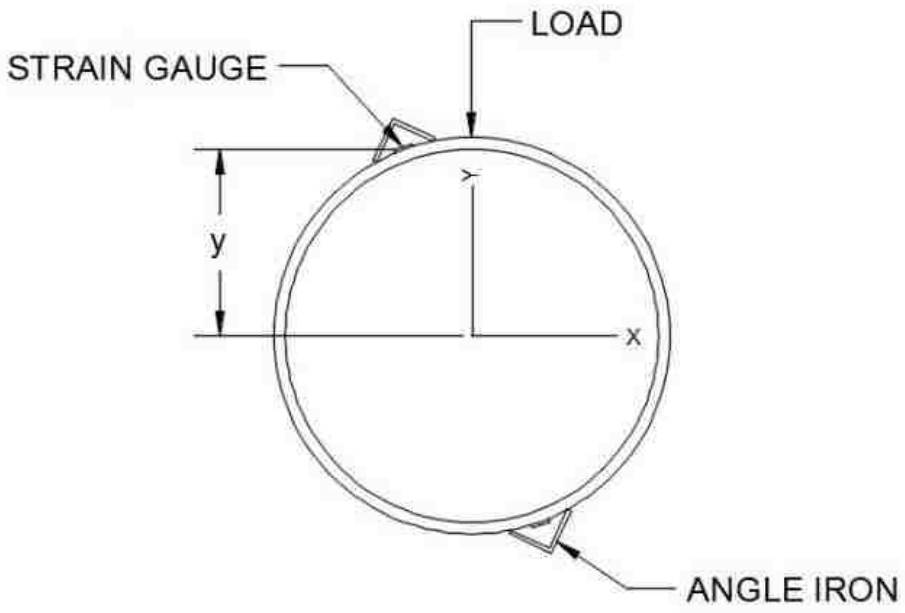

Figure 5-35: Corrected y measurement to account for pile rotation.

Bending moment is plotted versus depth below the surface for each pile at several pile head loads in Figure 5-36 through Figure 5-39. The moments are taken from the one-minute time hold readings for each test. Maximum moments for 3 inches of pile head deflection range between 2,300 kip-in and 4,200 kip-in and are located between 9 feet and 4 feet below ground surface, respectively. Typically, as pile spacing from the wall increases the depth to the maximum moment decreases, with the exception of the 4.3D test. The 4.3D test had two bad strain gauges for the 6 foot interval and one bad strain gauge for the 9 foot interval, therefore the location of the maximum moment is poorly constrained. Based on the other pile tests and an LPILE moment analysis (discussed in Chapter 6), it is likely that the maximum moment for the 4.3D test was much greater and at a depth between 5 feet and 7 feet below the surface. The lack of good data caused key points on the graph to be omitted and therefore skewed the results.

Maximum moments generally increased with pile spacing, but this is likely due to the increased pile head loads to create similar pile head deflections. Based on the data from the figures, maximum moments for similar pile head load values were similar. For example, at loads ranging from 20.1 and 21 kips, the maximum moment was 1,300 to 1,500 in-kips. Note that 5D data was interpolated using Figure 5-39 to get a load of 21 kips and a moment of approximately 1,500 in-kips. Again, the 4.3D pile is the exception and it is likely that the induced maximum moment was actually higher than measured data indicates as discussed previously.

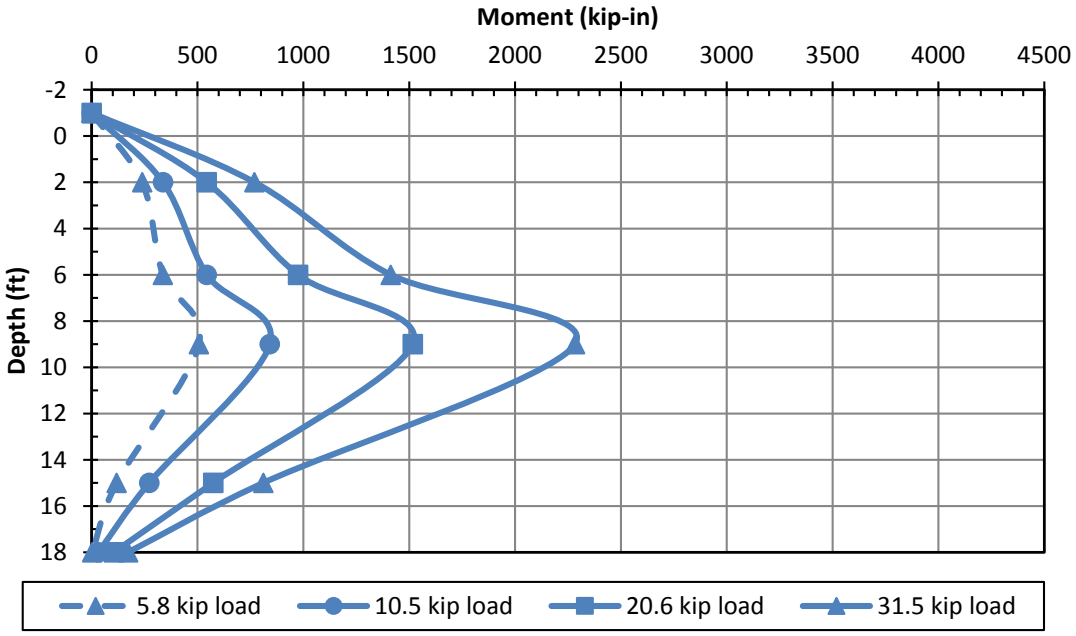

Figure 5-36: Bending moment versus depth of several pile head loads for the 1.8D test.

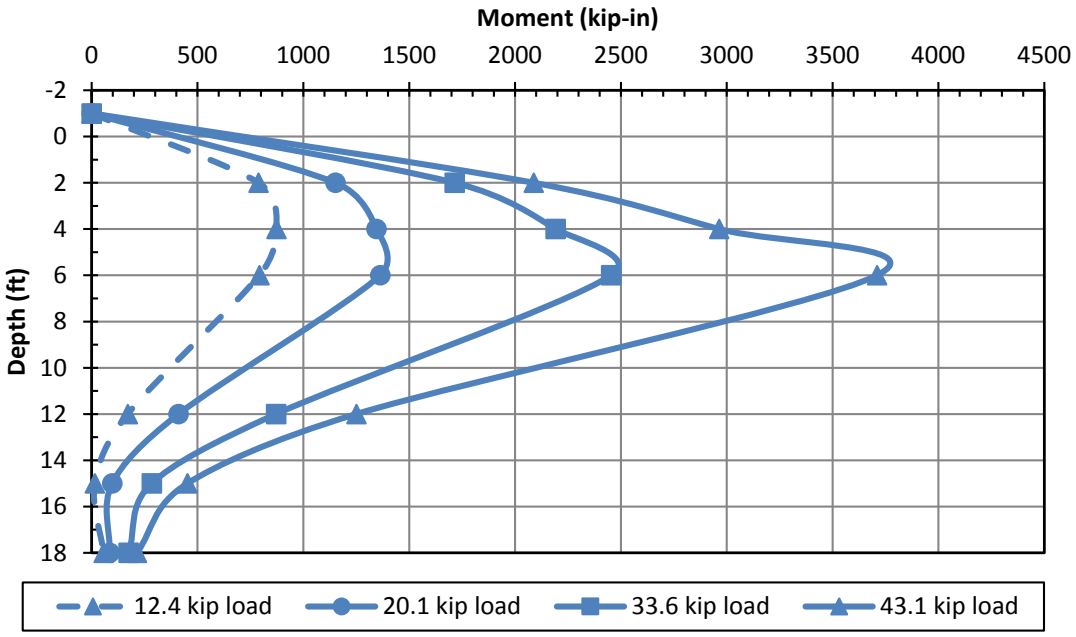

Figure 5-37: Bending moment versus depth of several pile head loads for the 3.4D test.

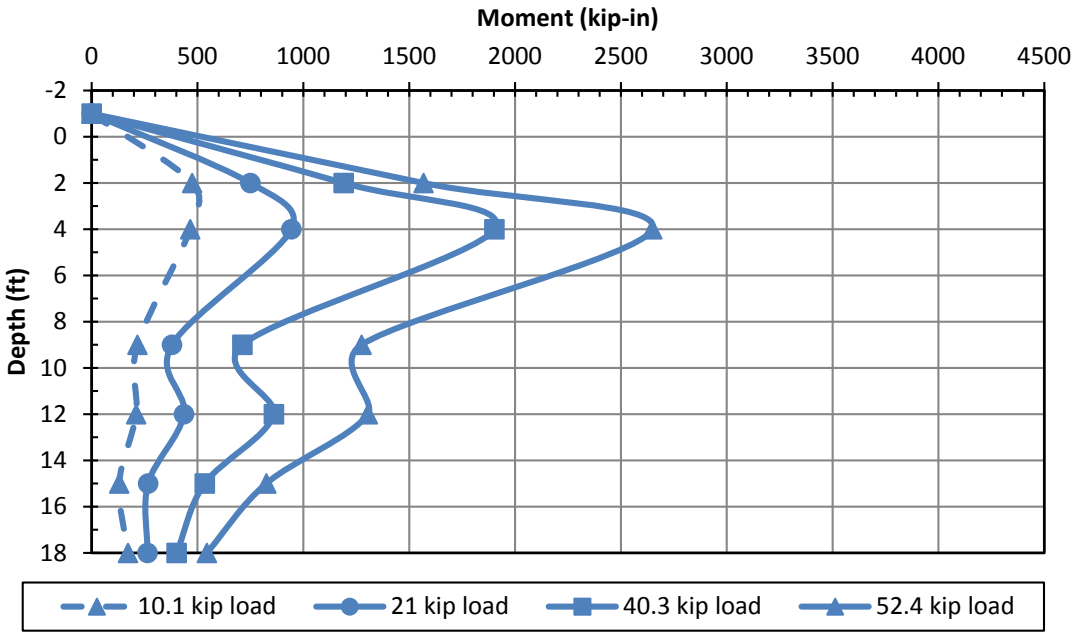

Figure 5-38: Bending moment versus depth of several pile head loads for the 4.3D test.

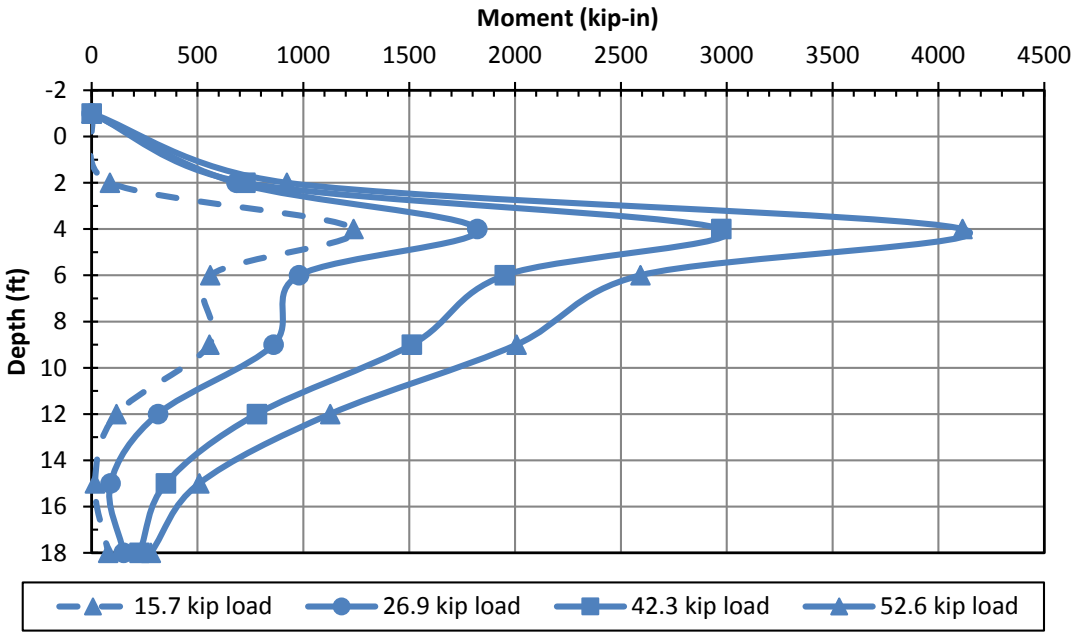

Figure 5-39: Bending moment versus depth of several pile head loads for the 5.2D test.

6 LATERAL PILE LOAD ANALYSES

Lateral pile load for this project was analyzed using the computer program LPILE 2015. As discussed in Chapter 2, LPILE is a finite difference program that models the pile as a beam and iteratively solves for deflection using the p-y method. In this method, the soil is modeled using p-y springs which account for horizontal soil resistance (p) and horizontal deflection (y). Input parameters for LPILE include the pile material, size and type as well as the soil layering and properties. Different soil types were programmed into LPILE based on previously researched full-scale load tests including clay, sand and a number of specialty soils. The program also allows manual entry of soil parameters.

The LPILE program was used to produce plots of pile head load vs. deflection, pile head load vs. rotation, and bending moment vs. depth for comparison with the measured curves. After calibration of the LPILE model based on performance of the pile furthest from the wall, p-multipliers were back-calculated in an effort to account for the reduction in lateral soil resistance owing to the presence of the MSE wall. The following sections will describe the material properties used as input parameters in LPILE and will discuss a comparison of the test results with the curves computed by LPILE.

LPILE was used to model the test piles as elastic, non-yielding steel pipe piles with an outside diameter of 12.75-inches. A moment of inertia of 314 in^4 was used to account for the pile

section with the steel angle iron welded onto the sides of each pile. The soil plug in the bottom 10 to 11 feet of the pile was neglected as it had little impact on the pile response.

As mentioned in previous chapters, the piles were driven about 18 feet into native soil and granular backfill was compacted to a depth of approximately 20 feet around the piles leaving a two foot length of pile above the ground surface. API Sand (O'Neill) was used to model the compacted backfill in the upper 20 feet and the native soil in the bottom 18 feet. Because the pre-cast concrete blocks only imposed a surcharge on the soil behind the test piles, this surcharge effect could not be modeled accurately using LPILE. LPILE can only model a continuous, uniform surcharge. To provide bounds on the computed behavior, two analyses were performed for each test pile. One analysis employed a continuous surcharge and one did not account for any surcharge. To account for surcharge in an LPILE model, a user must define a thin soil layer with no shear strength, but having a unit weight that produces a weight equal to the desired surcharge. In this case, the surcharge was modeled with a layer of soil 3-inches thick with a unit weight of 2,400 pcf to produce the surcharge pressure (q) of 600 psf. Friction angle and stiffness parameters were set to zero.

Input parameters for each soil layer consisted of an effective unit weight (γ), friction angle (φ), and the modulus of subgrade reaction (k). Each input parameter and associated soil layer is shown in Table 6-1 for the non-surcharge analysis and in Table 6-2 for the applied surcharge analysis. The soil unit weight was based on the average moist unit weight obtained from the nuclear density tests described previously. Friction angle, ϕ, and stiffness, k, were determined from the back analysis as described subsequently. Material properties in the native soil layer had relatively little effect on computed pile performance.

Table 6-1: Soil layers and input parameters without surcharge.

Soil Type	Layer Thickness (ft)	Unit Weight, γ (pcf)	Friction Angle, ϕ (degrees)	Modulus of Subgrade Reaction, k (pci)
API Sand (O'Neill)	20	126.8	38	220
API Sand (O'Neill)	18	125	34	115

Table 6-2: Soil layers and input parameters with surcharge.

Soil Type	Layer Thickness (ft)	Unit Weight, γ (pcf)	Friction Angle, ϕ (degrees)	Modulus of Subgrade Reaction, k (pci)
User-Defined	0.25	2,400	-	-
API Sand (O'Neill)	20	126.8	30	38
API Sand (O'Neill)	18	125	34	115

In LPILE the load was applied at the top of the model pile one foot above the ground surface with a pinned-head boundary condition to match field loading conditions. Loads were input for each deflection interval and the LPILE model was used to compute deflection.

6.1 LPILE Analysis Results

LPILE was used to back-calculate appropriate p-multipliers for each pile load test. Initially, the pile furthest from the wall (5.2D) was analyzed and the soil properties necessary to match the measured load-deflection curve were determined. Based on the assumption that the pile furthest from the MSE wall would be relatively unaffected by the presence of the wall, a p-multiplier of 1.0 was assumed for this case indicating no wall interaction. In calibrating the soil model, both ϕ and k affect the computed load-deflection curve; however, k has more effect on the curve at small deflection levels while ϕ has a greater effect at larger deflections as the soil layers begin to reach

failure. Generally, the k value was selected based on the correlation with friction angle for soil above the water table shown in Figure 6-1 as specified by API. However, some adjustment was allowed to improve agreement with the measured curve.

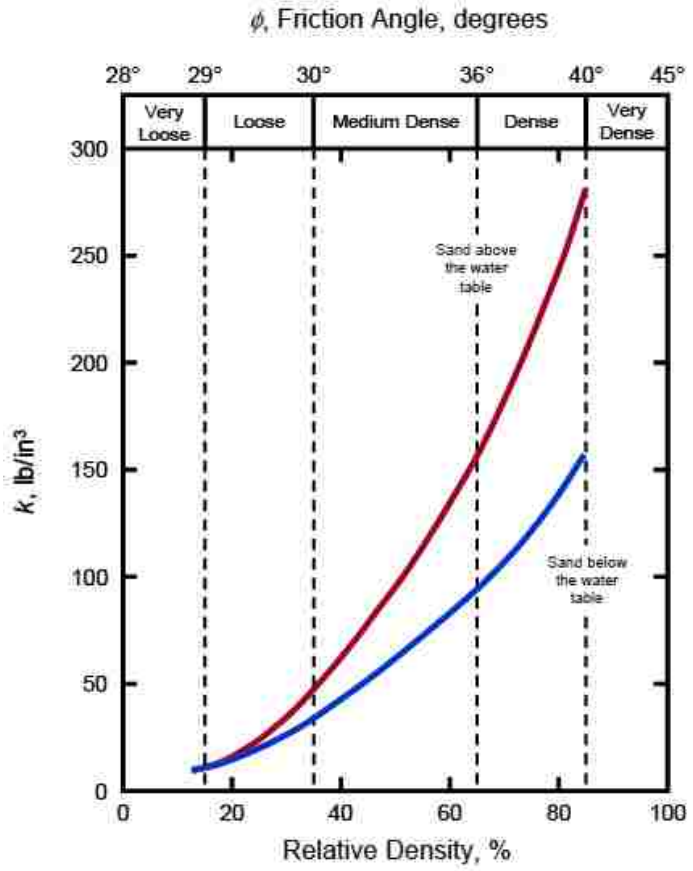

Figure 6-1: Soil modulus reaction based on friction angle or relative density of soil (API, 1982).

For piles located closer to the wall, these back-calculated soil parameters were then held constant for each pile and a constant p-multiplier was back-calculated to produce agreement with the measured load-deflection curve for that pile. P-multipliers are factors that are multiplied by the normal lateral soil resistance to account for the reduced lateral soil resistance for piles near an MSE wall. Separate analyses were performed with LPILE using both the no-surcharge and

surcharge models. Once the appropriate soil parameters and p-multipliers had been determined, computed pile load versus pile rotation and pile bending moment versus depth curves were also compared with measured curves.

6.1.1 Load Deflection Curves

As mentioned previously, load-deflection curves were calculated in LPILE by inputting soil and load parameters from the 5.2D test into LPILE to get a load-deflection curve similar to the measured load-deflection curve. A best fit curve was found by back-calculating ϕ and k values, which are found in Table 6-1 and Table 6-2. Load-deflection curves were generated with LPILE to account for both surcharge loading (q=600 psf) and non-surcharge loading (q=0 psf) and are shown in Figure 6-2 with the measured load-curve for the 5.2D pile. A p-multiplier of 1.0 was assigned to the 5.2D test with the assumption that it is spaced far enough behind the wall to not be affected by the walls presence. Best-fit load-deflection curves were then assigned to the measured load-deflection curves for the 4.3D, 3.4D and 1.8D tests, as shown in Figure 6-3 through Figure 6-5, by assigning different p-multipliers in LPILE until the desired curve was found for each test. P-multipliers for each test are shown in Table 6-3. LPILE curves were matched to the measured load-deflection curves by matching the top three deflection points of each curve. The top three points used as the criteria for the best fit line because the 4.3D test had bad data for the first 1.5 inches of deflection and the 1.8D load-deflection curve would have more realistic values at higher deflections after the loosely placed fill had time to mobilize and compact from axial pile loading.

Table 6-3: P-multiplier for each test pile

Pile	P-mult (q=0 psf)	P-mult (q=600 psf)
5.2D	1.00	1.00
4.3D	0.95	0.95
3.4D	0.68	0.71
1.8D	0.30	0.38

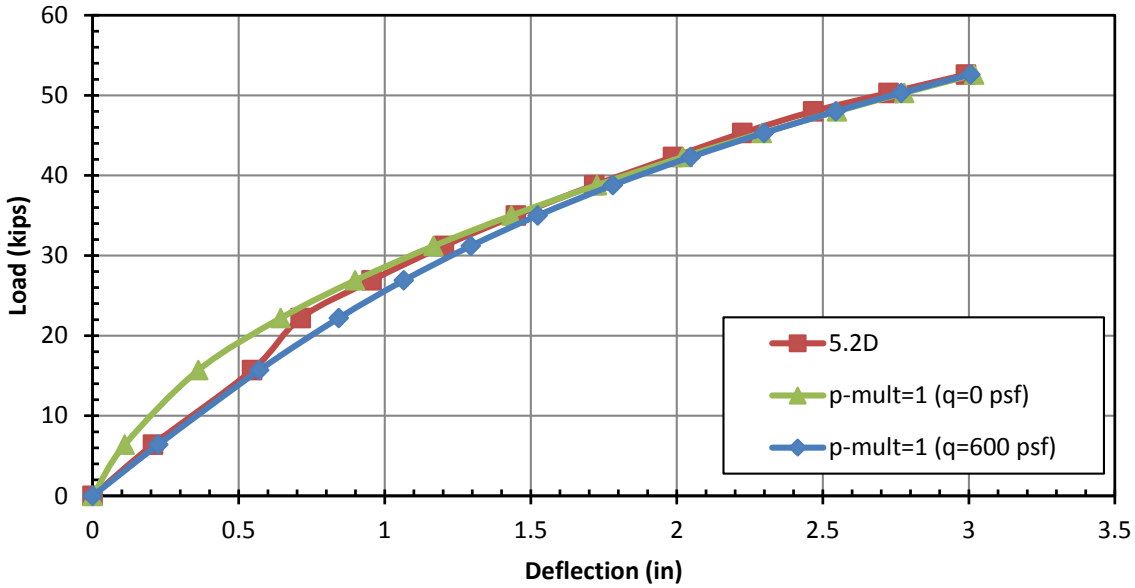

Figure 6-2: Comparison of load-deflection curves between measured and calculated results for the 5.2D test.

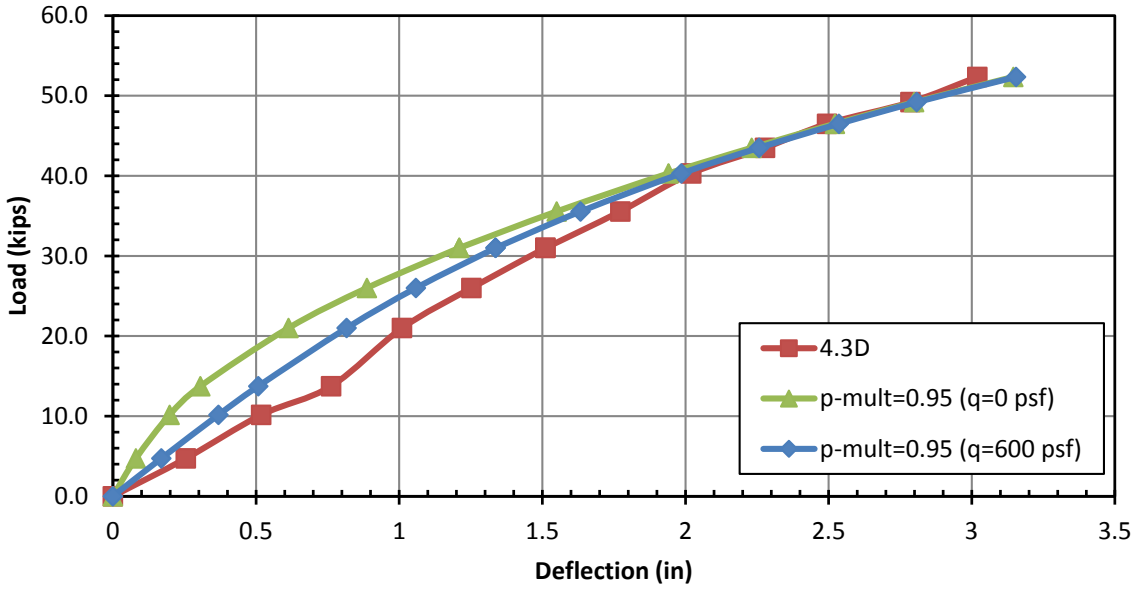

Figure 6-3: Comparison of load-deflection curves between measured and calculated results for the 4.3D test.

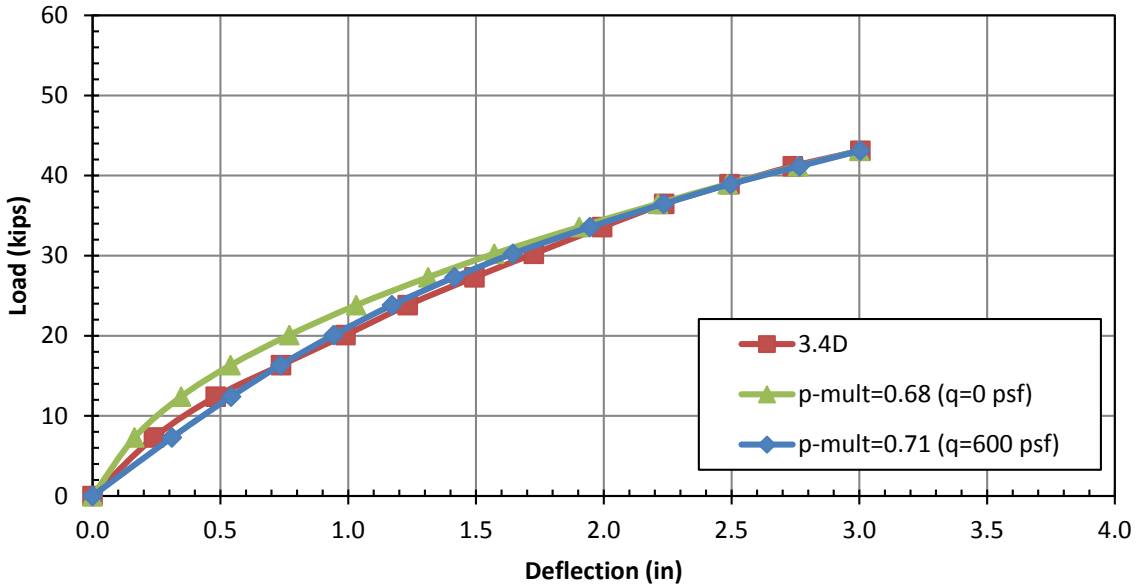

Figure 6-4: Comparison of load-deflection curves between measured and calculated results for the 3.4D test.

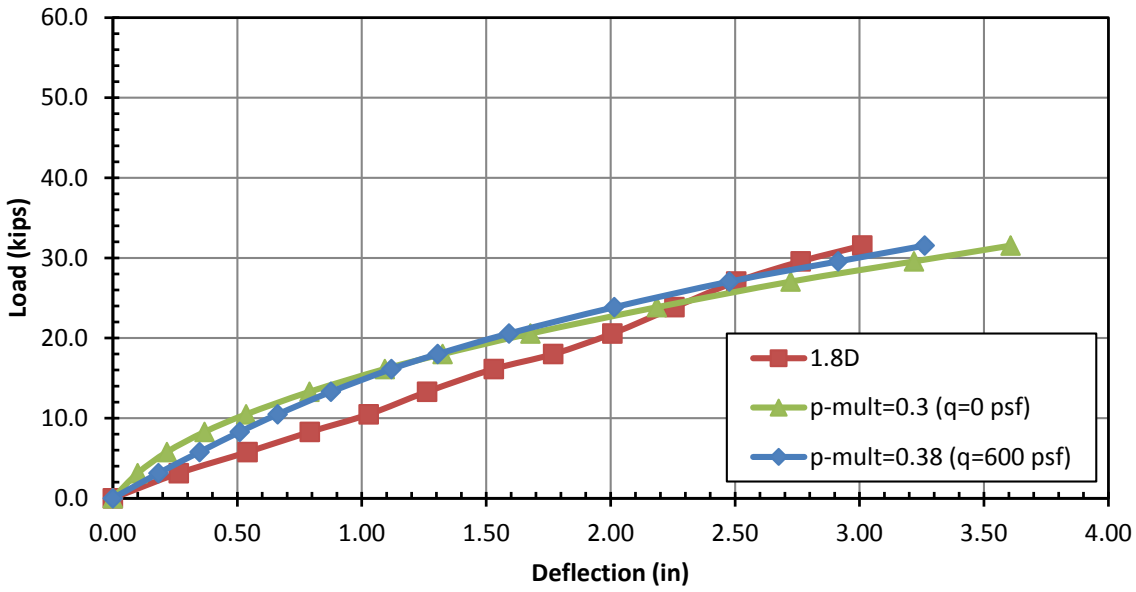

Figure 6-5: Comparison of load-deflection curves between measured and calculated results for the 1.8D test.

In general, the p-multiplier curves with surcharge fit the measured curves better than the non-surcharge curves. However, the field test curve should fit somewhere between the non-surcharge and surcharge curves since the surcharge load was only in a limited area whereas LPILE models the surcharge load as an infinite layer. Both of the LPILE curves fit the measured load-deflection curves reasonably well for the 5.2D and the 3.4D tests. As mentioned previously, the 1.8D test was close enough to the wall that compaction was difficult. As a result, the soil resistance was lower and was likely the reason for lower than expected pile loads. As discussed in section 5.1, low pile loads on the 4.3D test were caused by the hydraulic pump malfunctioning during the first half of the test. Loads from 0 to 1.5 inches of deflection were recorded much lower than what was actually produced. Figure 6-6 shows a comparison of the 15-foot and 20-foot SSL tests for the 4.3D pile and demonstrates that higher loads than those recorded likely occurred during the first half of the 20-foot test. The dashed lines in the figure represent the portion of the 4.3D test

that were recorded low and manually adjusted, but which likely need adjusted to match closer to the 15-foot test.

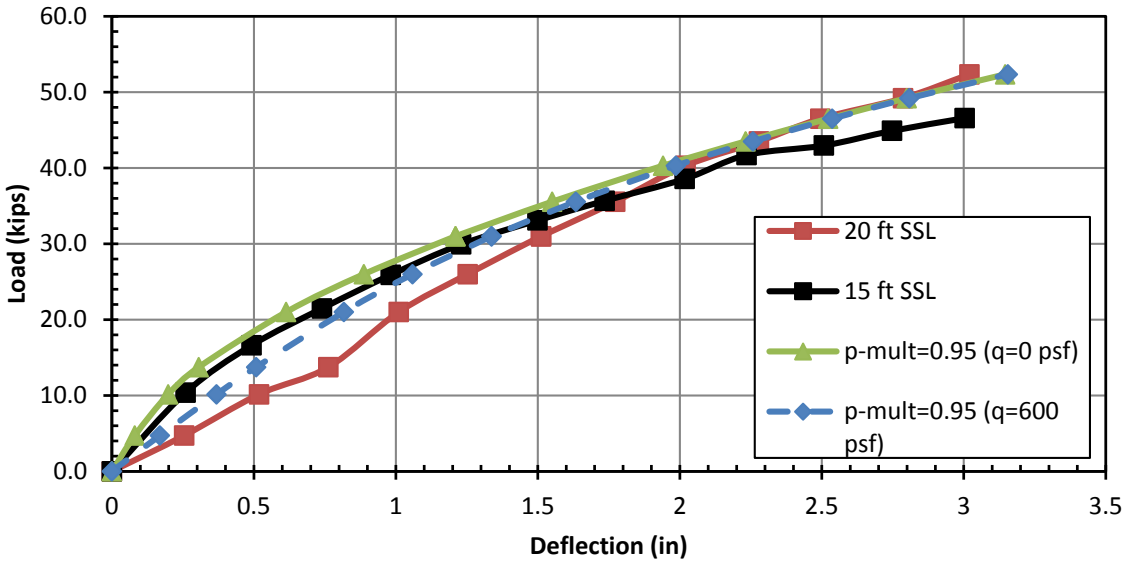

Figure 6-6: Comparison of 4.3D pile load-deflection tests for the 15-foot and 20-foot tests.

6.1.2 P-Multipliers and Pile Spacing Curves

P-multipliers are plotted versus distance from the wall in Figure 6-7 for all load tests on steel piles published to date. P-multipliers used in Figure 6-7 are of the non-surcharge condition to be consistent with other studies. However, this would not change the figure too much because the difference of the p-multiplier values for the different surcharge conditions is relatively small. The piles used for these tests were all round pipe piles ranging in diameter from 12.75 inches to 16.0 inches. A total of 24 p-multiplier points were used in Figure 6-7. The red data points (Nelson 2013, Han 2014, Besendorfer 2015) are test results using galvanized steel strip reinforcement. The blue data points (Price 2012, Hatch 2014, and this test) are test results using the galvanized welded-wire grid reinforcement. All tests have an L/H ratio ranging between 0.72 and 1.42. In general,

neither the L/H ratio nor the type of steel reinforcement used appears to affect the p-multiplier for steel pipe piles behind an MSE wall.

A linear regression analysis was performed to evaluate the p-multiplier as a function of normalized pile spacing data that was a distance of less than four diameters from the wall. The best fit relationship for P_{mult} is given by the equations:

$$P_{mult} = 0.32\frac{S}{D} - 0.23 \qquad \text{for S/D} < 3.9 \qquad (6\text{-}1)$$

$$P_{mult} = 1.0 \qquad \text{for S/D} > 3.9$$

where

S is the distance from the back face of the wall to the center of the pile; and

D is the outside diameter of the pile.

The linear regression equation indicates that a p-multiplier of 1.0 will result from a normalized spacing greater than 3.9. A p-multiplier of 1.0 indicates that the presence of the wall has no effect on the lateral resistance or alternatively that the reinforcement is sufficient to provide as much lateral restraint as if the wall were not present. For normalized spacings less than 3.9 the p-multipliers appear to decrease nearly linearly with normalized distance. The equation for a p-multiplier of less than 3.9 was generated by taking a linear regression of all but two points in Figure 6-7 that were less than 4.0 pile diameters away from the wall. The 2.8D and 2.9D tests by Besendorfer were considered outliers and removed from the equation. By removing the two outliers, the R^2 value increases from 0.79 to 0.89 and the equation is nearly identical to that developed initially. As more data from testing is completed the linear regression equation will be refined and become more accurate.

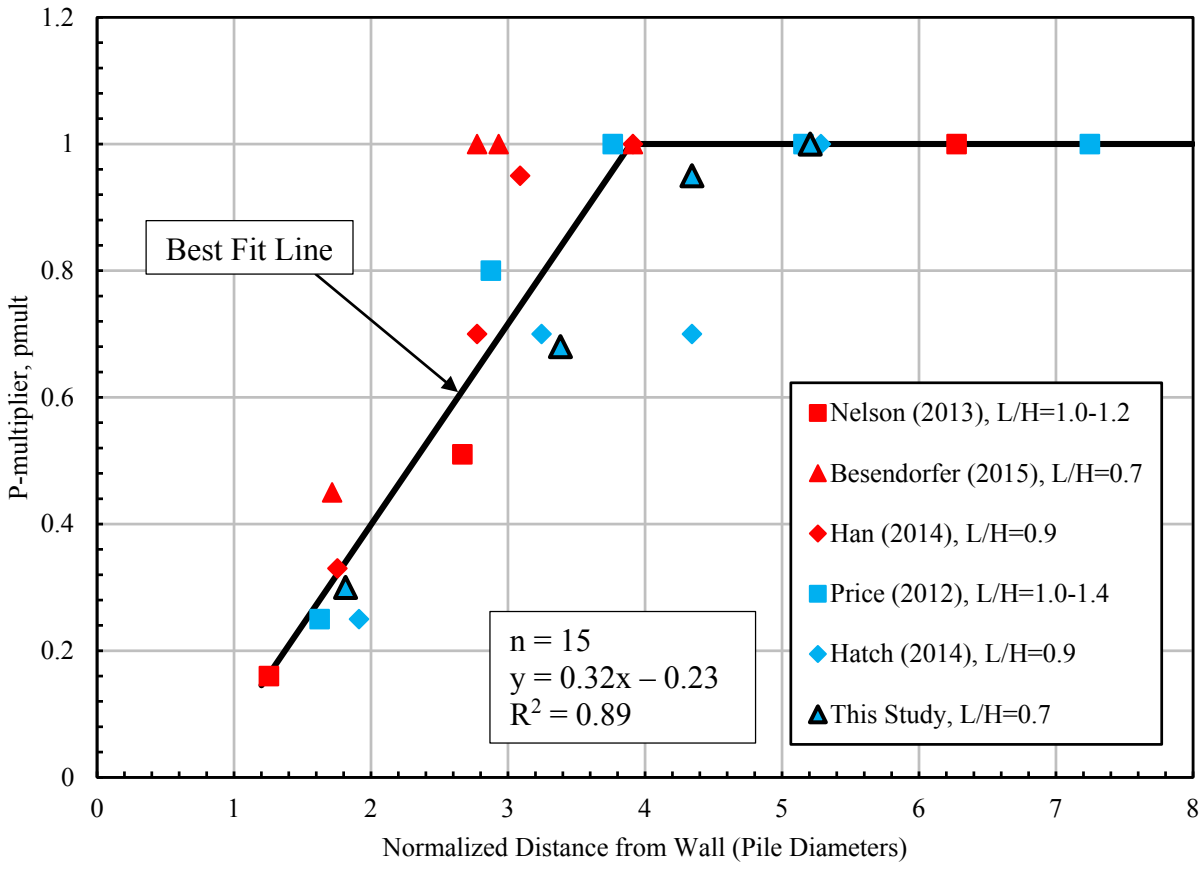

Figure 6-7: P-multiplier curve versus normalized distance for all known steel piles to date.

6.1.3 Pile Head Load versus Rotation Curves

As discussed in Section 5.6, pile head rotation was measured by taking the difference of the deflection measured by the two string potentiometers and using simple trigonometry to solve for the angle of rotation at the load point. The load vs. rotation curves from each test are compared with curves obtained with an LPILE analysis with and without an applied surcharge load in Figure 6-8 through Figure 6-11. In general, the measured curve for each test pile agrees reasonably well with the curves computed by LPILE, with the exception of the 4.3D pile. The 4.3D pile matches well with LPILE analyses after approximately 40 kips of load or 2 inches of pile deflection. As

mentioned in earlier sections, complications were encountered during the 4.3D pile load test when the hydraulic pump yielded unrealistically low normal pressure readings which appear to be in error. Although the load readings were manually corrected for pile head deflections of 1.0 through 1.5 inches, errors in other deflection intervals likely occurred causing lower deflection readings. It should be noted that the 3.4D pile showed negative rotation for the first 0.75 inches of pile deflection. Since this was not the case, 0.25 inches was added to the deflection difference in order to account for the error in the pile rotation. In general, as the distance from the pile to the wall increases the soils ability to resist pile head rotation increases.

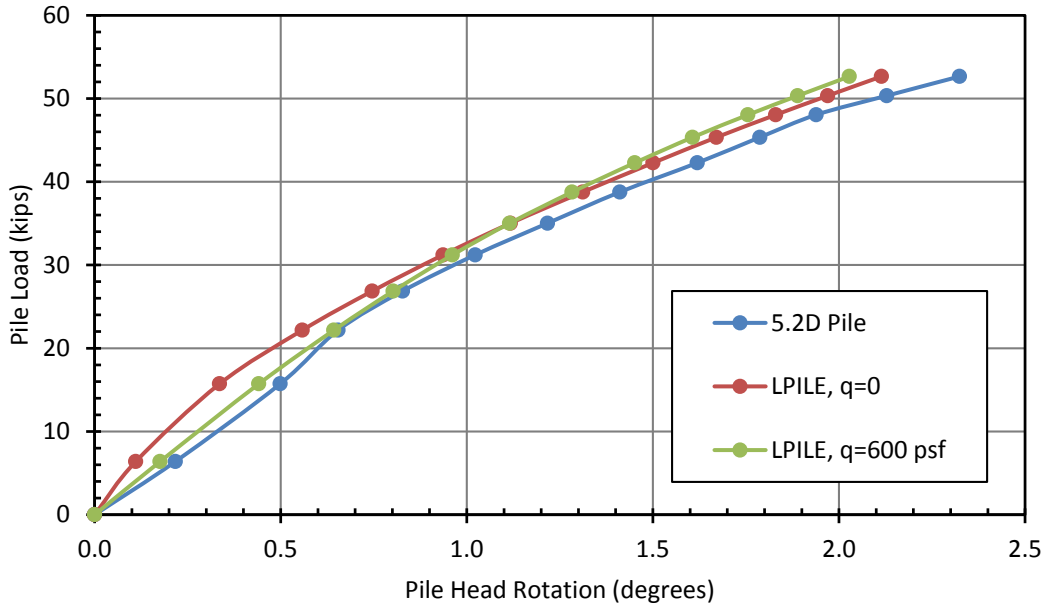

Figure 6-8: Comparison of the pile head load versus pile head rotation for the 5.2D test and LPILE analyses with and without surcharge.

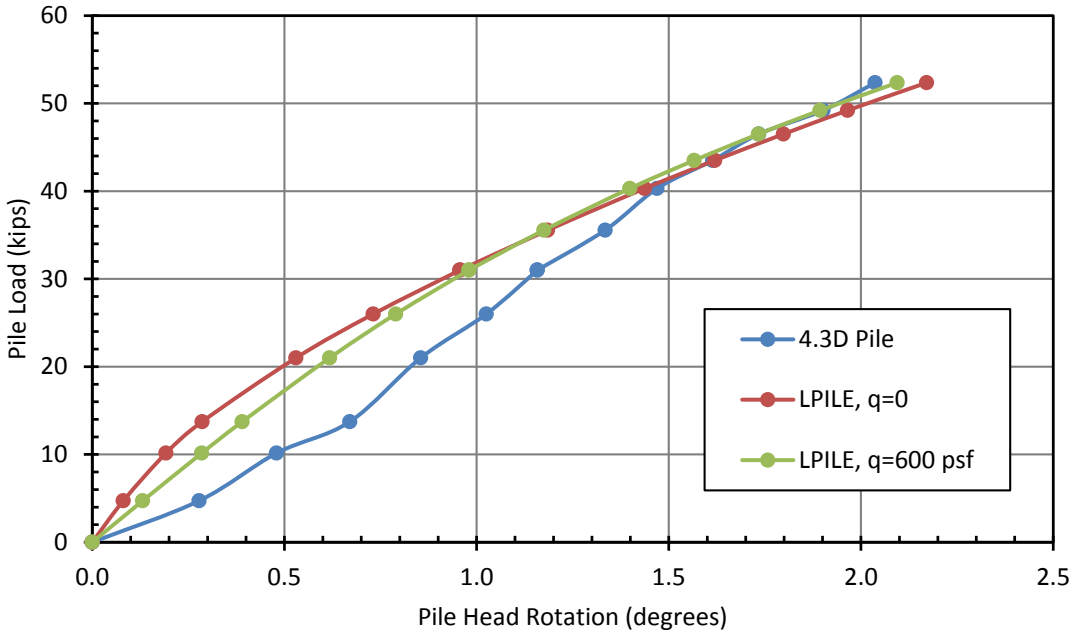

Figure 6-9: Comparison of the pile head load versus pile head rotation for the 4.3D test and LPILE analyses with and without surcharge.

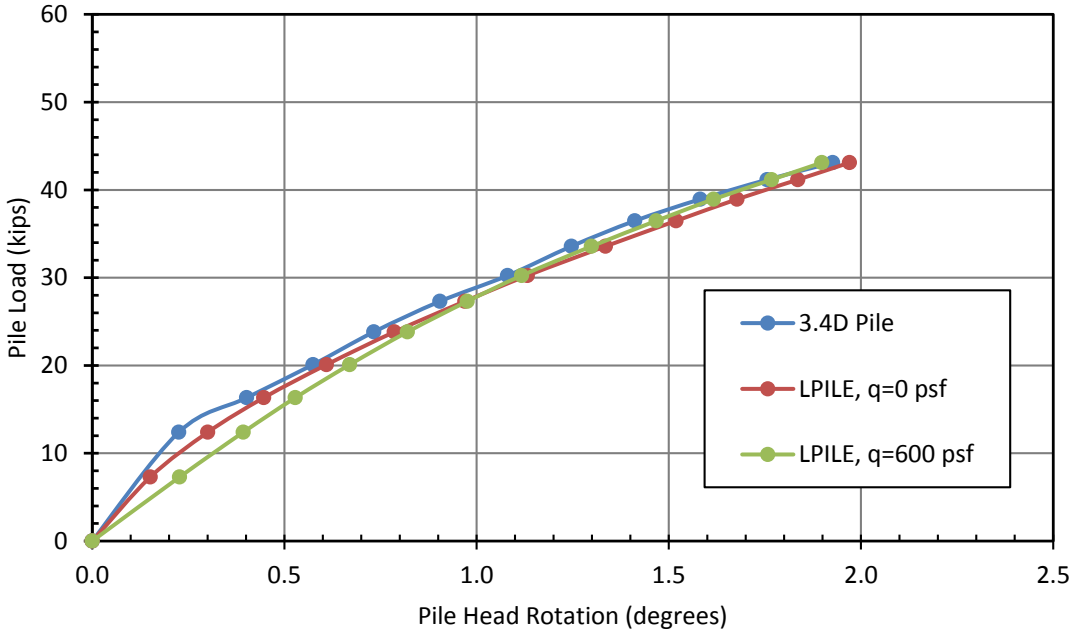

Figure 6-10: Comparison of the pile head load versus pile head rotation for the 3.4D test and LPILE analyses with and without surcharge.

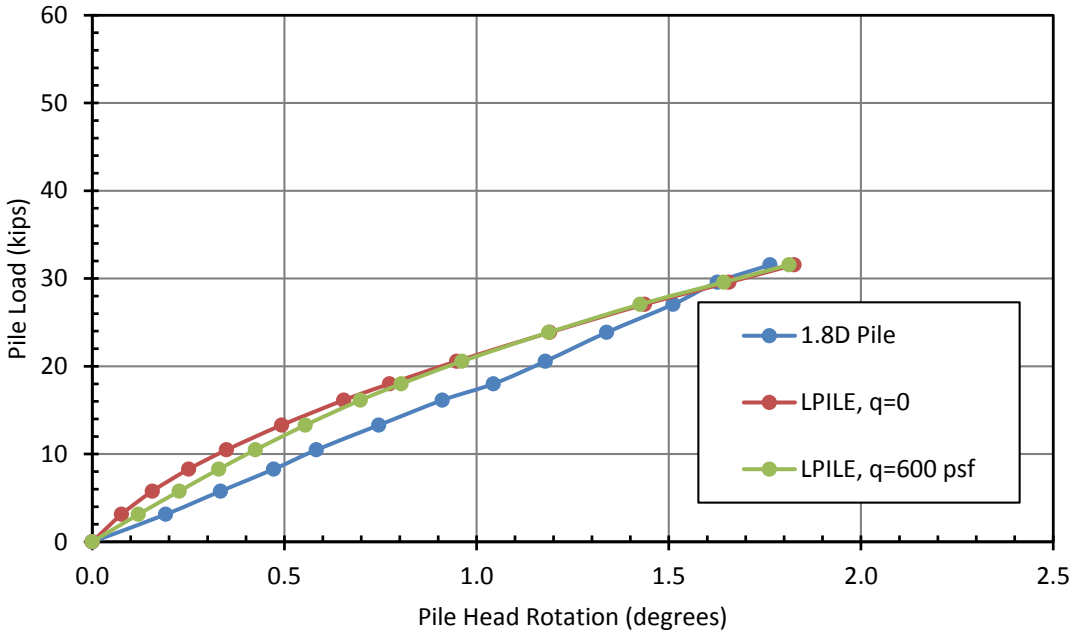

Figure 6-11: Comparison of the pile head load versus pile head rotation for the 1.8D test and LPILE analyses with and without surcharge.

6.1.4 Bending Moment versus Depth Curves

Bending moments along the length of the pile were determined using data from strain gauges obtained during testing and Equation 5-4 as described previously in Section 5.6. LPILE with the back-calculated p-multipliers described previously was also used to calculate bending moment versus depth curves for each pile test with and without surcharge load applied. Bending moment versus depth curves obtained from the strain gauge measurements for the 0.5-inch and 3.0-inch pile head deflection increments are shown in Figure 6-12 through Figure 6-15 along with the curves from the LPILE analyses with and without the applied surcharge load.

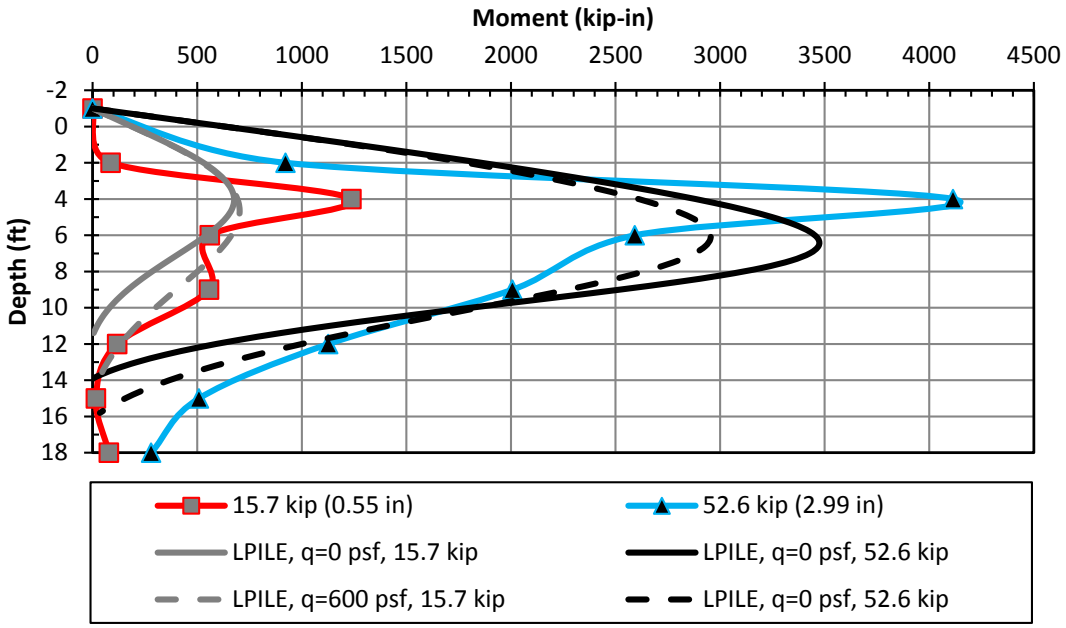

Figure 6-12: Measured and computed pile bending moment for the 5.2D test pile.

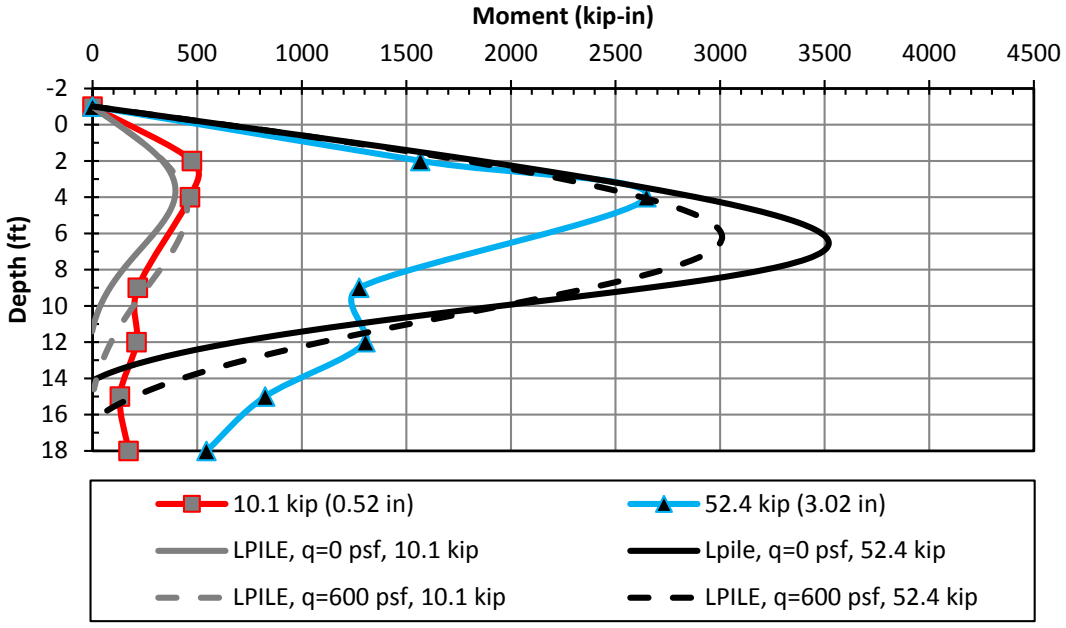

Figure 6-13: Measured and computed pile bending moment for the 4.3D test pile.

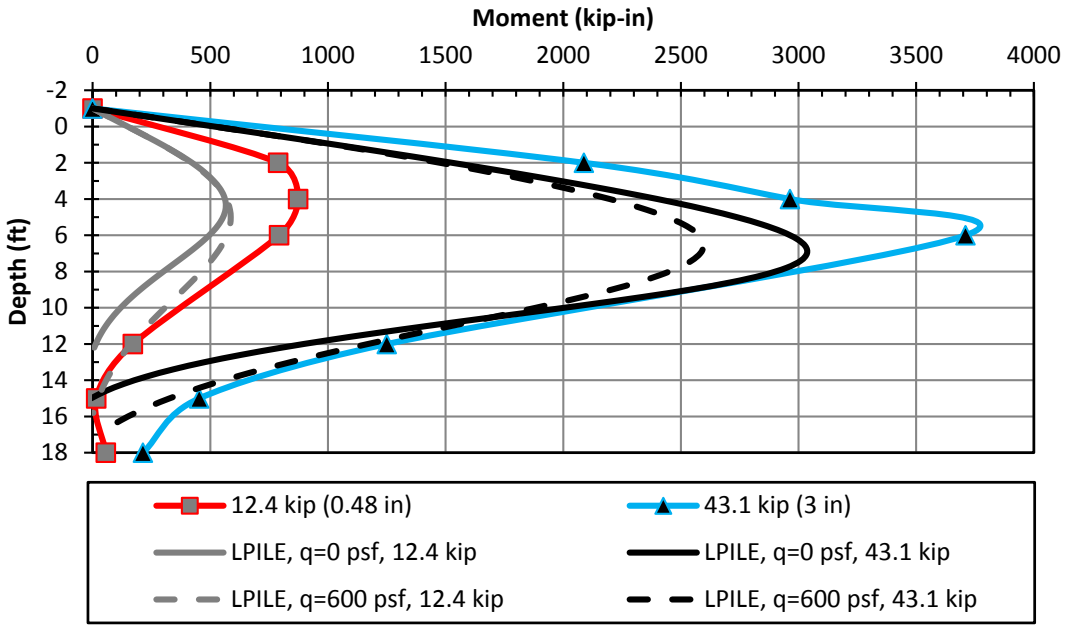

Figure 6-14: Measured and computed pile bending moment for the 3.4D test pile.

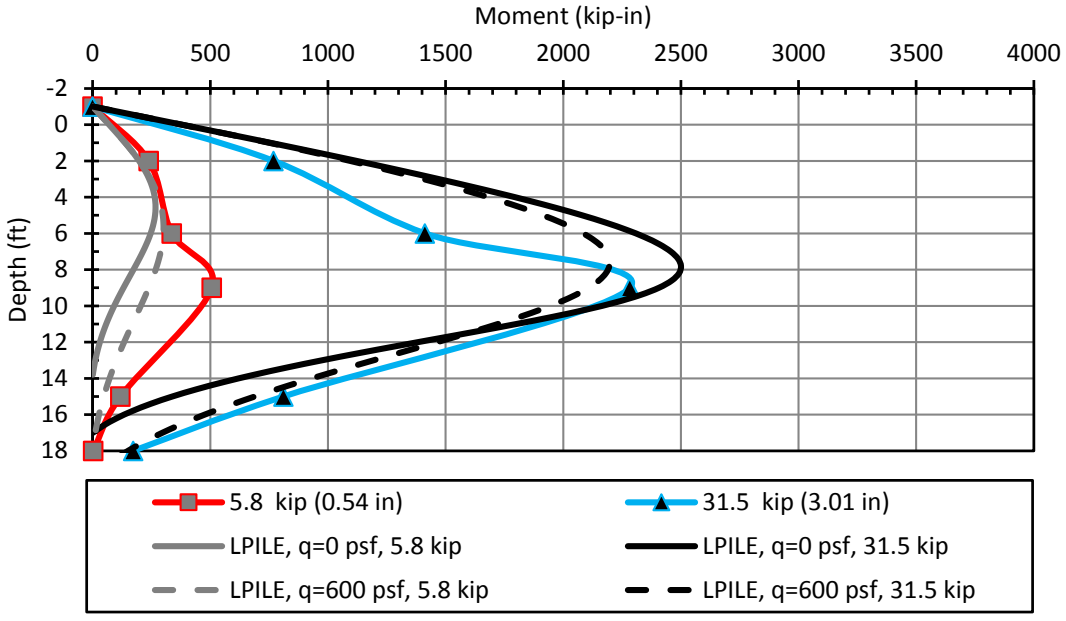

Figure 6-15: Measured and computed pile bending moment for the 1.8D test pile.

In general, the measured maximum bending moment agrees well with the maximum bending moment data calculated by LPILE. The maximum moment depth is defined as the depth where the maximum moment occurs. At three inches of pile head deflection for each test, the measured maximum bending moment is typically within 25% of the LPILE moment envelope created using q=0 psf and q=600 psf for the surcharge load. In addition, the measured depth to the maximum moment is within 2.5 feet of the calculated maximum moment depth for the load associated with three inches of pile head deflection. In cases such as the 4.3D pile, erroneous strain gauge data occurred in the location where LPILE predicted the maximum moment would occur. Therefore, it is likely that the measured maximum moment would be greater and the depth to the maximum moment would be deeper. For the 3.4D and 5.2D tests, both maximum moments are approximately 25% higher than the calculated moments from LPILE. Higher recorded moments could be the result of pile locations being directly behind the center of the panels. The combined panel and soil reinforcement resistance could have caused a higher resistance than the normal soil conditions that LPILE models. Although the difference in the LPILE calculations with and without surcharge loads does not affect the results by much, it gives a good range of where the test pile data should be theoretically, assuming all other variables are constant.

At 0.5 inches of pile head deflection, the measured maximum bending moment for the 1.8D, 3.4D, 4.3D and the 5.2D test piles are 68%, 48%, 5% and 76% more than that calculated by LPILE. The 1.8D measured and calculated maximum bending moments are within 5% of each other to a depth of approximately 6 feet below ground surface, after which the measured forces are much higher. The larger measured bending moment at a depth of nine feet is likely because one of the strain gauges was not reading correctly, so the measured value of the working strain gauge was used as the average value. Measured and calculated bending moments for the 5.2D test pile varied

by as much as 76% in the upper 5 feet, after which the measured and calculated values typically remained within 20% of each other. The depth of the maximum moment is generally within 1.5 feet of the calculated maximum moment depth, with the exception of the 1.8D test which varied by approximately 4 feet. The difference between the measured and calculated maximum moment could be caused by limitations in LPILE to account for soil reinforcement.

7 CONCLUSIONS

Full-scale load tests were performed on four 12.75”x0.375” pipe piles spaced at distances of 1.8, 3.4, 4.3 and 5.2 pipe diameters behind a 20-ft high MSE wall. The purpose of this study was to measure reduced lateral pile load displacement curves for piles at varying distance from an MSE wall; measure the distribution of reinforcement tensile force induced by lateral pile loading; develop reduction factors to account for reduced pile resistance based on spacing and reinforcement type; and to develop a design approach to predict reinforcement loads induced by pile loading. This chapter addresses conclusions made from this study regarding lateral pile resistance and induced forces in soil reinforcement and provides recommendations for further research.

7.1 Conclusions Regarding Steel Pipe Pile and MSE Wall Interaction

1. Lateral pile resistance decreases as pile spacing behind the MSE wall decreases below about four pile diameters behind the wall. Relative to the pile furthest from the wall, average pile load decreased approximately 4, 21 and 51 percent for piles spaced at 4.3D, 3.4D and 1.8D from the MSE wall face, respectively.
2. For similarly loaded piles, pile head rotation also decreases as pile spacing increases.
3. Based on this study and previous test data, a simple p-multiplier approach provides reasonably accurate estimates of lateral load-displacement curves as well as bending

moment versus depth curves. Lateral soil resistance remains relatively constant (p-multiplier of 1.0) for piles located greater than approximately 3.9 pile diameters (3.9D) behind an MSE wall with inextensible reinforcements. For piles spaced closer than 3.9D, a linear reduction in the p-multiplier was observed.

4. Reinforcement length to height (L/H) ratios and inextensible reinforcement types do not appear to significantly affect p-multiplier relationships.
5. In contrast to tests involving extensible (geosynthetic) reinforcements, lateral wall deformation for the concrete MSE wall panels were generally less than 0.4 inches with the inextensible reinforcements even at large pile head loads (60 kips) and deflections (3 inches).

7.2 Conclusions Regarding Pile and Welded-Wire Grid Reinforcement Interaction

1. Maximum tensile forces occur in the soil reinforcement near the pile location.
2. Maximum induced tensile forces increase as pile loads and pile distance from the wall face increase.
3. Maximum tensile forces decrease as transverse distances between the soil reinforcement and the pile center increase.
4. The statistical regression equation developed in this study accounts for approximately 79% of the variation in maximum induced tensile force for all welded-wire grid reinforcements tested to date. Variables affecting maximum induced tensile force are pile load, transverse distance from the pile load, vertical stress, pile spacing and L/H ratio.

7.3 Recommendations for Further Research

Piles for this study were loaded laterally using a pinned head connection. However, a fixed head connection is more representative of real life construction as piles are grouped together by a pile cap supporting a bridge abutment. A fixed connection would hinder pile head rotation and would create a different load distribution induced in the soil reinforcement. Research has shown that laterally loaded pile groups have a reduced resistance capacity in comparison with single piles (Rollins et al. 2006). Therefore, a group pile test is recommended behind an MSE wall to understand the differences that fixed and pinned head connections have on the induced load capacities of the reinforcement and to understand if reduction factors for pile groups behind an MSE wall are similar to those previously studied.

Piles for this study were loaded at ¼ in. cumulative deflection intervals that represent static loading conditions. Lateral loading of piles supporting a bridge abutment typically comes from thermal expansion or earthquake loads, both of which are cyclic loads. It is recommended that further full-scale testing be performed on piles behind MSE walls representing cyclic loads and their effects on induced forces in soil reinforcement and wall deflection.

Backfill compaction was approximately 92% between the test piles and the back face of the wall. Compaction affects the lateral resistance of the loaded pile, as well as the soil's ability to resist pullout of the reinforcement. During construction of MSE walls it may be hard to achieve exact compaction of backfill according to specifications and it is more likely that a range of relative compaction actually occurs near the face. Therefore, it is recommended that further testing behind an MSE wall be performed on piles spaced equal distances behind the back face of the wall with varied relative compaction. Data from compaction tests could then be used to calculate a range of

p-multipliers and reinforcement loads based on relative compaction for a specified pile spacing and correlations made for different pile spacings.

Piles located behind wall joints appeared to increase wall deflection and induced load in soil reinforcements compared with those located behind the center of the wall panel. Further research could be performed to better understand the relationship between pile location and wall joint location and to include a location reduction factor, if needed.

REFERENCES

API Recommended Practice for Planning, Designing, and Constructing Fixed Offshore Platforms. (1982). American Petroleum Institute, 13th Edition, Washington, D.C.

Berg, R.R., Christopher, B.R., and Samtani, N.C. (2009). "Design of Mechanically Stabilized Earth Walls and Reinforced Soil Slopes" *FHWA, Washington, D.C., Report No. FHWA-NHI-10-024.*

Besendorfer, J. (2015). "Lateral Resistance of Pipe Piles Near 20-ft Tall MSE Abutment Wall with Strip Reinforcements" MS Thesis, Department of Civil and Environmental Engineering, Brigham Young University, Provo, UT.

Han, J. (2014). "Lateral Resistance of Piles Near 15 Foot Vertical MSE Abutment Walls Reinforced with Ribbed Steel Strips" MS Thesis, Department of Civil and Environmental Engineering, Brigham Young University, Provo, UT.

Hatch, C. (2014). "Lateral Resistance of Piles Near Vertical MSE Abutment Walls" MS Thesis, Department of Civil and Environmental Engineering, Brigham Young University, Provo, UT.

Hild, F., and Roux, S. (2006). "Digital Image Correlation: from Displacement Measurement to Identification of Elastic Properties - a Review." Strain, 42(2), 69–80.

Isenhower, W.M., Wang S. (2015). "Technical Manual for LPILE 2015 (Using Data Format Version 8)", Ensoft Inc., Austin, TX.

Lawson, W., Jayawickrama, P., Wood, T., and Surles, J. (2013). "Pullout Resistance Factors for Inextensible Mechanically Stabilized Earth Reinforcements in Sandy Backfill." *Transportation Research Record: Journal of the Transportation Research Board*, 2363, 21–29.

"Measurement Principles of DIC." *Digital Image Correlation (DIC) Measurement Principles*, <http://www.dantecdynamics.com/measurement-principles-of-dic> (Aug. 11, 2015).

Nelson, K.R. (2013). “Lateral Resistance of Piles Near Vertical MSE Abutment Walls at Provo Center Street” MS Thesis, Department of Civil and Environmental Engineering, Brigham Young University, Provo, UT.

Parsons, R. L., Pierson, M., Han, J., Brennan, J. J., and Brown, D. A. (2009). “Lateral Load Capacity of Cast-in-Place Shafts behind an MSE Wall.” *Contemporary Topics in In Situ Testing, Analysis, and Reliability of Foundations*.

Pierson, M., Parsons, R. L., Han, J., Brown, D., and Thompson, W. R. (2009). “Capacity of Laterally Loaded Shafts Constructed Behind the Face of a Mechanically Stabilized Earth Block Wall”, *Kansas Department of Transportation, Report No. K-TRAN: KU-07-6.*

Pierson, M. C., Parsons, R. L., Han, J., Brennan, J. J., and Huang, J. (2011). “Influence of Geogrid Stiffness on Shaft Lateral Capacities and Deflections behind an MSE Wall.” Geo-Frontiers 2011.

Price, J.S. (2012). “Lateral Resistance of Piles Near Vertical MSE Abutment Walls” MS Thesis, Department of Civil and Environmental Engineering, Brigham Young University, Provo, UT.

Rollins, K. M., Olsen, K. G., Jensen, D. H., Garrett, B. H., Olsen, R. J., and Egbert, J. J. (2006). “Pile Spacing Effects on Lateral Pile Group Behavior: Analysis.” *J. Geotech. Geoenviron. Eng. Journal of Geotechnical and Geoenvironmental Engineering*, 132(10), 1272–1283.

Rollins, K.M., Price, J.S., and Nelson, K.R. (2013). “Lateral Resistance of Piles Near Vertical MSE Abutment Walls”, *Utah Department of Transportation, Report No. UT-1X.13*.

Source: “Test Site.” 40°27’14.08” N and 111°53’53.60” W. GOOGLE EARTH. June 4, 2013. June 15, 2015.

APPENDIX A – PULLOUT CALCULATIONS

MSE Wall- Phase 2

MSE Wall Properties

Wall Height	H	20	ft
Total Height	H_1	24.8	ft
Panel Width	w_p	9.94	ft
Panel Height	h_p	4.94	ft
Reinforcements per Panel Along Wall Length		2	

$$H_1 = H + H_{eq}$$

Soil Properties

Reinforced Backfill Moist Unit Weight	γ_r	126.2	pcf
Friction Angle	ϕ_r'	38	deg
		0.66	rad
Active Earth Pressure Coefficient	K_a	0.238	[Eqn. 4-25]

$$K_a = \tan^2\left(45 - \phi_r'/2\right)$$

Grid Reinforcement Properties

Approximate Vertical Spacing	S_v	2.5	ft
Approximate Horizontal Spacing	S_h	5	ft
Length of Reinforcement	L	18	ft
Longitudinal Grid Spacing	S_l	8	in
Scale Effect Correction Factor	α	1	[p. 3-16]
Reinforcement Effective Unit Perimeter	C	2	[pp. 3-16, 4-49]
Nominal Transverse Wire Thickness, W11	t	0.374	in

$$F^* = 20(t/S_t) \qquad F^* = 10(t/S_t)$$

Boundaries for			
Depth Below Top of wall, Z	K_r/K_a	F* (Top Layer)	F* (Other Layers)
0	2.5	1.247	0.623
20	1.2	0.623	0.312

Depth, Z [ft]		rcement Length in Resistance Zone,	
at Z = 0	0	10.57	$L_e = L - 0.3H_1$
at Z = $H_1/2$	12.38	10.57	$L_e = L - 0.3H_1$
at Z = H_1	24.8	18	$L_e = L$

$$L = L_a + L_e \qquad L_a = 0.3H$$

Surcharge

Unit Weight of Surcharge	γ_{eq}	126.2	pcf
Equivalent Surcharge Height	H_{eq}	4.8	ft
Surcharge (Dead Load)	q	600	psf

Load Factor for Maximum Permanent Loads	$\gamma_{EV\text{-}MAX}$	1.35	[Table 4-2]
Resistance Factor for Pullout	ϕ_p	0.9	[Table 4-7]

			[Fig. 4-10]			[Sim. to Eqn. 4-3	[Eqn. 4-32a]		[Eqns. 3-6, 3-7]	[Fig. 4-9 and Eqns. 4-37, 4-40]		[Fig. 3-3]	[Fig. 3-3]	[Sim. to Eqn. 4-35]	
Reinforcement Level	Wire Type	Depth to Layer, Z [ft]	K_r/K_a	Horizontal Earth Pressure Coefficient, K_r	Vertical Stress, $\sigma_v=\gamma_r(Z+H_{eq})$ [psf]	Factored Horizontal Stress, $\sigma_H=K_r(\gamma_r(Z+h_{eq}))\gamma_{EV\text{-}MAX}$ [psf]	Reinforcement Demand, $T_{max}=\sigma_H(Sv)$ [k/ft]	Transverse Grid Spacing, S_t [in]	Reinforcement Pullout Friction Factor, F*	Length of Reinforcement in Resistance Zone, L_e [ft]	Length of Reinforcement in Active Zone, L_a [ft]	Grid Reinforcement Width, b [ft]	Grid Reinforcement Coverage Ratio, $R_c=b/S_h$	Factored Pullout Resistance, $P_r=\phi_p F^* \alpha \sigma_v L_e C R_c$ [k/ft]	Capacity to Demand Ratio, $CDR=P_r/T_{max}$
1	1X0.50	1.25	2.42	0.58	758	589	1.47	6	1.208	10.57	7.43	3.33	0.667	11.61	7.89
2	1X1.00	3.75	2.26	0.54	1073	778	1.94	12	0.565	10.57	7.43	2.67	0.533	6.15	3.17
3	1X1.00	6.25	2.09	0.50	1389	934	2.33	12	0.526	10.57	7.43	2.67	0.533	7.41	3.18
4	1X1.00	8.75	1.93	0.46	1704	1057	2.64	12	0.487	10.57	7.43	2.67	0.533	8.42	3.19
5	1X1.00	11.25	1.77	0.42	2020	1147	2.87	12	0.448	10.57	7.43	2.67	0.533	9.19	3.20
6	1X1.00	13.75	1.61	0.38	2335	1205	3.01	12	0.409	11.40	6.60	3.33	0.667	13.07	4.34
7	1X1.00	16.25	1.44	0.34	2651	1229	3.07	12	0.370	12.90	5.10	3.33	0.667	15.18	4.94
8	1X1.00	18.75	1.28	0.30	2966	1221	3.05	12	0.331	14.40	3.60	3.33	0.667	16.97	5.56
														Average CDR:	**4.43**

APPENDIX B – MSE WALL PLANS

APPENDIX C – LABORATORY RESULTS FOR BACKFILL PROPERTIES

GENEVA ROCK PRODUCTS, INC.
1565 West 400 North • P.O. Box 538 • Orem, UT 84059 • (801) 765-7800 • Fax (801) 765-7830 • www.genevarock.com

AGGREGATE SUBMITTAL

Report of Physical Properties

GRP Material Description: Fill - 3/8" HARDPAC
GRP Material Code: FINE
Source Location/Code: North Hansen / 527
Report Date: April 15, 2014
Reviewed by: Victor Johnson
Report No. 527FINE00114

TEST RESULTS

Standard	PHYSICAL PROPERTIES		Result	Test Source
ASTM C 29 AASHTO T19	Unit Weight	Unit Weight, lbs./cu.ft. =	112.0	
		Voids, % =	30	
		☐ Jigged ☐ Loose ☑ Rodded		
ASTM D1557 AASHTO T180	Modified Proctor	Max. density, lbs./cu.ft. =	133.0	
		Optimum Moisture, % =	7	
ASTM D698 AASHTO T99	Standard Proctor	Max. density, lbs./cu.ft. =	128.0	
		Optimum Moisture, % =	7.6	
ASTM D4318 AASHTO T89/90	Liquid Limit	Liquid Limit=	0	
	Plastic Limit	Plastic Limit=	0	
	Plasticity Index	Plasticity Index=	NP	
ASTM C131 AASHTO T96	L.A. Abrasion	Small Coarse Loss, % =		
		Grading/Revolutions, =		
ASTM C535	L.A. Abrasion	Large Coarse Loss, % =		
		Grading/Revolutions, =		
ASTM C 128 AASHTO T84	Fine Specific Gravity & Absorption	Bulk Specific Gravity (dry) =	2.581	
		Bulk Specific Gravity, SSD =	2.599	
		Apparent Specific Gravity =	2.628	
		Absorption, % =	0.7	
ASTM C 127 AASHTO T85	Coarse Specific Gravity & Absorption	Bulk Specific Gravity (dry) =		
		Bulk Specific Gravity, SSD =		
		Apparent Specific Gravity =		
		Absorption, % =		
ASTM D2419 AASHTO T176	Sand Equivalent	Sand Equivalent, % =	34	
ASTM C 88 AASHTO T104	Soundness	Coarse Soundness Loss, % =		
		Magnesium No. of Cycles =		
	Soundness	Fine Soundness Loss, % =	1.0	
		Sodium Sulfate No. of Cycles =		
ASTM C 1252 AASHTO T304	Fine Aggregate Angularity	Uncompacted Voids, % =	48.3	
		Method C (as received material)		
ASTM C40 AASHTO T21	Organic Impurities	Coarse Aggregate, % =	Lighter Plate # 1	
		Fine Aggregate, % =		
ASTM C142 AASHTO T112	Clay / Friable Particles	Coarse Aggregate, % =		
		Fine Aggregate, % =	0.0	
ASTM C123 AASHTO T113	Lightweight Pieces	Coarse Aggregate, % =		
		Fine Aggregate, % =		
ASTM D1883 AASHTO T193	CBR	Surcharge = 10 lbs. CBR @ 0.1"=	50	
		Swell% = 0.0% CBR @ 0.2"=	99	
ASTM D5821	Fractured Face	1 or 2 Faces =		
		Fractured Face, % =		
ASTM D2487	Soil Classification	Group Symbol =	GW-GM	
		Group Name =	Well-graded gravel with silt and sand	
ASTM D2488	Soil Description & Identification	Group Symbol =	Cu=66.7 Cc=1.8	
		Group Name =		

SIEVE ANALYSIS

ASTM C136 AASHTO T27

Sieve Size	% Passing	Spec.
450 mm (18")		
375 mm (15")		
300 mm (12")		
250 mm (10")		
225 mm (9")		
200 mm (8")		
150 mm (6")		
125 mm (5")		
100 mm (4")		
75.0 mm (3")		
63.0 mm (2-1/2")		
50.0 mm (2")		
37.5 mm (1-1/2")		
25.0 mm (1")		
19.0 mm (3/4")		
12.5 mm (1/2")	100	
9.5 mm (3/8")	100	
6.3 mm (1/4")		
4.75 mm (No.4)	77	
2.36 mm (No.8)	52	
2.00 mm (No.10)		
1.18 mm (No.16)	37	
0.600 mm (No.30)	30	
0.425 mm (No.40)		
0.300 mm (No.50)	25	
0.180 mm (No.80)		
0.150 mm (No.100)	20	
0.075 mm (No.200)	14	
ASTM D422 Hydrometer =		
ASTM C566 AASHTO T255 Moisture Content, % =		
ASTM C136 AASHTO T27 Fineness Modulus (FM) =		
AASHTO M145 Classification of Soils =	A1B	
ASTM D4791 Ratio = Flat & Elongated =		

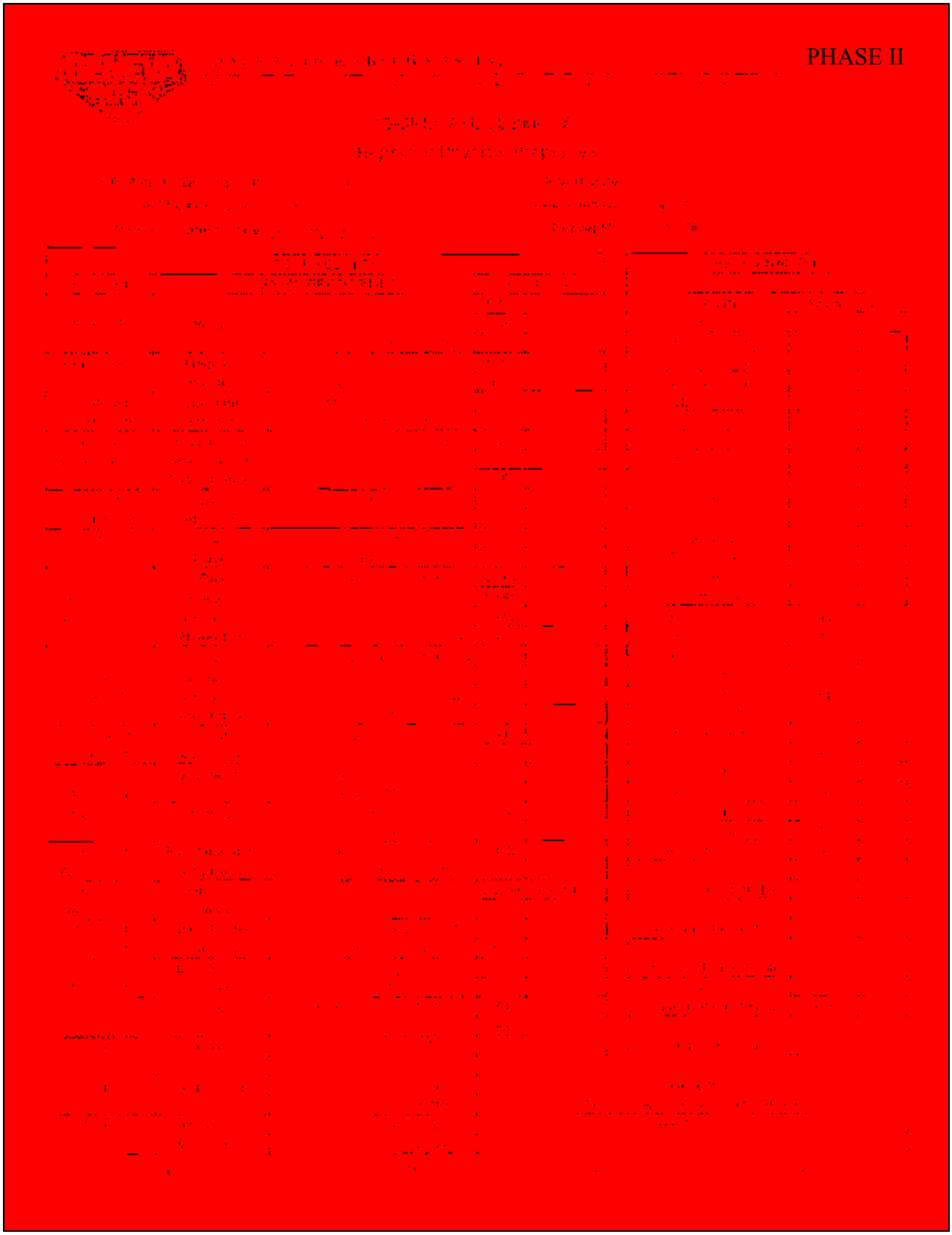
PHASE II

APPENDIX D – LOAD-DEFLECTION CURVES

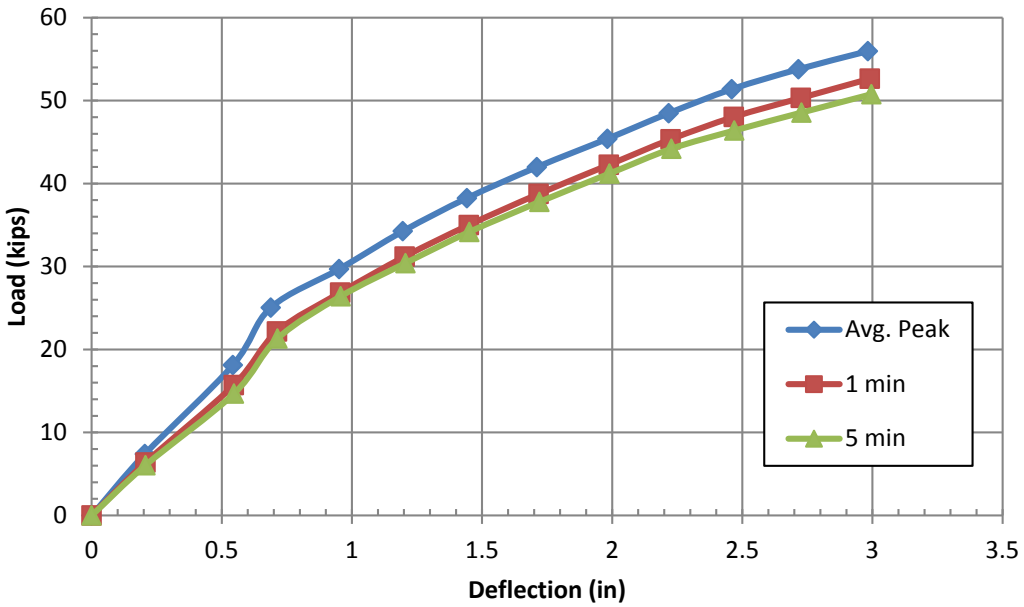

Figure D-1: Load-deflection curves for the 5.2D test.

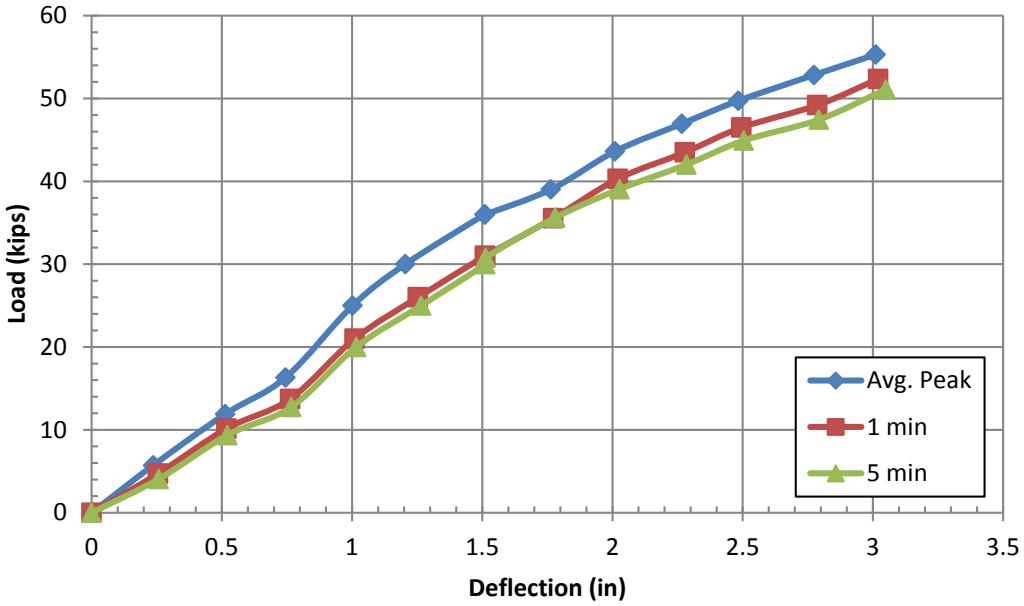

Figure D-2: Load-deflection curves for the 4.3D test.

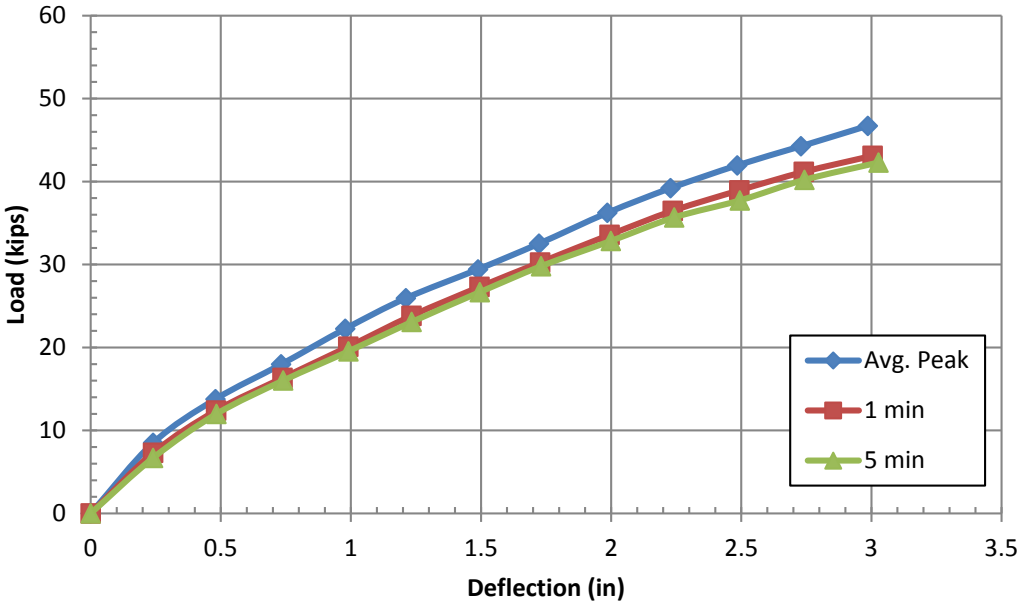

Figure D-3: Load-deflection curves for the 3.4D test.

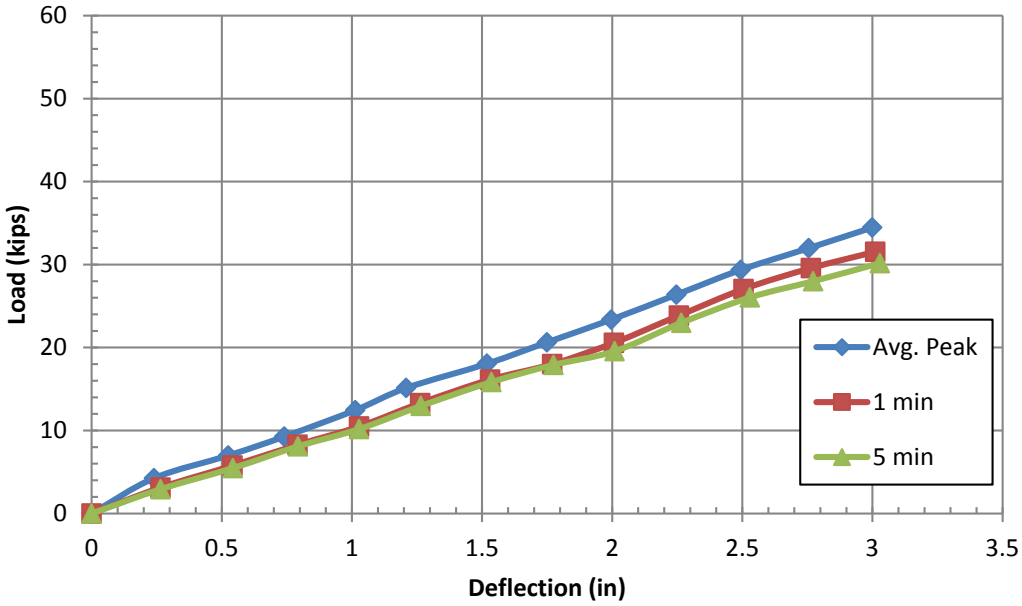

Figure D-4: Load-deflection curves for the 1.8D test.

APPENDIX E – GROUND DISPLACEMENT CURVES

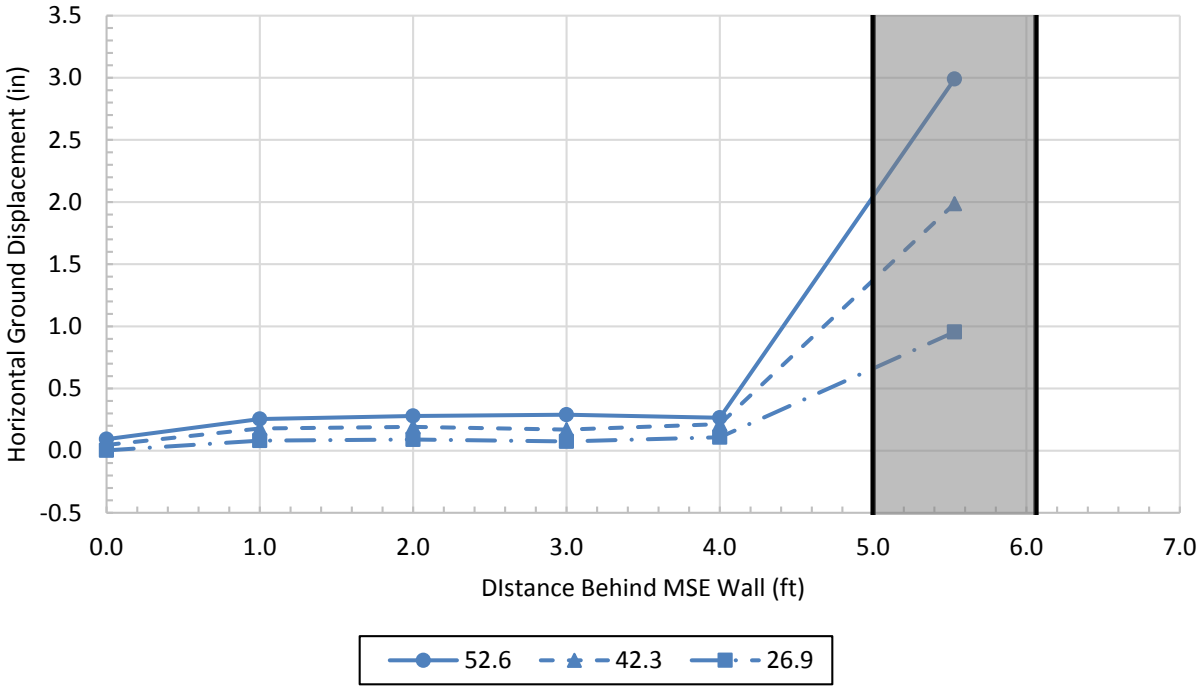

Figure E-1: Horizontal ground displacement for the 5.2D test.

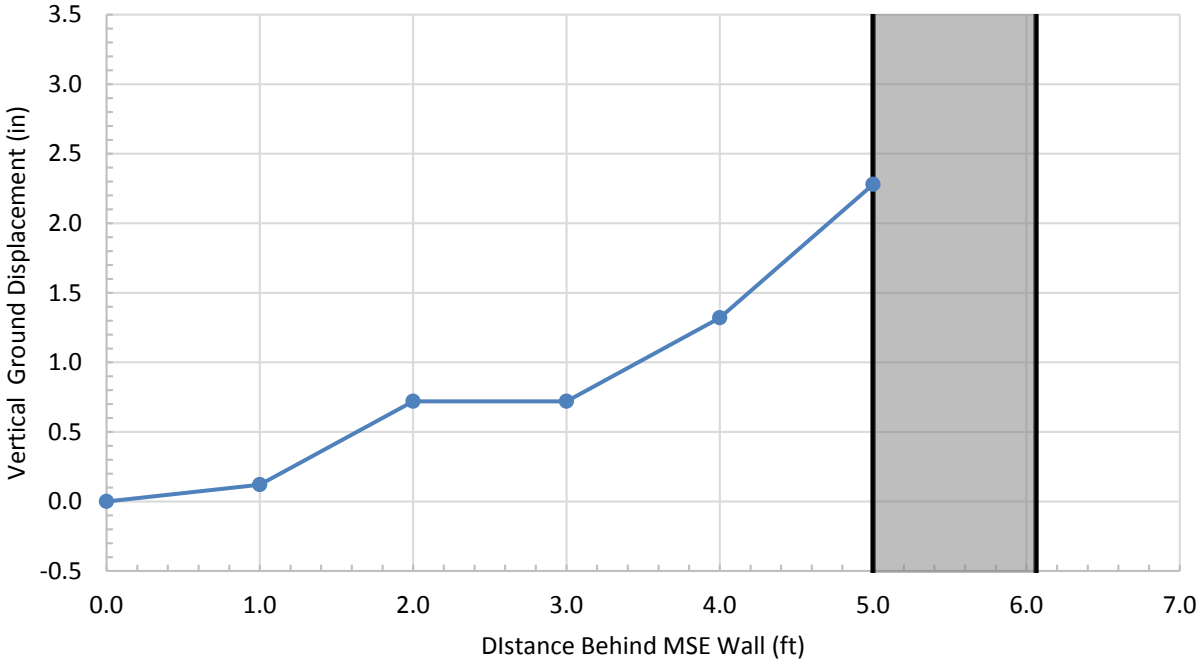

Figure E-2: Vertical ground displacement for the 5.2D test.

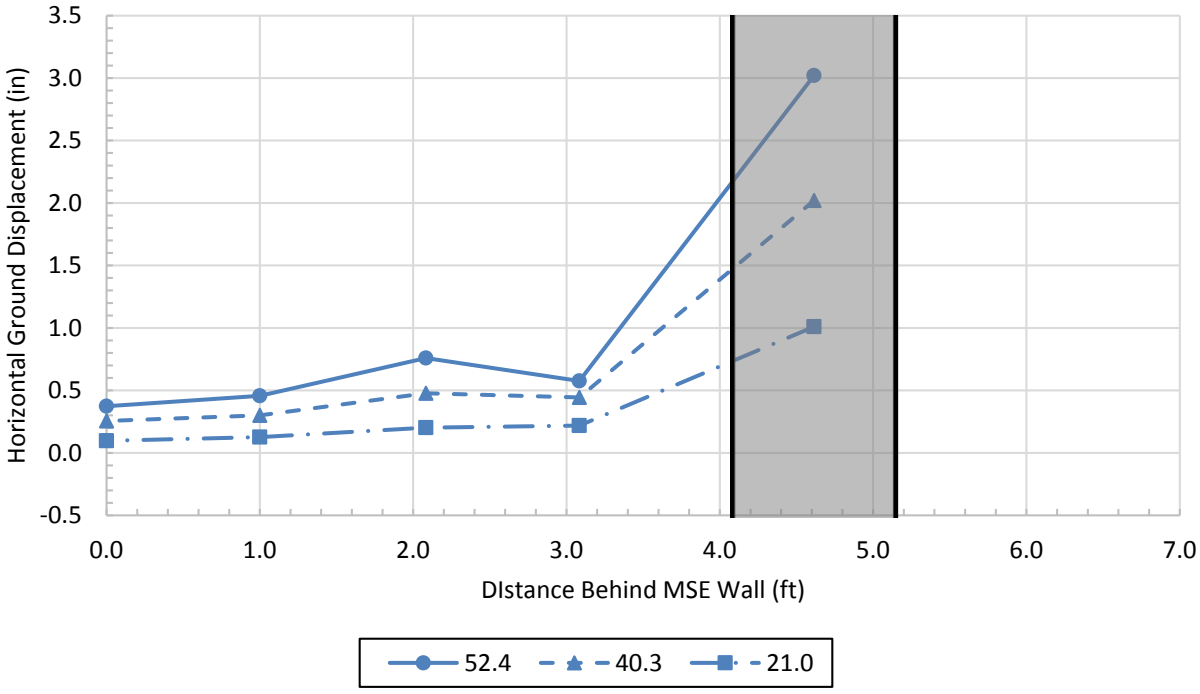

Figure E-3: Horizontal ground displacement for the 4.3D test.

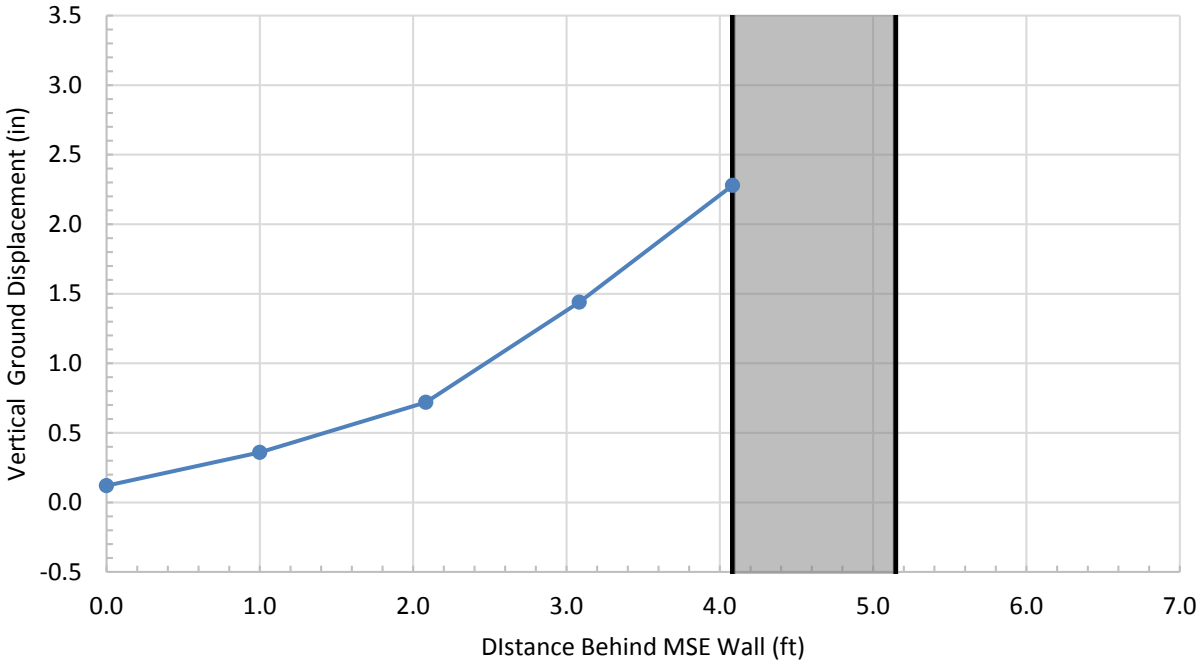

Figure E-4: Vertical ground displacement for the 4.3D test.

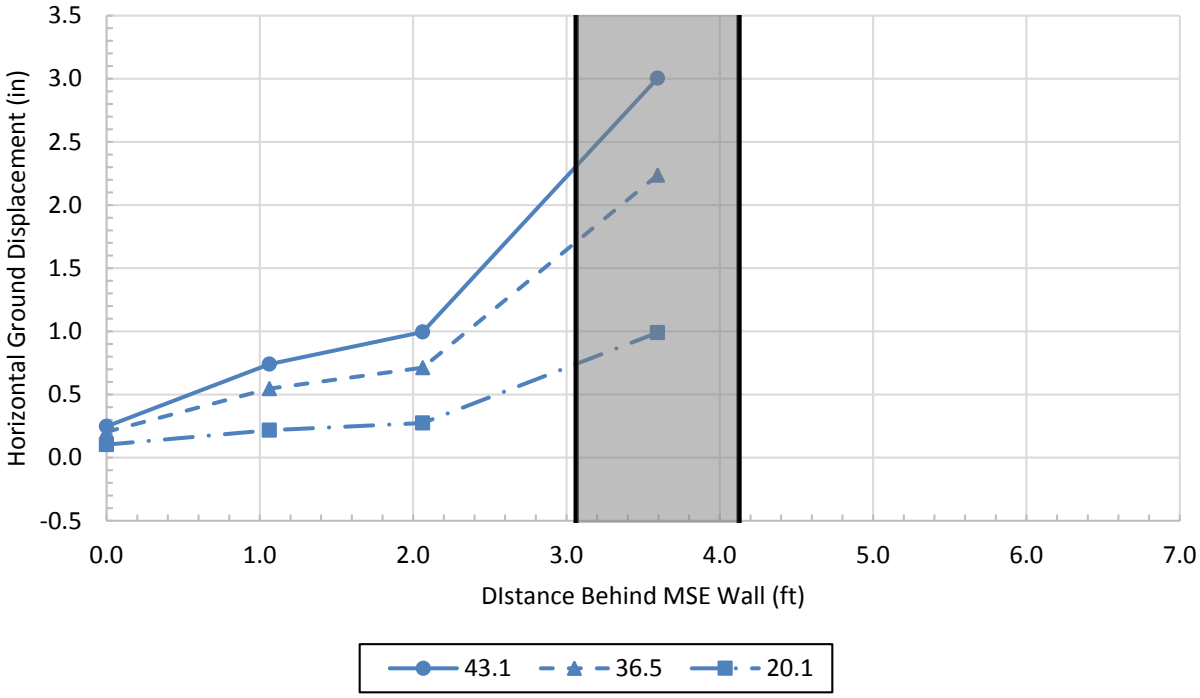

Figure E-5: Horizontal ground displacement for the 3.4D test.

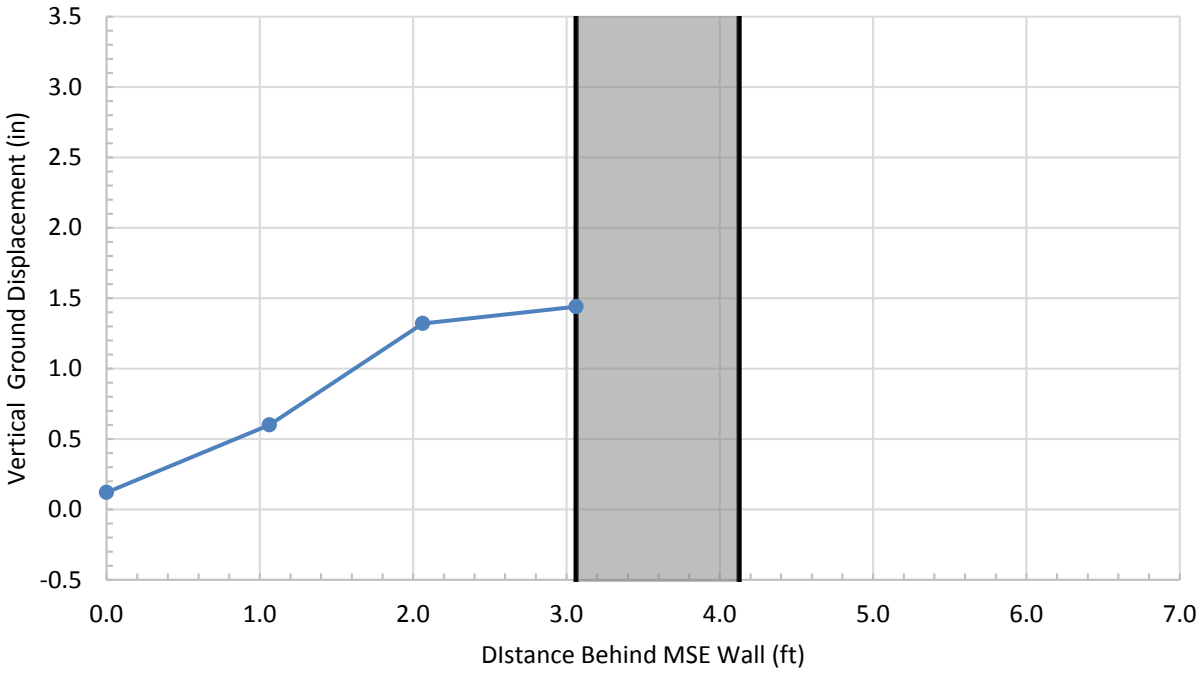

Figure E-6: Vertical ground displacement for the 3.4D test.

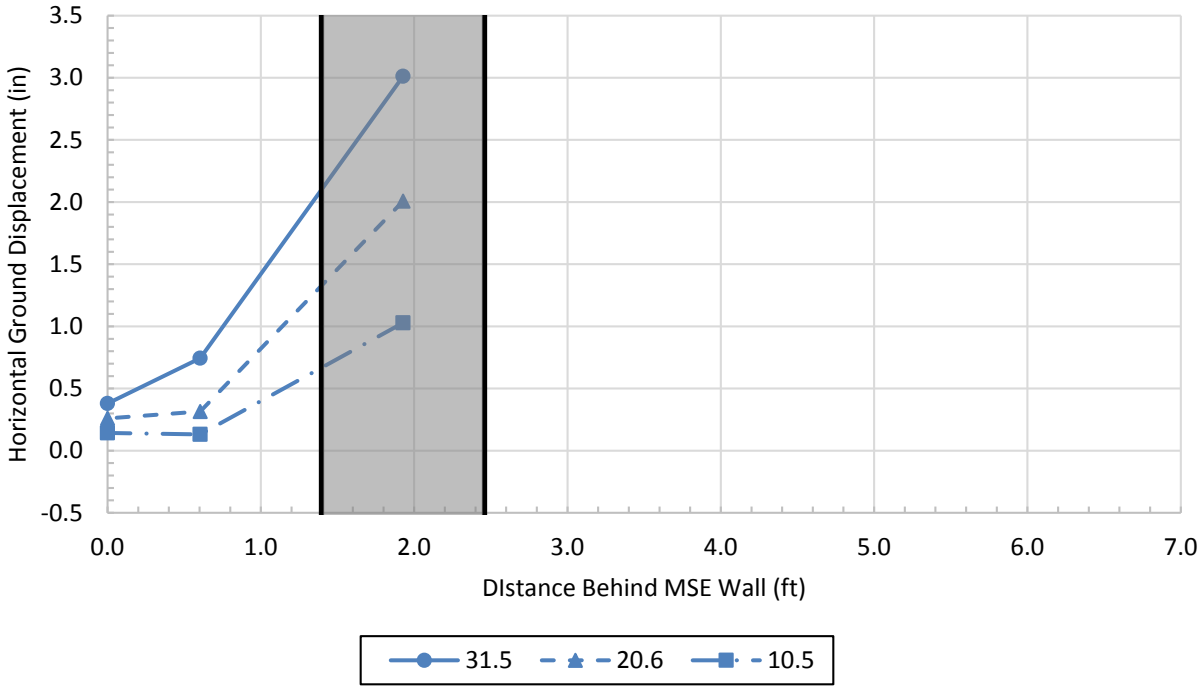

Figure E-7: Horizontal ground displacement for the 1.8D test.

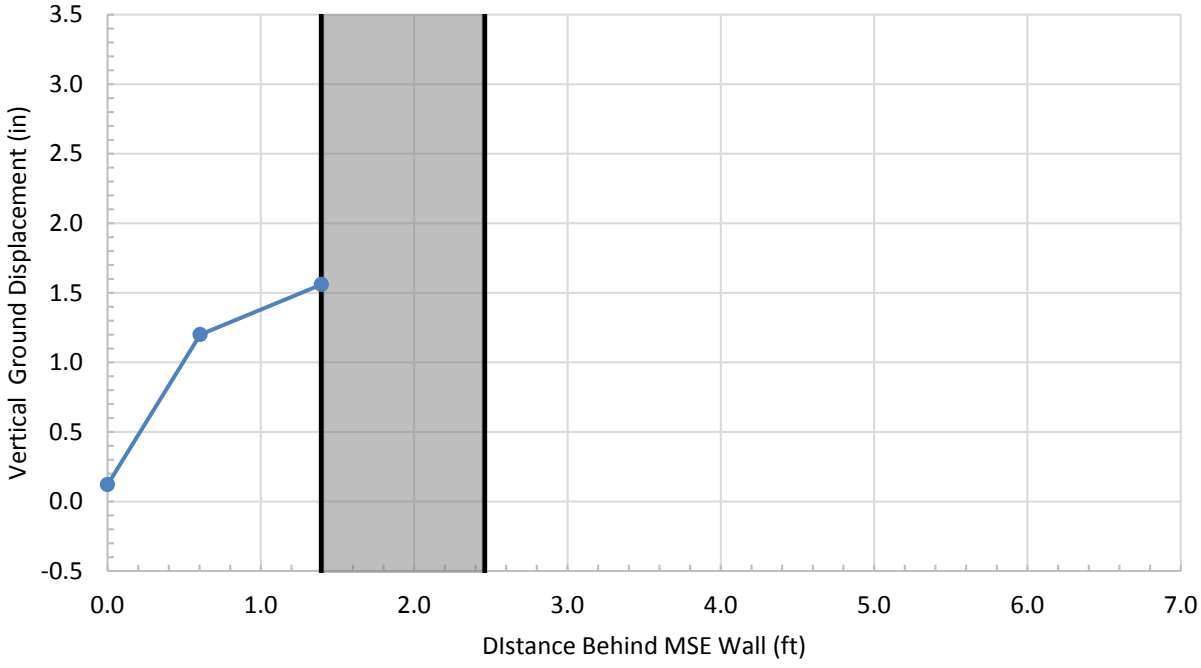

Figure E-8: Vertical ground displacement for the 1.8D test.

APPENDIX F – SOIL REINFORCEMENT INDUCED LOAD CURVES

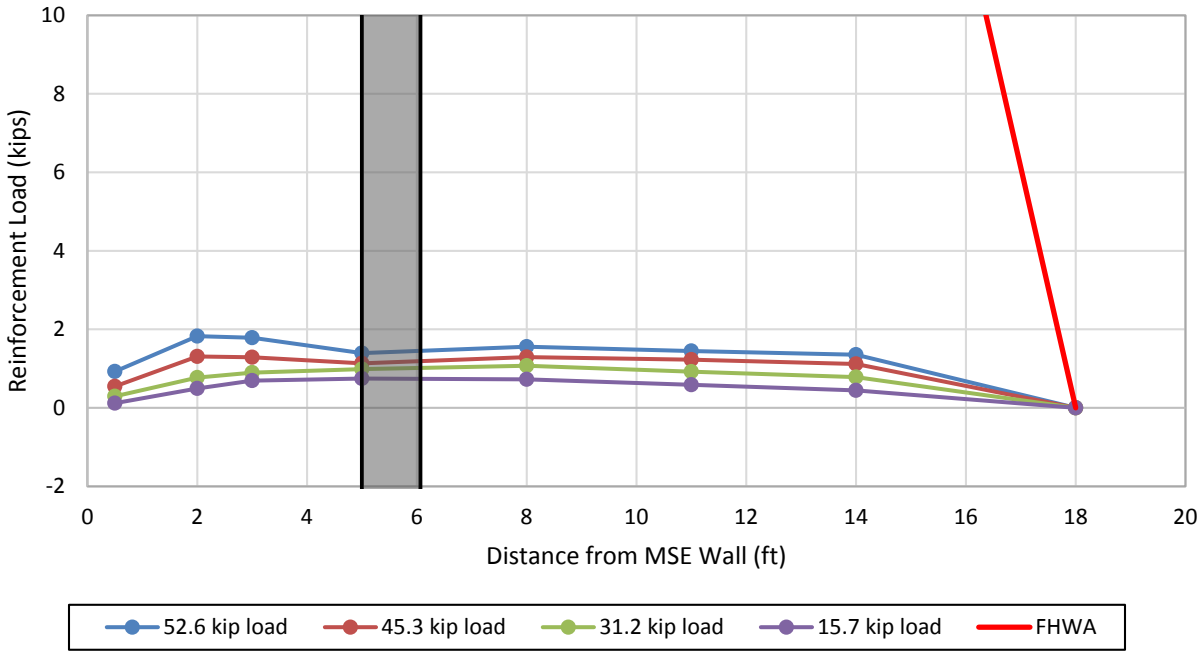

Figure F-1: Induced loads in the soil reinforcement at different pile head loads relative to distance from the back of the MSE wall (5.2D pile, layer L1, 46.5 in. transverse spacing).

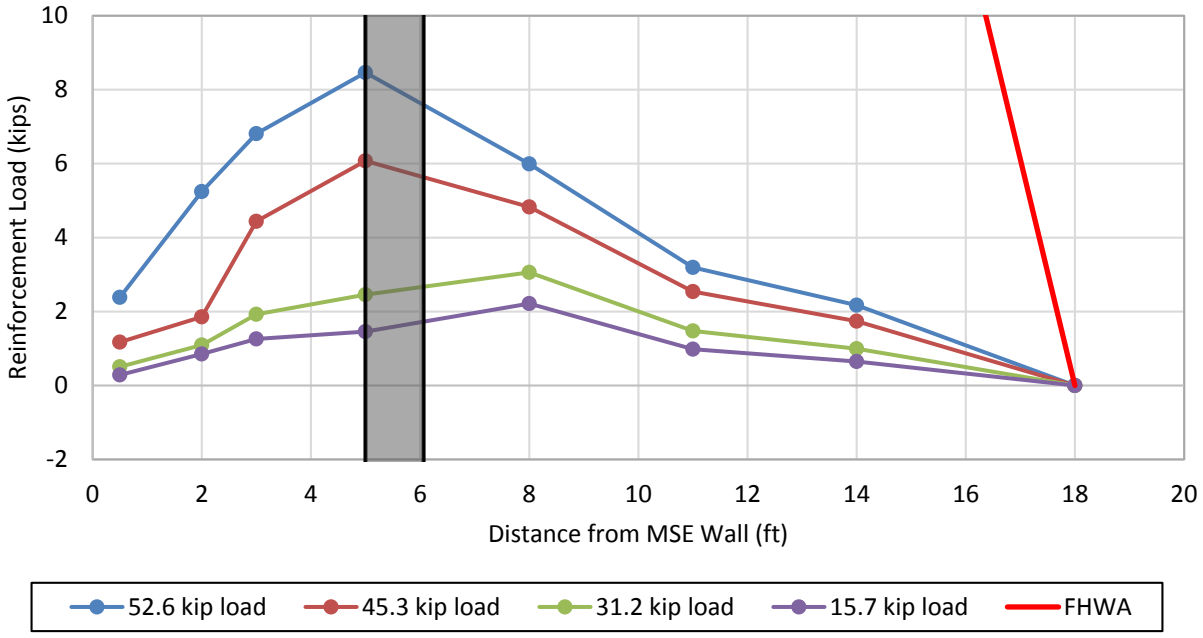

Figure F-2: Induced loads in the soil reinforcement at different pile head loads relative to distance from the back of the MSE wall (5.2D pile, layer L1, 15 in. transverse spacing).

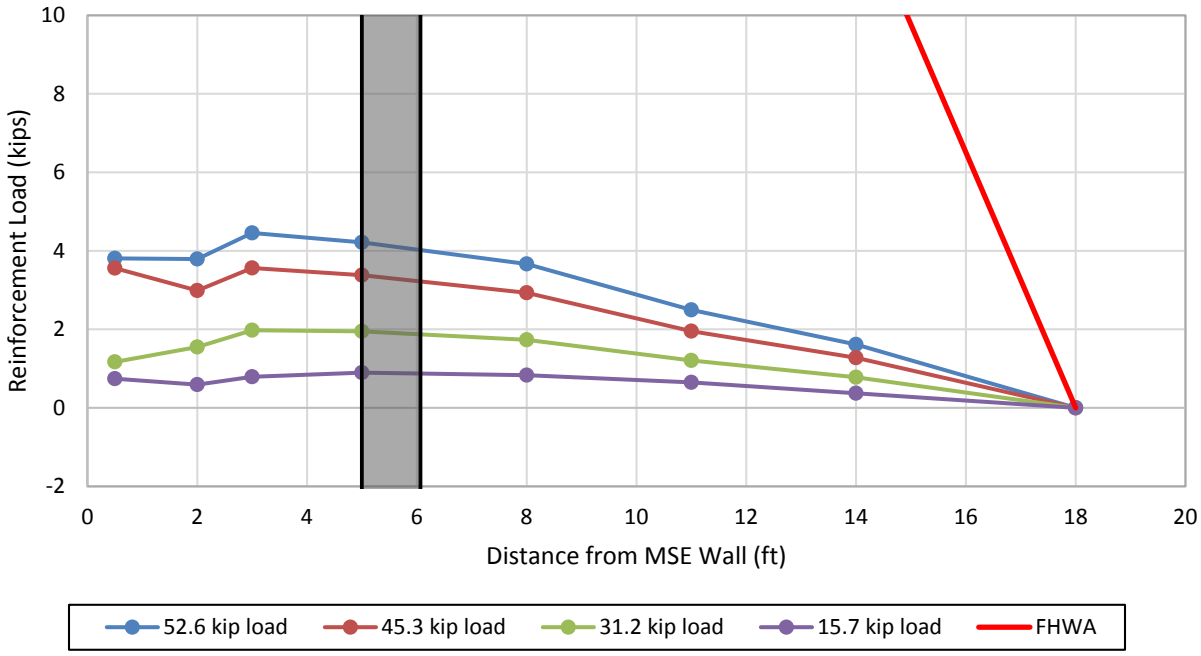

Figure F-3: Induced loads in the soil reinforcement at different pile head loads relative to distance from the back of the MSE wall (5.2D pile, layer L2, 38.5 in. transverse spacing).

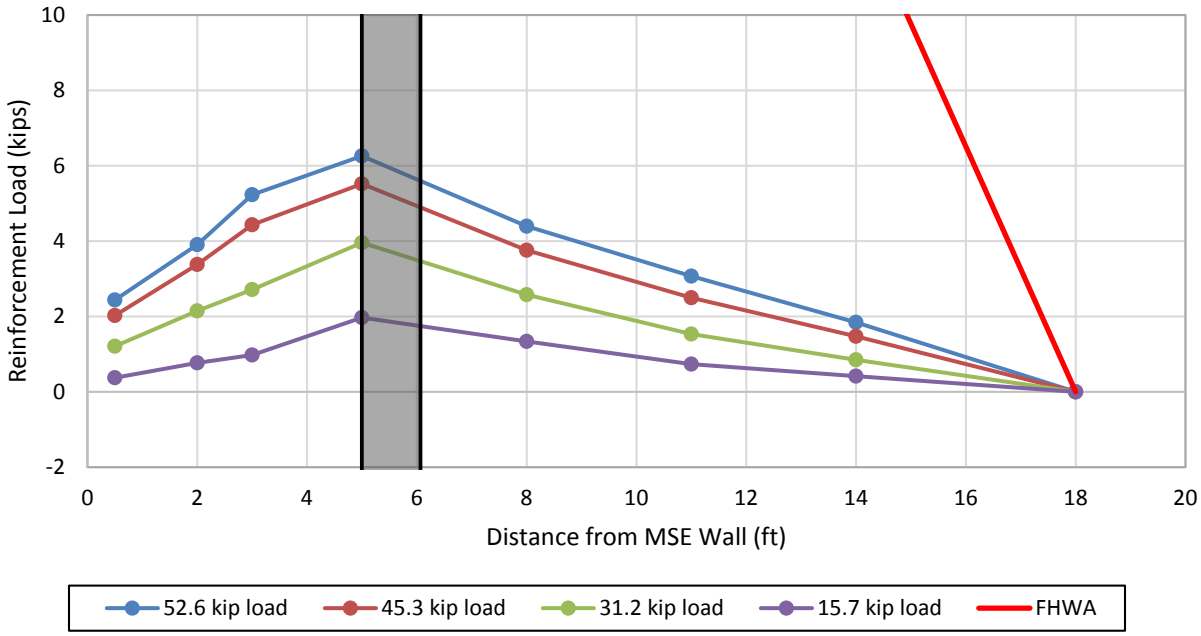

Figure F-4: Induced loads in the soil reinforcement at different pile head loads relative to distance from the back of the MSE wall (5.2D pile, layer L2, 22.5 in. transverse spacing).

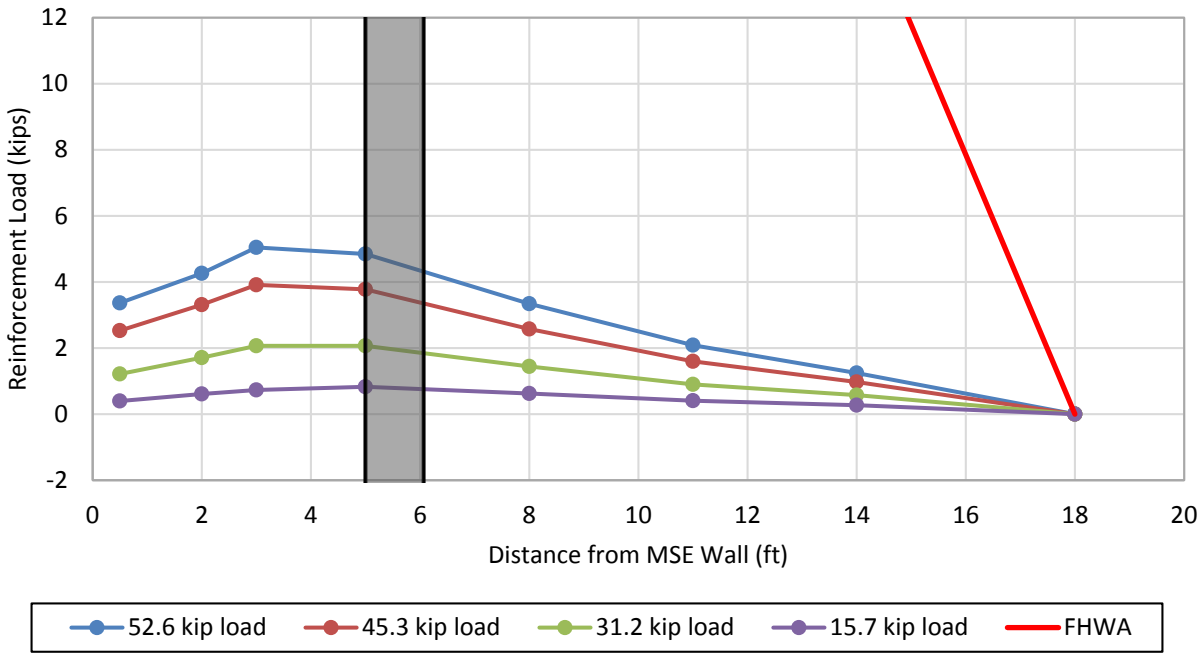

Figure F-5: Induced loads in the soil reinforcement at different pile head loads relative to distance from the back of the MSE wall (5.2D pile, layer L3, 46 in. transverse spacing).

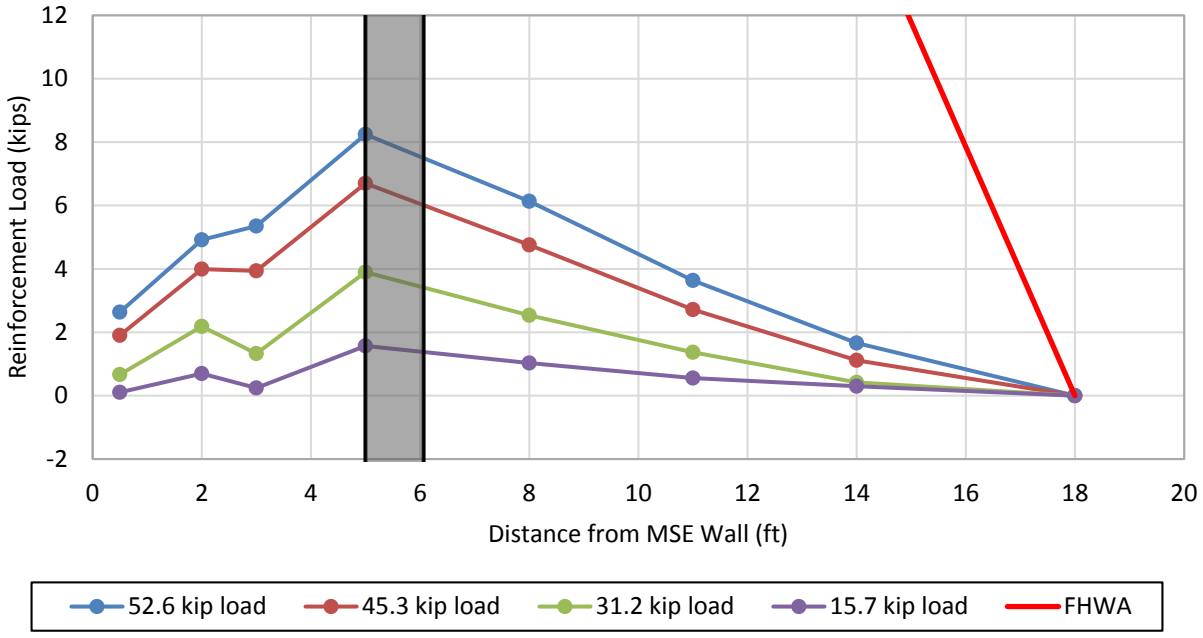

Figure F-6: Induced loads in the soil reinforcement at different pile head loads relative to distance from the back of the MSE wall (5.2D pile, layer L3, 21.5 in. transverse spacing).

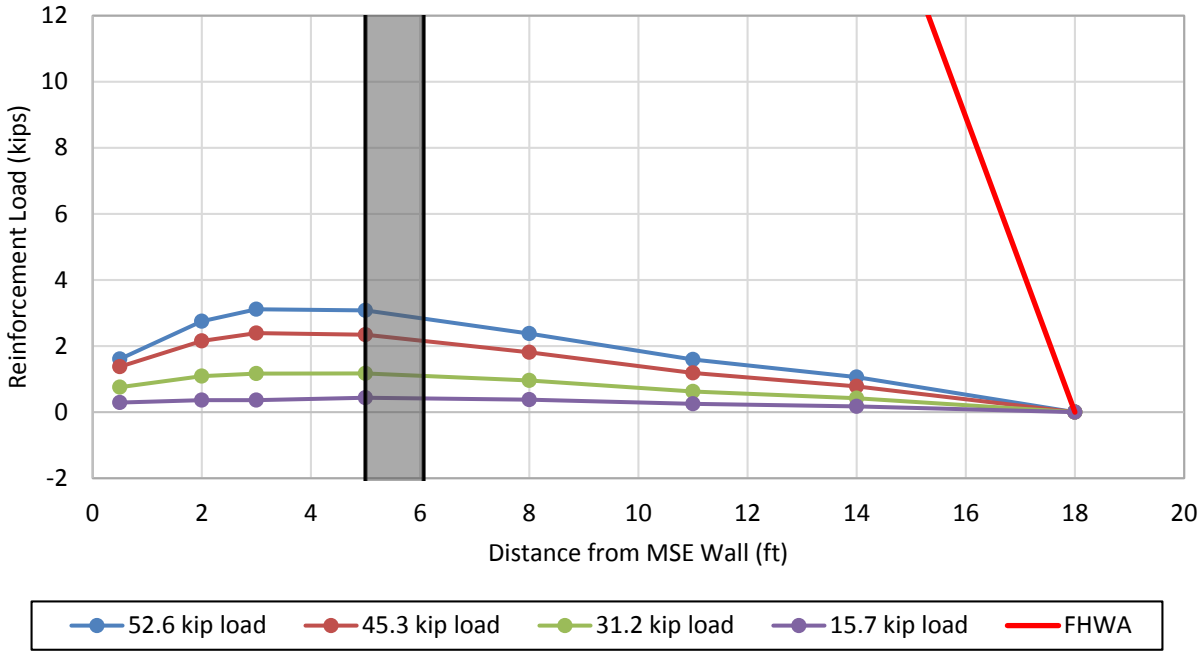

Figure F-7: Induced loads in the soil reinforcement at different pile head loads relative to distance from the back of the MSE wall (5.2D pile, layer L4, 39 in. transverse spacing).

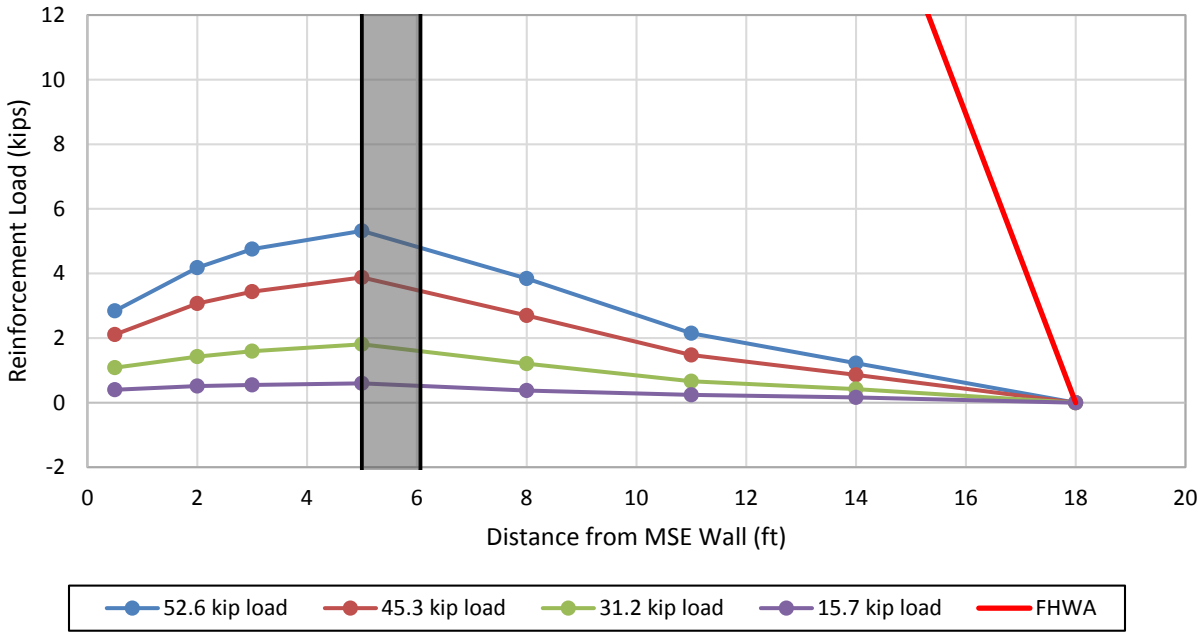

Figure F-8: Induced loads in the soil reinforcement at different pile head loads relative to distance from the back of the MSE wall (5.2D pile, layer L4, 23 in. transverse spacing).

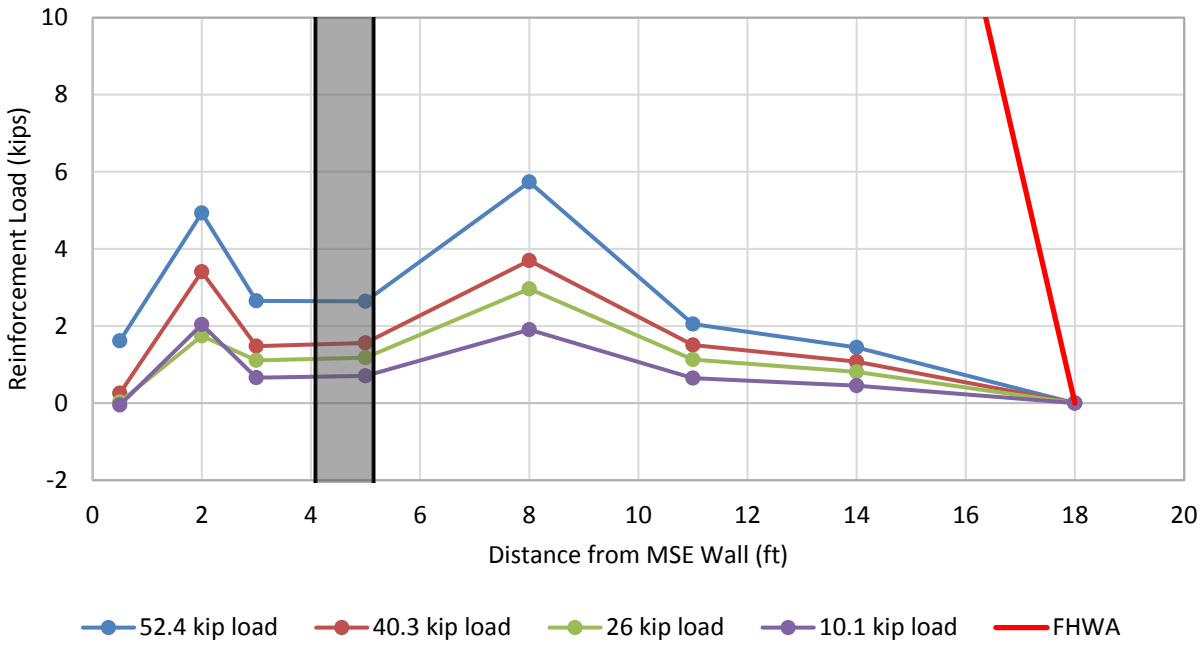

Figure F-9: Induced loads in the soil reinforcement at different pile head loads relative to distance from the back of the MSE wall (4.3D pile, layer L1, 40.5 in. transverse spacing).

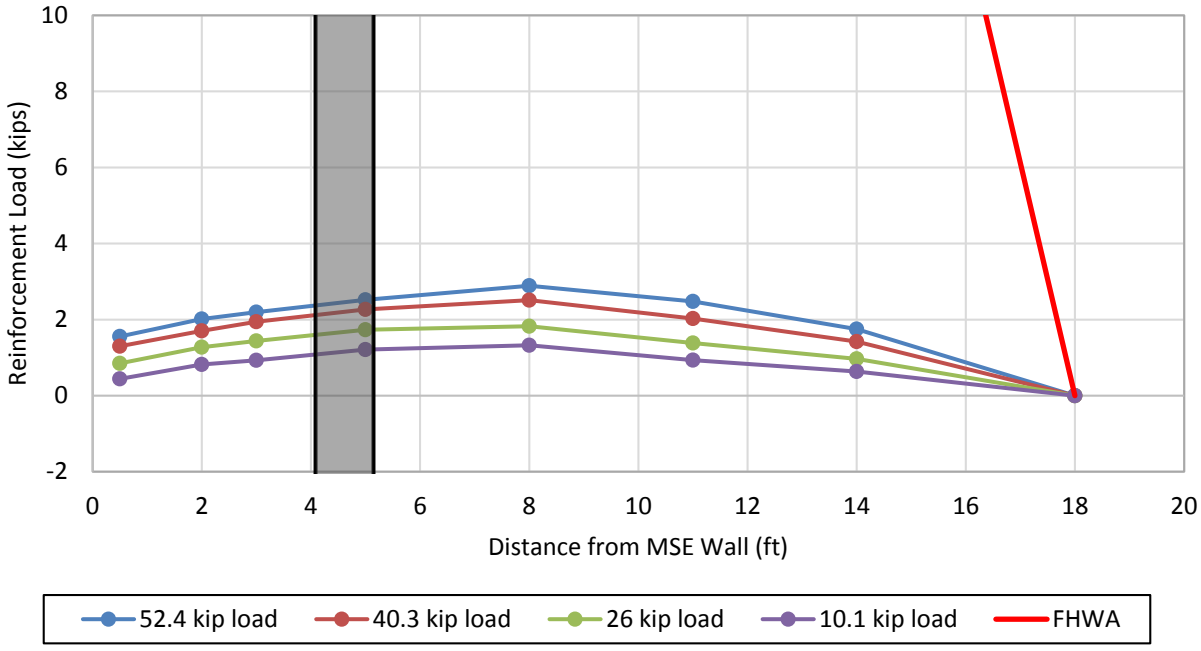

Figure F-10: Induced loads in the soil reinforcement at different pile head loads relative to distance from the back of the MSE wall (4.3D pile, layer L1, 17.5 in. transverse spacing).

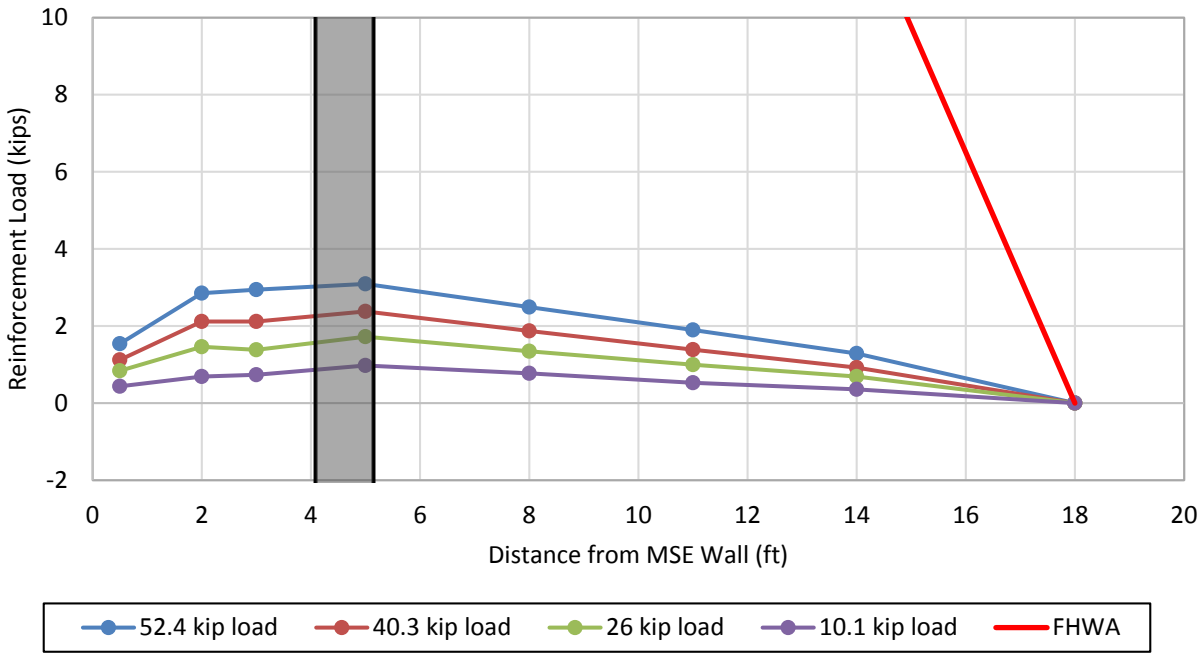

Figure F-11: Induced loads in the soil reinforcement at different pile head loads relative to distance from the back of the MSE wall (4.3D pile, layer L2, 33.5 in. transverse spacing).

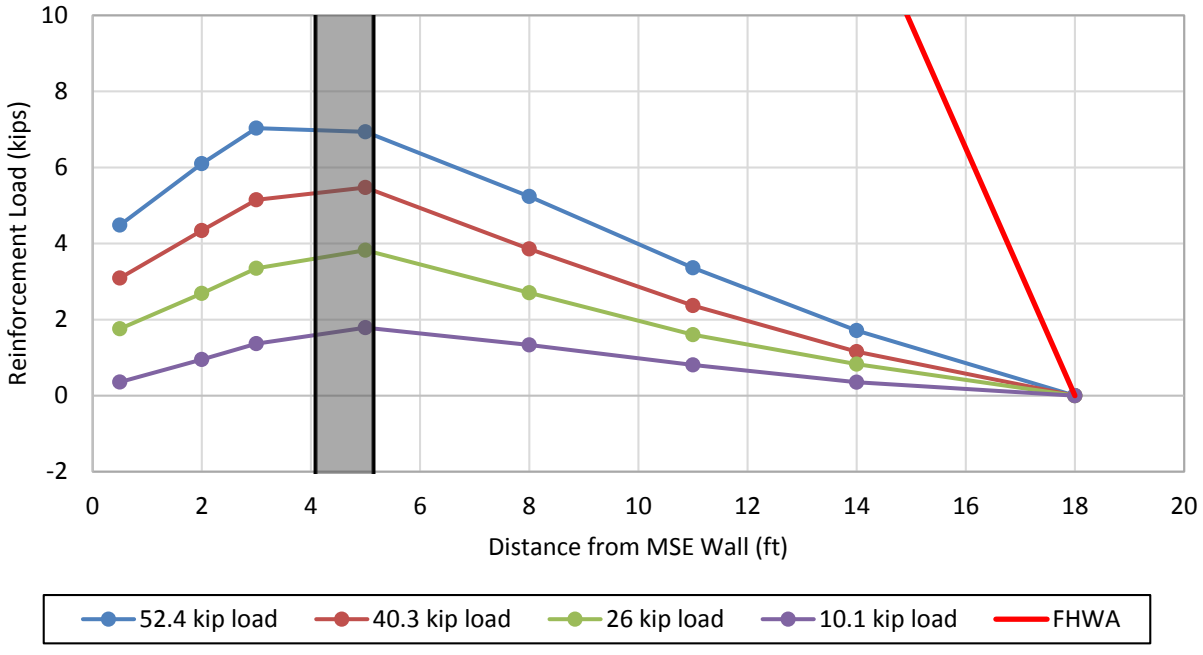

Figure F-12: Induced loads in the soil reinforcement at different pile head loads relative to distance from the back of the MSE wall (4.3D pile, layer L2, 18.5 in. transverse spacing).

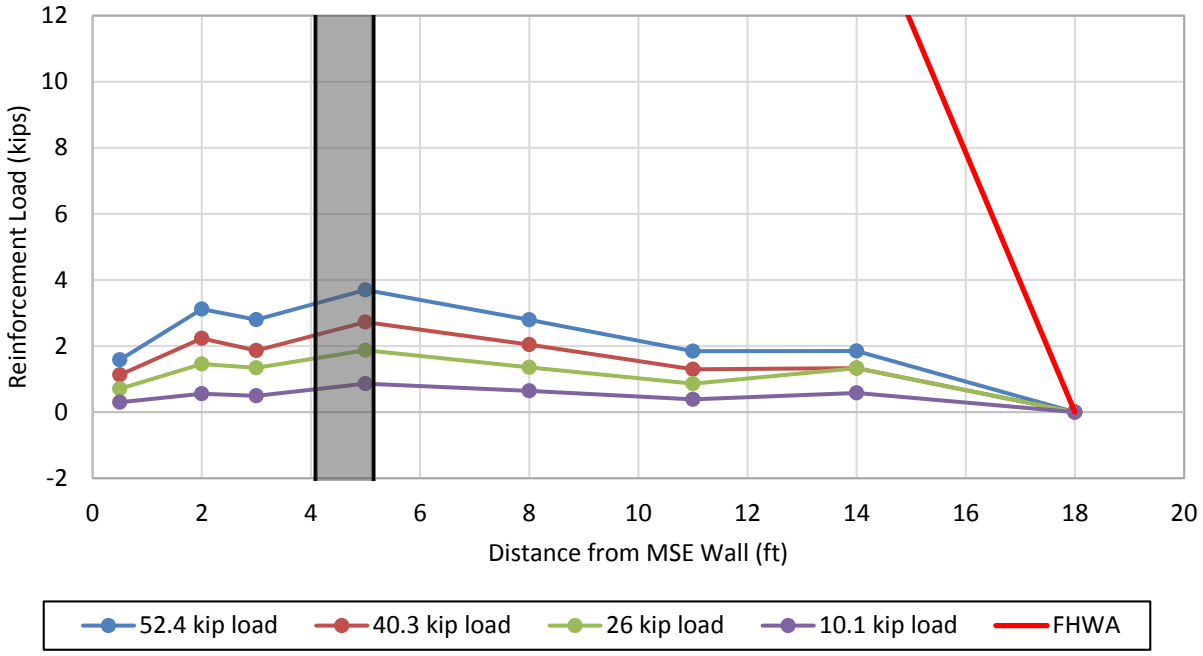

Figure F-13: Induced loads in the soil reinforcement at different pile head loads relative to distance from the back of the MSE wall (4.3D pile, layer L3, 34.5 in. transverse spacing).

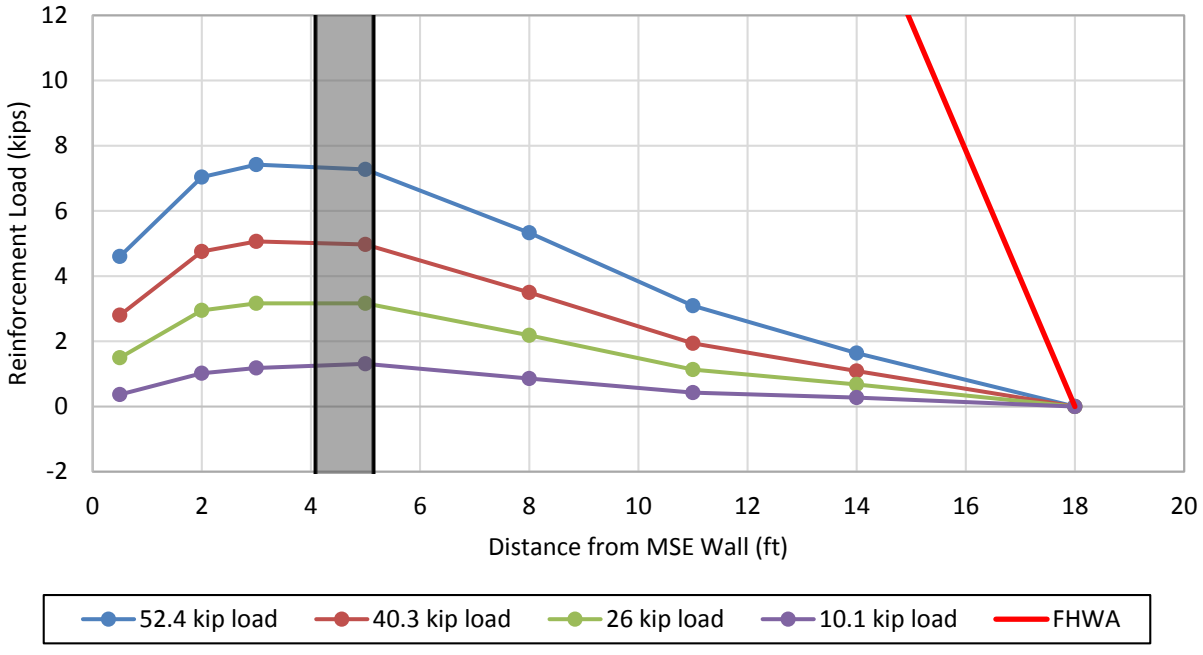

Figure F-14: Induced loads in the soil reinforcement at different pile head loads relative to distance from the back of the MSE wall (4.3D pile, layer L3, 17.5 in. transverse spacing).

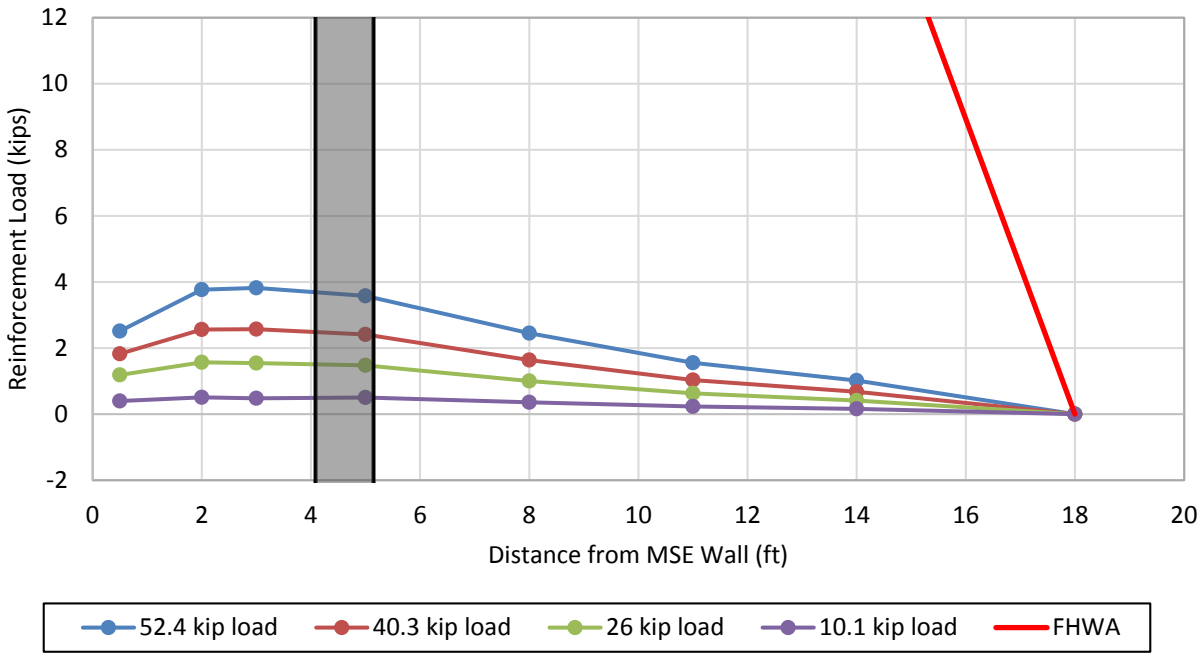

Figure F-15: Induced loads in the soil reinforcement at different pile head loads relative to distance from the back of the MSE wall (4.3D pile, layer L4, 34 in. transverse spacing).

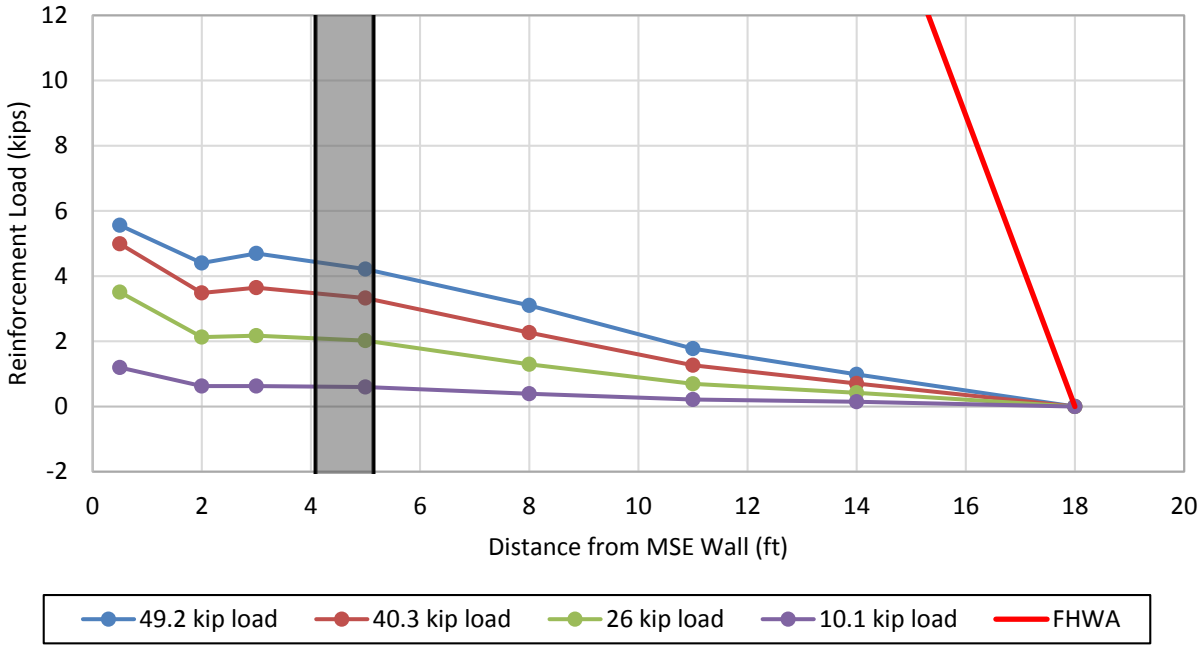

Figure F-16: Induced loads in the soil reinforcement at different pile head loads relative to distance from the back of the MSE wall (4.3D pile, layer L4, 19 in. transverse spacing).

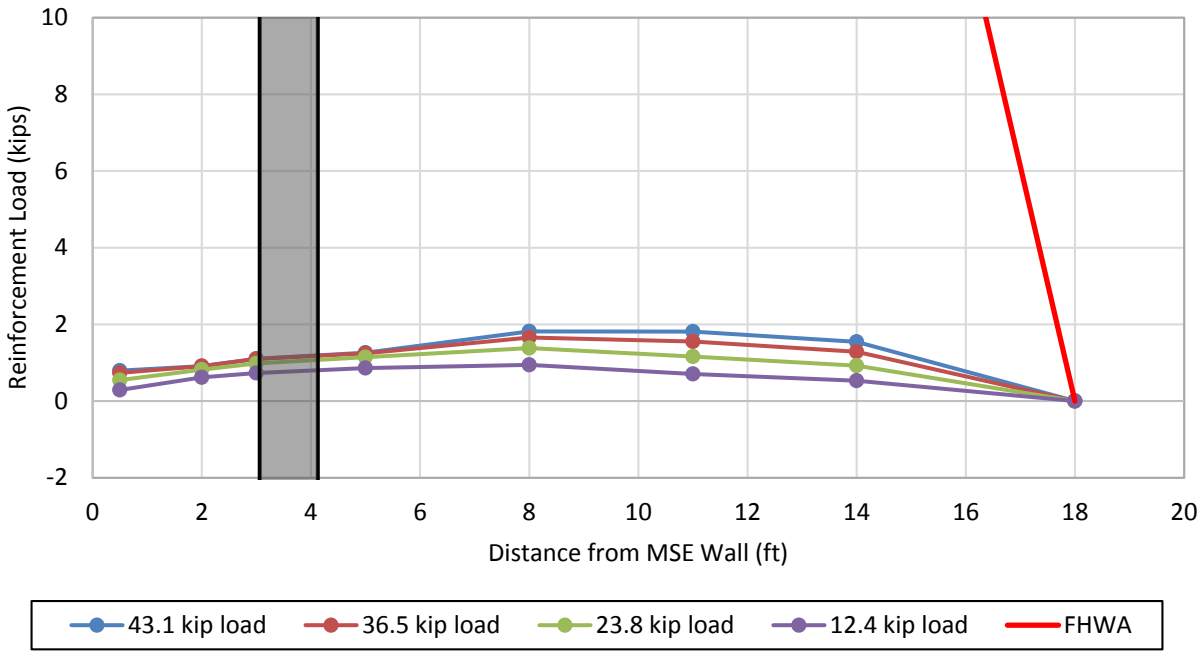

Figure F-17: Induced loads in the soil reinforcement at different pile head loads relative to distance from the back of the MSE wall (3.4D pile, layer L1, 38 in. transverse spacing).

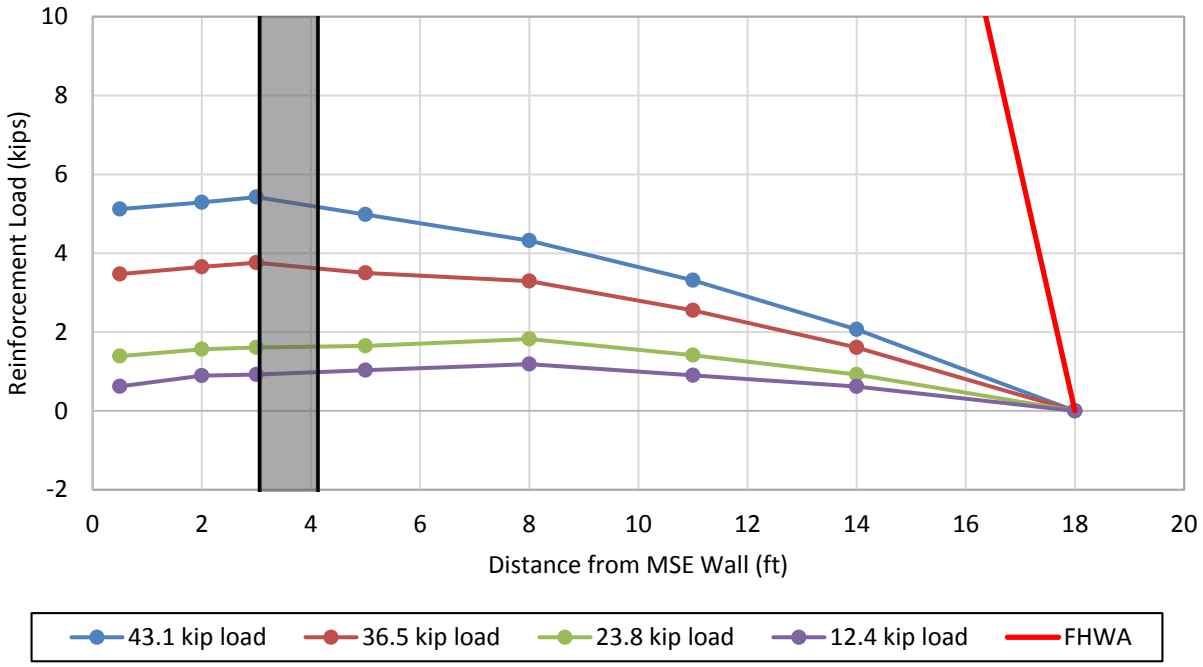

Figure F-18: Induced loads in the soil reinforcement at different pile head loads relative to distance from the back of the MSE wall (3.4D pile, layer L1, 24.5 in. transverse spacing).

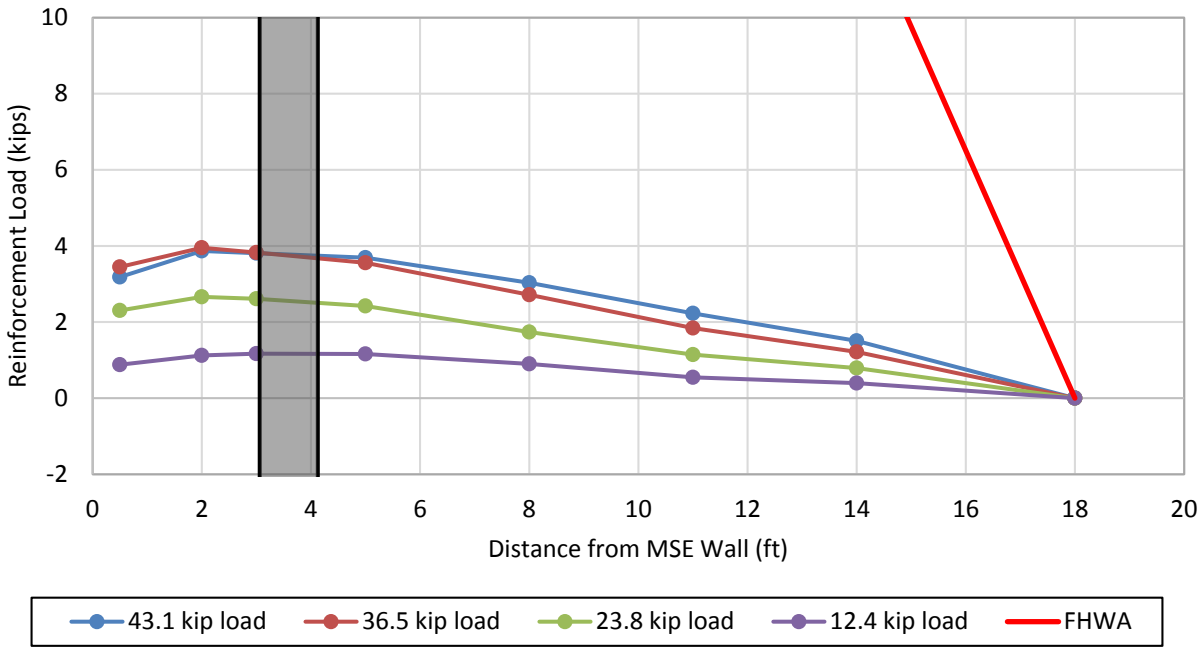

Figure F-19: Induced loads in the soil reinforcement at different pile head loads relative to distance from the back of the MSE wall (3.4D pile, layer L2, 37.5 in. transverse spacing).

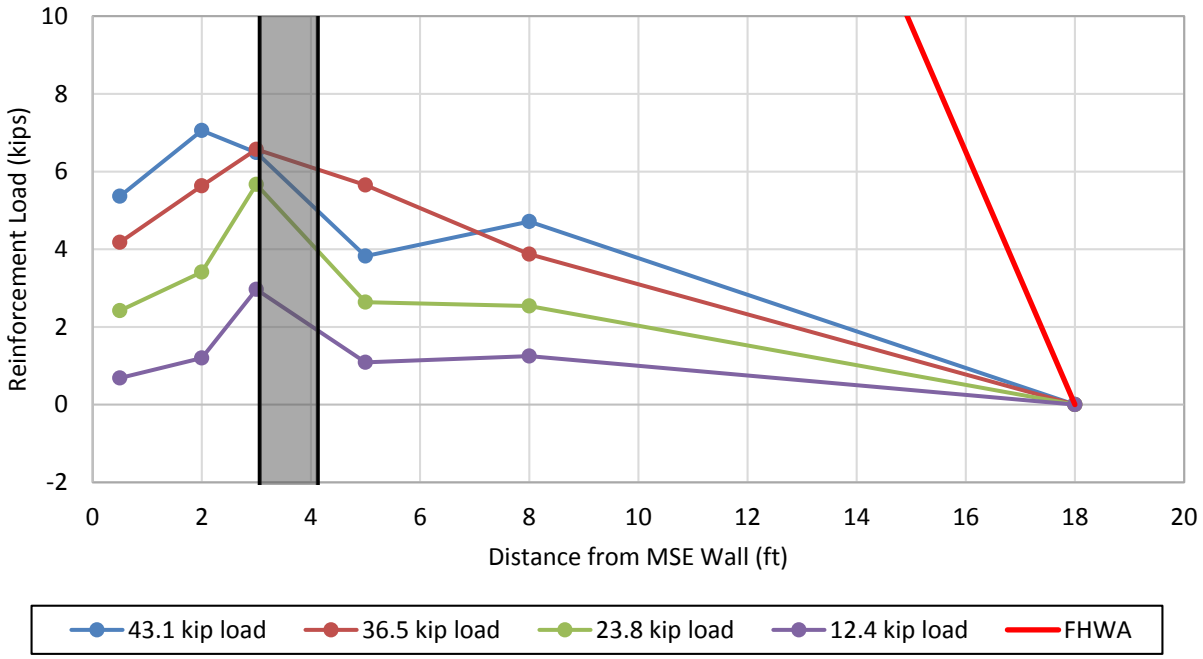

Figure F-20: Induced loads in the soil reinforcement at different pile head loads relative to distance from the back of the MSE wall (3.4D pile, layer L2, 23 in. transverse spacing).

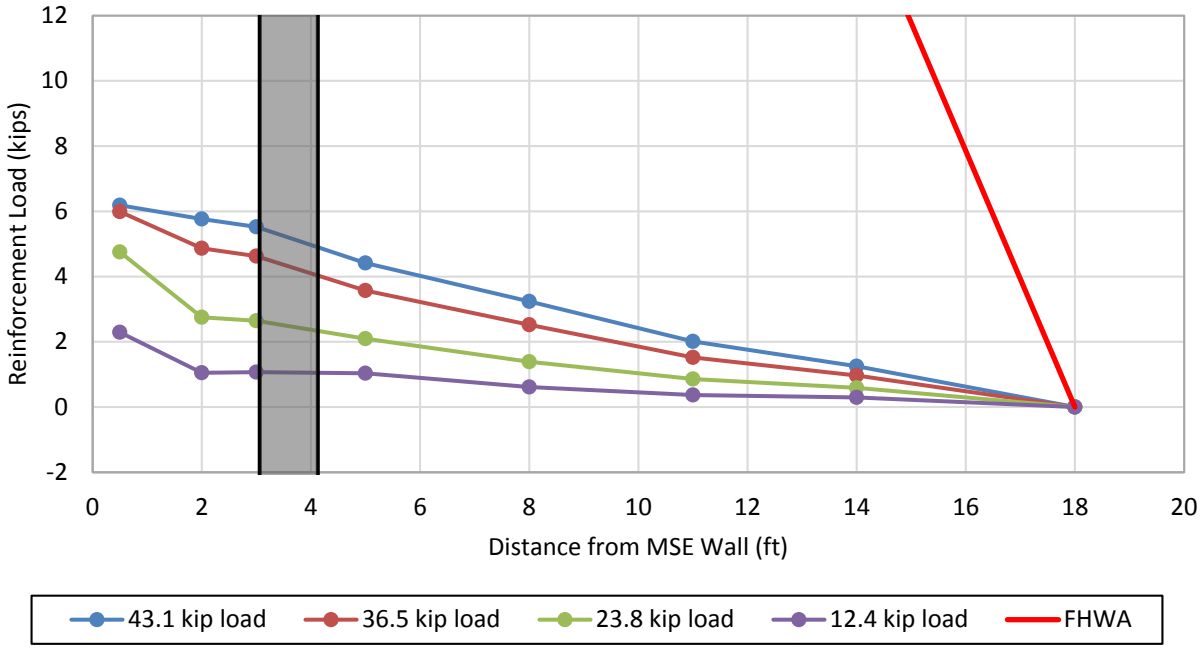

Figure F-21: Induced loads in the soil reinforcement at different pile head loads relative to distance from the back of the MSE wall (3.4D pile, layer L3, 38 in. transverse spacing).

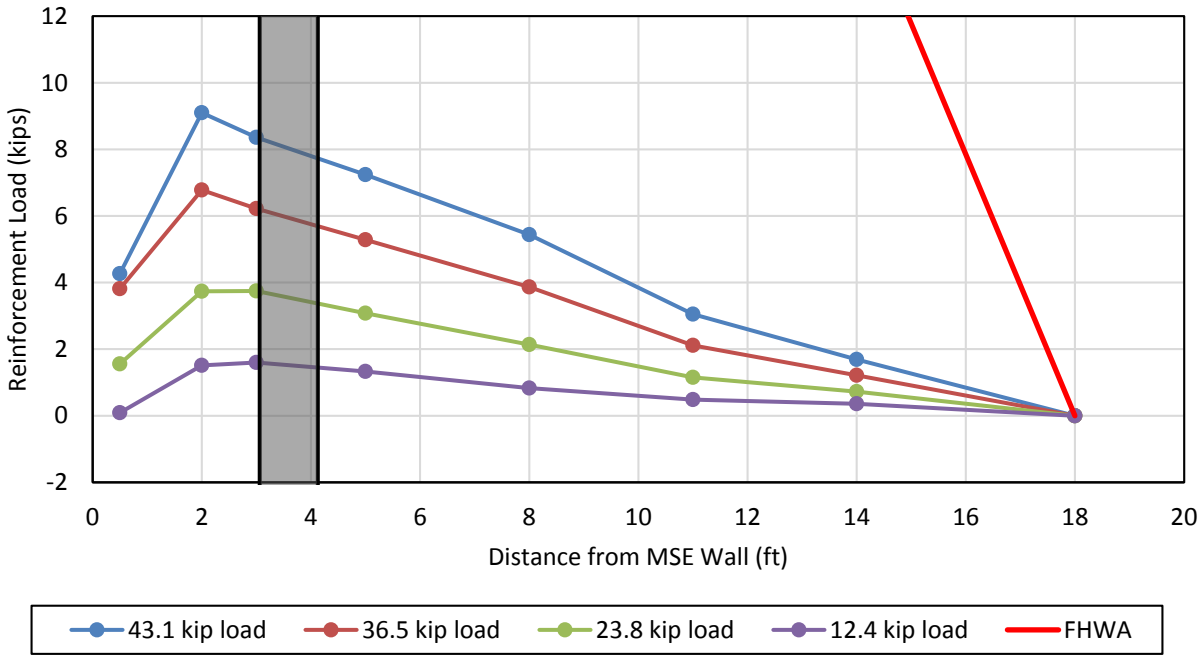

Figure F-22: Induced loads in the soil reinforcement at different pile head loads relative to distance from the back of the MSE wall (3.4D pile, layer L3, 23 in. transverse spacing).

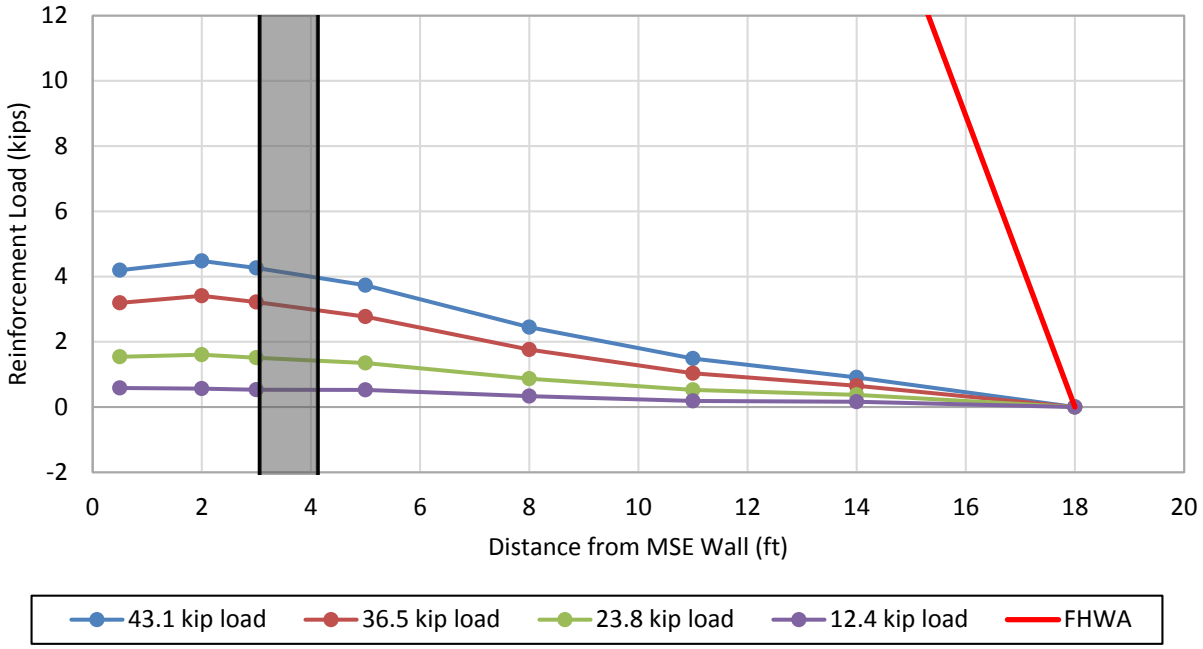

Figure F-23: Induced loads in the soil reinforcement at different pile head loads relative to distance from the back of the MSE wall (3.4D pile, layer L4, 38 in. transverse spacing).

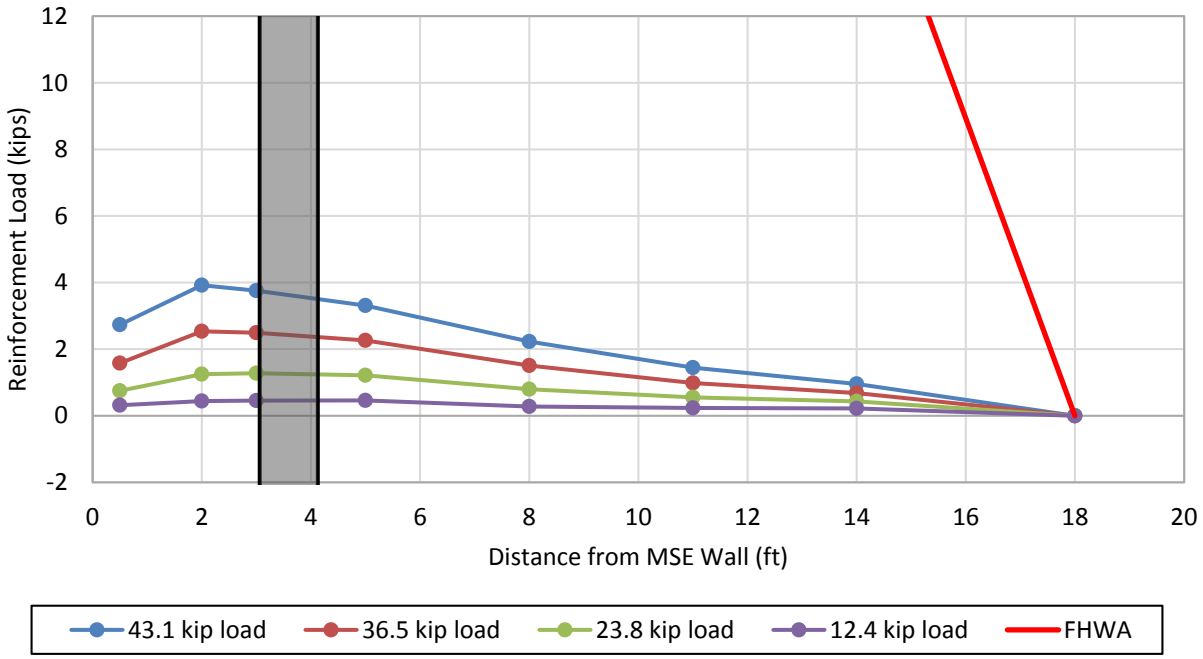

Figure F-24: Induced loads in the soil reinforcement at different pile head loads relative to distance from the back of the MSE wall (3.4D pile, layer L4, 31 in. transverse spacing).

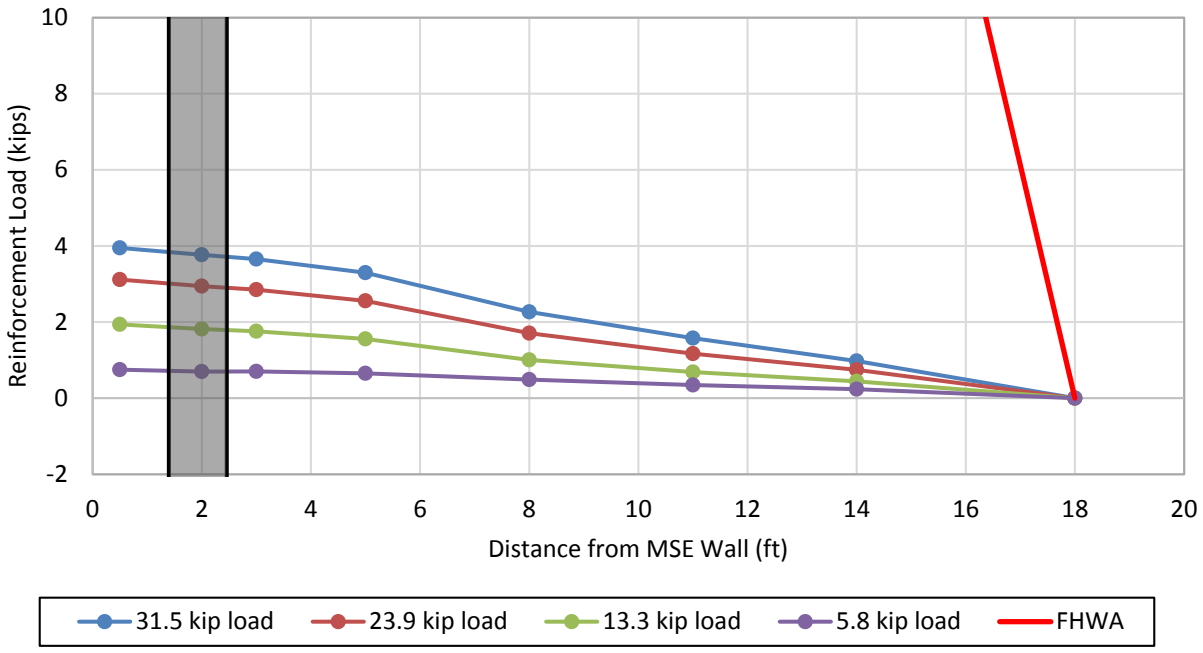

Figure F-25: Induced loads in the soil reinforcement at different pile head loads relative to distance from the back of the MSE wall (1.8D pile, layer L1, 42 in. transverse spacing).

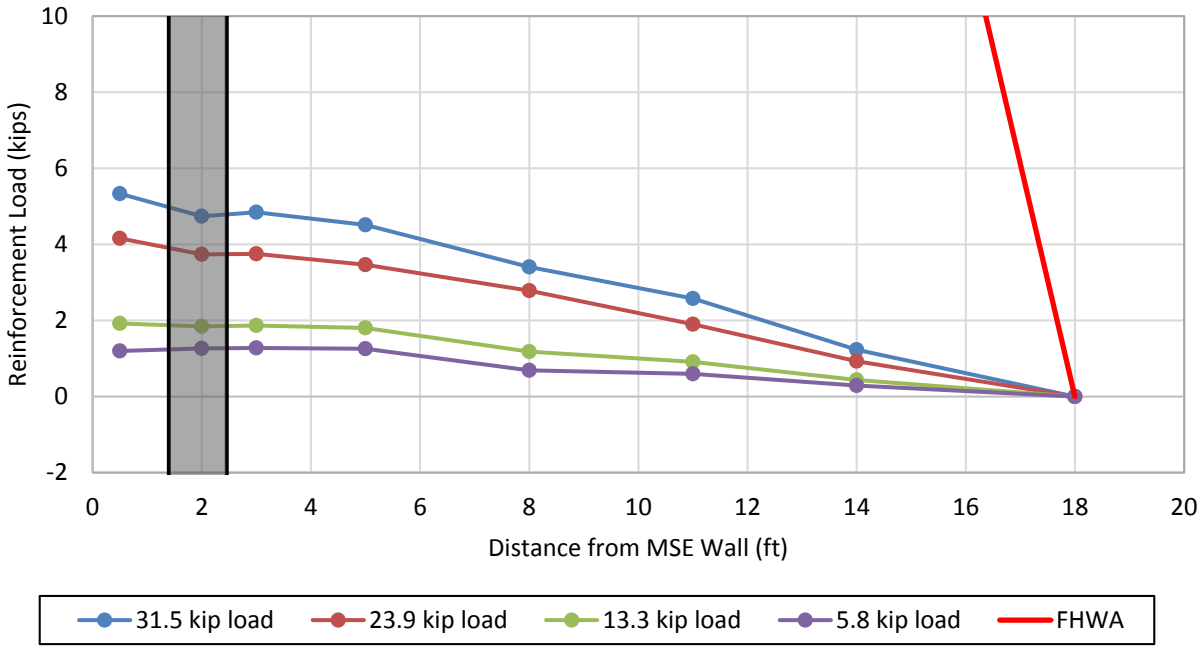

Figure F-26: Induced loads in the soil reinforcement at different pile head loads relative to distance from the back of the MSE wall (1.8D pile, layer L1, 17.5 in. transverse spacing).

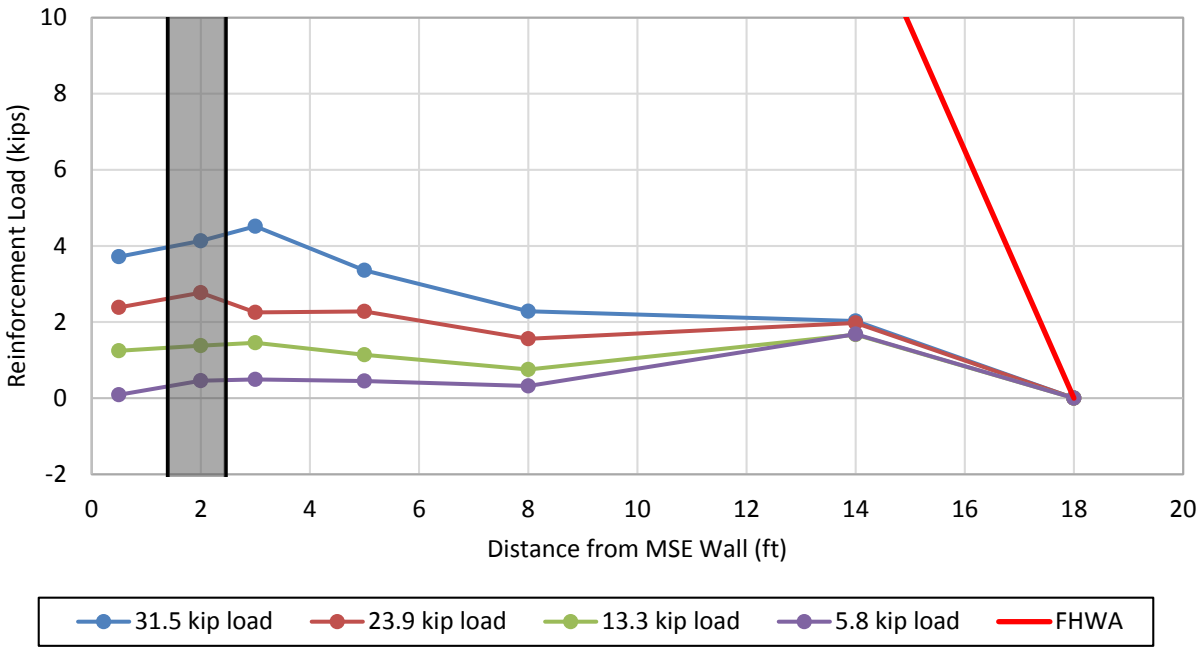

Figure F-27: Induced loads in the soil reinforcement at different pile head loads relative to distance from the back of the MSE wall (1.8D pile, layer L2, 43 in. transverse spacing).

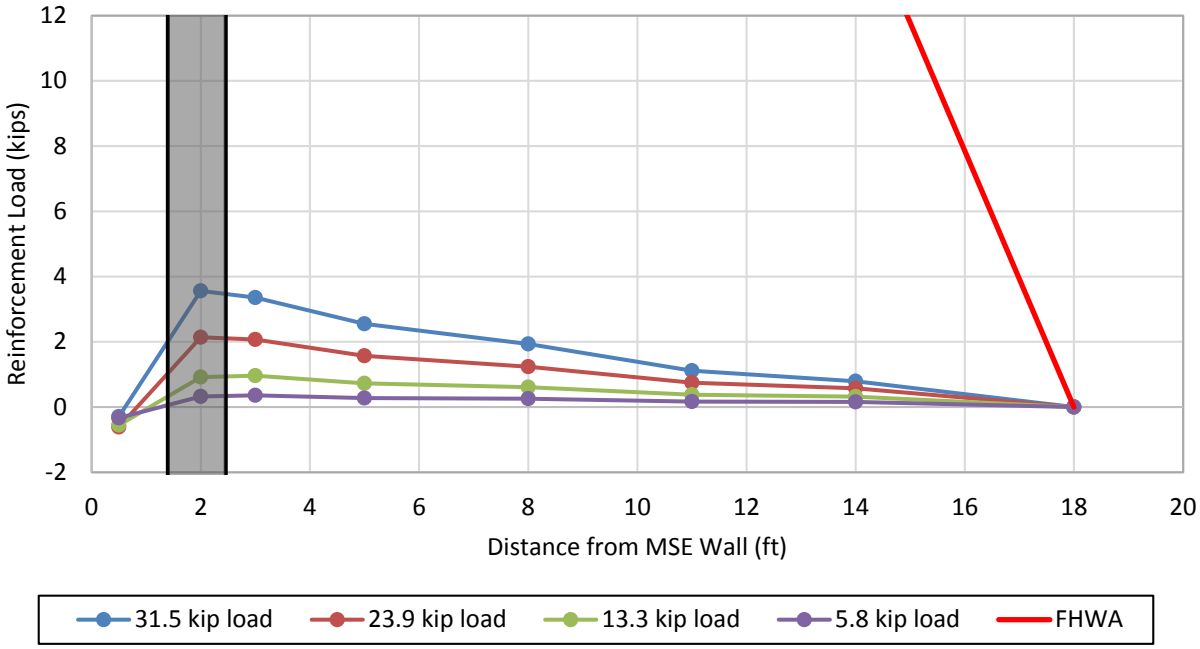

Figure F-28: Induced loads in the soil reinforcement at different pile head loads relative to distance from the back of the MSE wall (1.8D pile, layer L3, 43 in. transverse spacing).

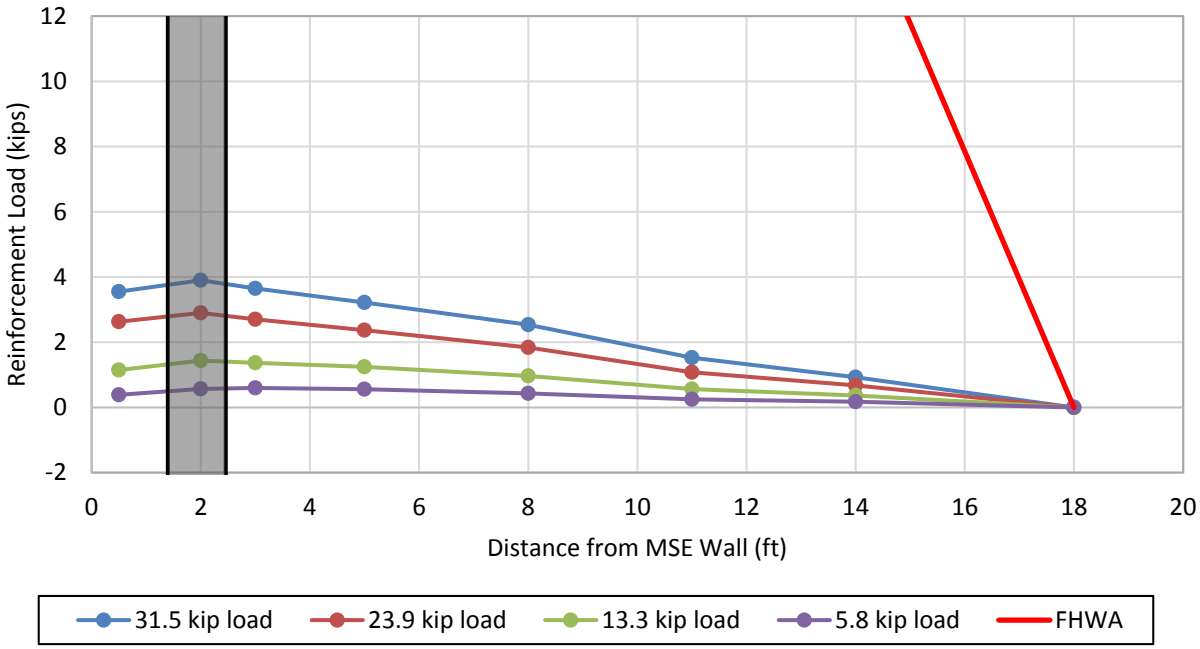

Figure F-29: Induced loads in the soil reinforcement at different pile head loads relative to distance from the back of the MSE wall (1.8D pile, layer L3, 22 in. transverse spacing).

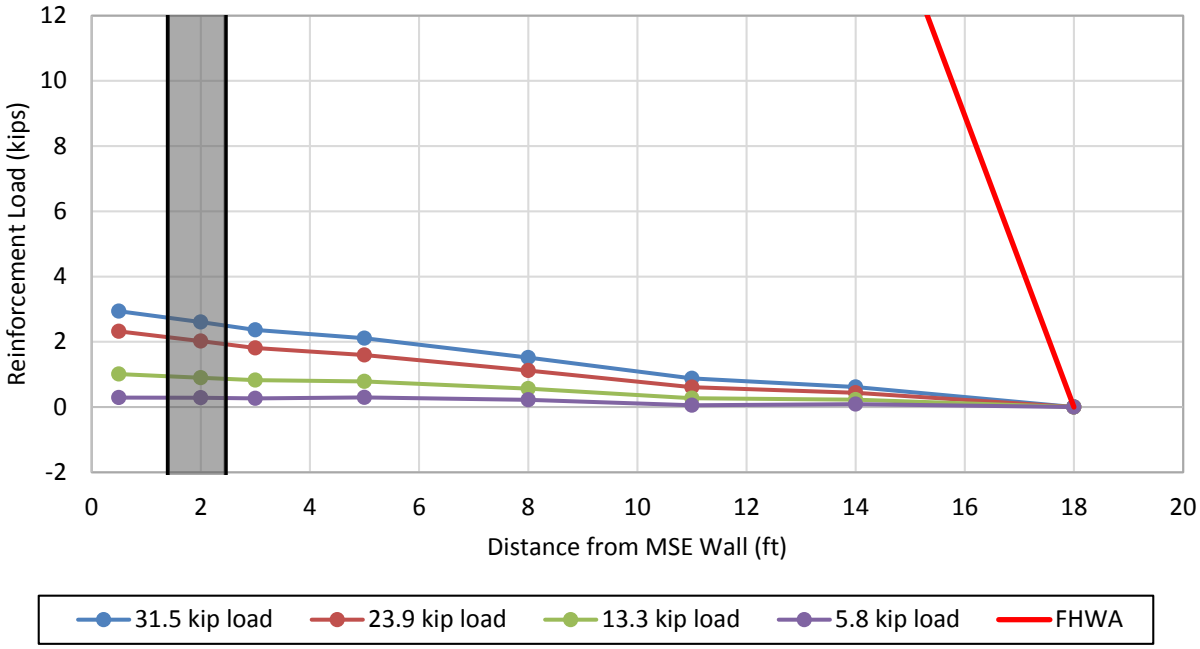

Figure F-30: Induced loads in the soil reinforcement at different pile head loads relative to distance from the back of the MSE wall (1.8D pile, layer L4, 35 in. transverse spacing).

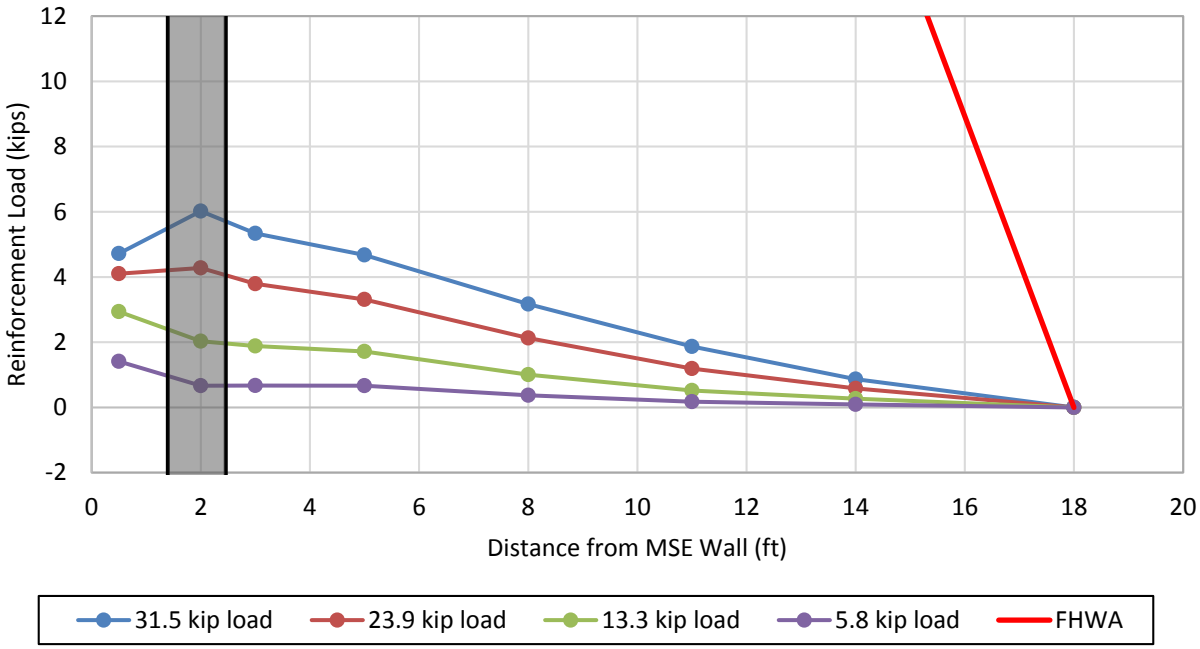

Figure F-31: Induced loads in the soil reinforcement at different pile head loads relative to distance from the back of the MSE wall (1.8D pile, layer L4, 17 in. transverse spacing).